

January 2014

Biomaterial Testing Methodology for Long-Term in vivo Applications: Silicon Carbide Corrosion Resistance, Biocompatibility and Hemocompatibility

Maysam Nezafati

University of South Florida, maysam@mail.usf.edu

Follow this and additional works at: <http://scholarcommons.usf.edu/etd>

 Part of the [Biomedical Engineering and Bioengineering Commons](#), [Electrical and Computer Engineering Commons](#), and the [Materials Science and Engineering Commons](#)

Scholar Commons Citation

Nezafati, Maysam, "Biomaterial Testing Methodology for Long-Term in vivo Applications: Silicon Carbide Corrosion Resistance, Biocompatibility and Hemocompatibility" (2014). *Graduate Theses and Dissertations*.
<http://scholarcommons.usf.edu/etd/5283>

This Dissertation is brought to you for free and open access by the Graduate School at Scholar Commons. It has been accepted for inclusion in Graduate Theses and Dissertations by an authorized administrator of Scholar Commons. For more information, please contact scholarcommons@usf.edu.

Biomaterial Testing Methodology for Long-Term *in vivo* Applications:
Silicon Carbide Corrosion Resistance, Biocompatibility and Hemocompatibility

by

Maysam Nezafati

A dissertation submitted in partial fulfillment
of the requirements for the degree of
Doctor of Philosophy in Electrical Engineering
Department of Electrical Engineering
College of Engineering
University of South Florida

Major Professor: Stephen E. Sadow, Ph.D.
Robert D. Frisina, Ph.D.
Andrew M. Hoff, Ph.D.
Christopher L. Frewin, Ph.D.
Laura Anderson, Ph.D.

Date of Approval:
June 27, 2014

Keywords: Semiconductor, Cytotoxicity,
ISO standard, Prosthetic implants, Neuroscience

Copyright © 2014, Maysam Nezafati

DEDICATION

To Behnaz H. Zaribaf, who has supported me unconditionally and never gave up on me.

ACKNOWLEDGMENTS

I want to show my gratitude to Dr. S. E. Sadow that without his valuable advice this project could not achieved its goals. I also want show my appreciation to Dr. R. Frisina, who has helped me a lot during my graduate studies in USF. I want to thank Dr. A. Hoff, Dr. L. Anderson and Dr. M. Jaroszeski to accept to be in my PhD committee and giving me the most valuable advice. Last but not least I want to thank Dr. Christopher Frewin who not only was my mentor but was a great friend. The author would like to acknowledge the assistance of NREC, Dr. K. Muffly, Leigh West, the Rosekamp laboratory crew and especially Dr. G. A. De Erausquin.

I am so grateful to have the most supportive person “Behnaz H Zaribaf” in my life who assisted me to pursue all of my dreams.

I also want to thank Kevin Kohler the most reliable lab assistant. I also am so happy to have had the help of my good friends Joe (Dr. Register) and Meralys (Dr. Reyes).

This work was sponsored by the Defense Advanced Research Projects Agency (DARPA) MTO under the auspices of Dr. Jack Judy through the Space and Naval Warfare Systems Center, Pacific Grant/Contract No. N66001-12-1-4026 - Biocompatibility of Advanced Materials for Brain Machine Interfaces.

TABLE OF CONTENTS

LIST OF TABLES	iii
LIST OF FIGURES	iv
ABSTRACT	viii
CHAPTER 1: INTRODUCTION	1
1.1. Need for <i>in vivo</i> Biomaterials	1
1.2. ISO 10993 Introduction	2
1.3. Biocompatibility of the Materials	4
1.4. Hemocompatibility of the Materials	5
1.5. Chemical Simulation of the Body Environment <i>in vitro</i>	6
1.6. Cell Biology	7
1.6.1. Fibroblast Cell Line (L 929 Cell Line)	7
1.6.2. Neuroglioma Cells (H4 Cell Line).....	8
1.6.3. Primary Neurons	9
1.7. Statistical Theories.....	9
1.8. Summary	10
CHAPTER 2: CORROSION AND MATERIALS DEGRADATION	12
2.1. Sample Preparation	12
2.2. Scientific Controls	15
2.2.1. Negative Control Selection	15
2.2.2. Positive Control Selection	18
2.3. Test Materials.....	20
2.3.1. (100) Silicon.....	20
2.3.2. Cubic Silicon Carbide (3C-SiC)	21
2.3.3. Silicon Carbide (<i>a</i> -SiC).....	22
2.4. Corrosion Testing in Simulated Solution.....	25
2.4.1. Scanning Electron Microscopy	26
2.4.2. Atomic Force Microscopy	30
2.5. Material Stability Tests on Silicon.....	31
2.5.1. Solvent Cleaning of Immersed Samples	33
2.5.2. Piranha Cleaning of Immersed Samples	33
2.5.3. Hydrofluoric (HF) Acid Cleaning of Immersed Samples.....	35
2.6. Surface Degradation of <i>a</i> -SiC and 3C-SiC	39
2.6. Summary	40

CHAPTER 3: BIOCOMPATIBILITY OF THE BIOMATERIALS	43
3.1. Sample Preparation	46
3.2. Cell Culture.....	47
3.2.1 Cell Plating.....	50
3.3. Extract Method.....	51
3.4. Direct Contact Method.....	55
3.5. Seeding Method	57
3.6. Direct Cell Plating (BAMBI Method)	59
3.7. Summary	65
 CHAPTER 4: HEMOCOMPATIBILITY OF BIOMATERIALS	 68
4.1. Flow Dynamics	70
4.2. Chandler’s Loop.....	72
4.3. Current Design.....	73
4.4. Method and Materials	75
4.4.1 Platelet Rich Plasma (PRP) Preparation	75
4.5. Static Hemocompatibility Experiment.....	78
4.7 Summary.....	81
 CHAPTER 5: SILICON CARBIDE NANOWIRES AS A BIOMATERIAL	 83
5.1. Silicon Carbide Nanowire Properties.....	83
5.2. SiCNW Fabrication Methods.....	86
5.2.1 Conversion of C or Si 1D Structures to 3C–SiC.....	86
5.2.2. SiCNW Growth Based on the Vapor–Liquid–Solid (VLS) Mechanism	87
5.3. Cytotoxicity Evaluation of SiCNWS	87
5.4. Cell Adhesion on SiCNWS.....	90
5.5. Summary	93
 CHAPTER 6: SUMMARY AND FUTURE WORKS	 95
6.1. Summary	95
6.2 Future Works	96
 REFERENCES	 99
 APPENDICES	 106
Appendix A: Copyright Permissions	107
Appendix B: Chemical Composition of Electrolytes.....	112

LIST OF TABLES

Table 2.1: The DI water grade requirements based on ISO-3696 [44].....	17
Table 2.2: Cleaning methods description.....	32
Table 2.3: AFM data extracted from <i>in vitro</i> tests.....	36

LIST OF FIGURES

Figure 2.1: Flowchart showing the sample preparation steps and sample distribution for the material stability (Blue - Chapter 2), biocompatibility (Green -Chapter 3) and hemocompatibility (Red – Chapter 4) tests based on ISO 10993.	14
Figure 2.2: The chemical structure of citric acid $C_6H_8O_7$	20
Figure 2.3: AFM micrographs of (left) 10×10 and (right) $5 \times 5 \mu m$ scans of 3C-SiC sample USF2-12-147.	21
Figure 2.4: Line scan of the $5 \times 5 \mu m$ AFM micrograph of Figure 2.3 of 3C-SiC sample USF2-12-147.	22
Figure 2.5: Cross-section showing the structure of type I <i>a</i> -SiC developed for testing in this research.	23
Figure 2.6: Cross-section showing the structure of type II <i>a</i> -SiC developed for testing in this research.	23
Figure 2.7: Cross-section showing the structure of type III <i>a</i> -SiC developed for testing in this research.	24
Figure 2.8: Cross-section showing the structure of type IV <i>a</i> -SiC developed for testing in this research.	24
Figure 2.9: The SEM micrographs of Au samples at 60° tilt angle, 25 kV acceleration voltage and 5000X magnification after soaking in 1X PBS at 37 and $60^\circ C$	27
Figure 2.10: The SEM micrographs of Cu samples at 60° tilt angle, 25kv acceleration voltage and 5000X magnification after soaking in 1X PBS at 37 and $60^\circ C$	27
Figure 2.11: The SEM micrographs of PE samples at 60° tilt angle, 25kv acceleration voltage and 5000X magnification after soaking in 1X PBS at 37 and $60^\circ C$	28
Figure 2.12: The SEM micrographs of PVC samples at 60° tilt angle, 25kv acceleration voltage and 5000X magnification after soaking in 1X PBS at 37 and $60^\circ C$	29
Figure 2.13: The SEM micrographs of parylene C samples at 60° tilt angle, 25kv acceleration voltage and 5000X magnification after soaking in 1X PBS at 37 and $60^\circ C$	29

Figure 2.14: Sample map showing the position of the patches in 5 regions studied for each sample and their corresponding designation.	30
Figure 2.15: 45×45 μm area AFM micrographs of silicon samples immersed in Cell Media+ H4 Cells (left column) , Cell Media (center column) and ACSF (right column) for 96 hours at 37°C.	34
Figure 2.16: SEM micrographs of silicon samples immersed in Cell Media+ H4 Cells, Cell Media and ACSF; for 96 hours at 37°C.	37
Figure 2.17: SEM results of silicon after in vitro testing.	38
Figure 2. 18: Surface degradation of positive controls.	39
Figure 2. 19: Surface roughness change of <i>a</i> -SiC, 3C-SiC, SiO ₂ and Si (100).	40
Figure 3.1: The schematic of material/ cell orientation in: Extract test based on ISO 10993-5 section 8.2 (left)[6], Direct test based on ISO 10993-5 section 8.3 (center)[6] and Seeding test (right)[12-15].	46
Figure 3.2: Photograph of the hemocytometer used for counting the cell concentration.	50
Figure 3.3: Live/ dead cell assay data.	54
Figure 3.4: Quantitative data of control materials Au, Cu, PE and PVC done with extract method on L929 cells.	55
Figure 3.5: Fluorescence micrographs of Au as negative control material after performing direct contact method with L929 cells.	56
Figure 3.6: Quantitative analysis of the direct contact test on control materials.	57
Figure 3.7: Fluorescence micrographs comparing PE after (a) direct surface seeding method, with b) the extract method with 100% media replacement.	58
Figure 3.8: Qualitative analysis of the control materials (Au, Cu, PE and PVC) using surface seeding method.	59
Figure 3.9: BAMBI method sample placement schematic showing the orientation of samples in the 6 well cell culture plate containing 2 coupons of test material, 1 coupon of positive control, 1 coupon of negative control, and 2 CTPC samples used as baseline.	60
Figure 3.10: Illustration of BAMBI method sample mounting on a cell treated polycarbonate slide and the cells seeded above them versus time.	61

Figure 3.11: BAMBI method fluorescence micrographs, at 10X magnification, of the wells that included the control materials (a) Au, (b) Cu, (c) polyethylene and (d) PVC organo-Sn. Cells present on the test materials are out of focus and thus appear black in the image (see Fig. 3.12 for cell images from the test materials).	62
Figure 3.12: BAMBI method fluorescence micrographs, at 10X and 50X magnifications, of the materials that included the control materials (a) Au, (b) Cu, (c) polyethylene and (d) PVC organo-Sn. (See Fig. 3.11 for well images corresponding to this data).	63
Figure 3.13: BAMBI method fluorescence micrographs of 3C-SiC, Cu as positive control, Au as negative control and 2 CTPC as baseline samples, from the wells at 10X and 50X magnification.	64
Figure 3.14: BAMBI method statistical analysis of control materials (Cu, Au, PVC org.-Sn, PE) and test materials (3C-SiC and <i>a</i> -SiC).	65
Figure 4.1: Human brain and neck blood vessel network (i.e., brain vasculature) [67] showing how dense is the brain vasculature.	68
Figure 4.2: Velocity vector distribution of a laminar flow pattern in a tube geometry.	71
Figure 4.3: The schematic of the modified Chandler’s circuit design in A) stage 0, the circuit is open and the tubes were rinsed with PBS B) stage 1 the circuit is still open but the blood source is connected and C) stage 2 the circuit is closed and the tubes are completely filled with PRP.	73
Figure 4.4: The current dynamic hemocompatibility test set up in Dr. Muffly’s lab in the USF College of Medicine.	74
Figure 4.5: Design and fabrication of a new, more cost-effective sample holder. USF SiC Group 3D printed nylon cell (Left), solid-works schematic (center), the sample holder machined out of Teflon by the USF engineering machine shop (right).	75
Figure 4.6: Formulation of PRP for hemocompatibility testing. a) Schematic that shows the three phases of the blood after centrifuge b) The 50 mL ACCUSPIN centrifuge tube including the separated PRP and Erythrocytes phases.	76
Figure 4.7: Static hemocompatibility test fluorescence micrographs using Rothamin as a fluorescence tag at 50 x of magnification. a) 3C-SiC b) <i>a</i> -SiC, c) SiO ₂ and d) Si (100). Scale bar is equal to 100 μm.	78
Figure 4.8: Static hemocompatibility histogram of platelet activation of the Si, <i>a</i> -SiC, SiO ₂ and 3C-SiC in static hemocompatibility test using standard deviation as the error bar.	79

Figure 4.9: Static hemocompatibility test fluorescence micrographs using Rothamin as a fluorescence tag at 50 x of magnification. a) 3C-SiC b) *a*-SiC, c) SiO₂ and d) Si (100). 80

Figure 4.10: Dynamic hemocompatibility histogram of platelet activation of the Si, *a*-SiC, SiO₂ and 3C-SiC using standard deviation as the error bar. 81

Figure A.1: Copyright permission to reuse the figures from Cambridge University Press, for figure 2.15 and 2.16. 108

Figure A.2: Copyright permission to reuse the figures from © to-BBB, for figure 4.1. 109

Figure A. 3: Copyright permission to reuse the figures from Elsevier, for figure 5.1. 110

Figure A. 4: Copyright permission to reuse the figures from institute of physics publishing, for figure 5.2 and figure 5.3. 111

ABSTRACT

Biomedical devices that function in-vivo offer a tremendous promise to improve the quality of life for many who suffer from disease and trauma. The most important consideration for these devices is that they interact with the physiological environment as designed without initiating a deleterious inflammatory response. ISO 10993 outlines the current international guideline for investigating the biocompatibility of such devices. Numerous groups report the use of ISO 10993 as the basis for their experimental evaluation of candidate materials for neuroprosthetics, as well as other biomedical devices, however most of these reports fail to completely comply with the standard. This leads to a lack of consistent results between R&D groups, which hinders progress in the implantable biomedical device field. For the first time, and to the best of our knowledge, we present a methodology that is in strict adherence to the methodologies presented in ISO 10993, namely direct contact and extract testing. In addition we show that the MTT assay, which has been used in multiple reports, suffers from a major flaw that can create false results especially for conductive materials. We also report on our application of ISO 10993-12 with respect to control materials and preparation methods. These materials are gold and polyethylene as negative reaction controls, and copper and polyvinyl chloride organotin (PVC-org. Sn) as positive reaction controls. The results of our tests are consistent to what has been previously reported, albeit in separate reports. We used silicon carbide, which is a very promising candidate material for neuroprosthetics, as our test materials. Not only have we confirmed the outstanding in-vitro response of 3C-SiC and amorphous SiC, we do this in strict

compliance to ISO 10993 thus showing that it is indeed possible to quantitatively assess the performance of materials in a statistically significant and highly repeatable fashion.

CHAPTER 1:INTRODUCTION

1.1. Need for *in vivo* Biomaterials

As a result of the evolution in health science the living condition for human beings has become longer and of higher quality. The discovery of new medicines, the invention of biomedical devices, the widespread use of prosthetic implants as well as new cures and treatment methods are examples of this progress. Many diseases and traumas that were not curable in the past can now easily can be treated with a prescription or prosthetic devices. The biomaterials described by Williams ,1987, and the materials that have been used for medical applications that are in close and persistent contact with the human body are in many cases implanted within tissue [1]. This raises the important point that biomedical devices, and the materials that they are made of, must be highly compatible with the human body for the lifetime of the treatment which, for highly complex prosthetics, is equivalent to the lifetime of the patient.

Biomedical devices offer a wide range of solutions to improve the life of humans who suffer from disease and trauma. This is a broad range of treatments, from diabetes management to dental/bone implants and, more recently, robotic prosthetics that enable the restoration of functionality after the loss of a limb or severe brain trauma. All of these devices share one thing in common – they must function inside the human body, i.e., *in vivo*, for long periods of time. Therefore implant and prosthetic device materials must possess certain critical characteristics, such as mechanical strength, surface hardness; wear resistance, chemical stability, corrosion

resistance, biocompatibility, and hemocompatibility. This doctoral dissertation research focused on developing a comprehensive strategy to evaluate materials for *in vivo* applications and was centered around the use of the international standard organization (ISO) standard for biomedical materials and devices, ISO 10993.

1.2. ISO 10993 Introduction

The ISO 10993 standard was established to standardize methodologies for the biological evaluation of medical devices and biomaterials, by determining the corrosion behavior, cytotoxic reactions of cells within physiological environments *in-vitro*, and hemocompatibility of the implant devices and materials.

ISO 10993 provides the minimum requirements for the testing of a new material and/or device that may be used in contact with the human body. The manufacturers must follow this guideline while they are developing their product if they are to be granted permission for clinical trials in humans. The Food and Drug Administration (FDA) in the USA requires the results of biocompatibility tests of these products before approval for device marketing, for example. Therefore following the protocols of ISO 10993 is mandatory by the FDA and it is mentioned in a blue book memorandum in 1995: #G95-1, entitled “Use of International Standard ISO 10993, Biological Evaluation of Medical Devices ” [2].

ISO 10993-5 provides a very reliable protocol to initially test novel biomaterials and biomedical devices *in vitro* by testing the toxicity of the implants. The latest edition of ISO 10993, published in 2009, consists of 20 sections. In this research we studied the methods that focused on material corrosion resistance (10993-14), biocompatibility (10993-5) and hemocompatibility (10993-4).

Sample preparation, test conditions, selection of controls, volume to surface area ratio and conditions of the equipment are described in section 12 of the ISO (i.e., ISO 10993-12), so this section was studied first. Strict adherence to the protocols in this section was the first priority since most of deviations from the ISO protocols happens when the researchers do not consider the details in this part of the ISO standard [3].

After material preparation, testing the chemical stability candidate materials in a physiological environment is the first step. The degradation of materials implanted in the body is important from several aspects; any released ions or particles from the device/implant can be toxic or at least can cause an abnormality in the concentration of chemicals within the human body. In addition any deterioration in the biomaterial can result in performance failure of the prosthetic device, in this case a second surgery would be inevitable. Section 14 and 15 of ISO 10993 provide the protocols which are useful in studying the degradation of materials [4, 5].

The major concern when a material is implanted or is in contact with the human body is if the material is non-toxic. Section 5 of ISO 10993 recommends several assays to study the *in vitro* cytotoxicity behavior of the materials. Direct contact of the cells with the actual device, preparing the extract from the materials under test and testing the extract liquid on the cells as well as testing cell viability using MTT [3-(4,5-dimethylthiazol-2-yl)-2,5-diphenyltetrazolium bromide] assays are the methods that are suggested in the ISO 10993-5 [6].

When a prosthetic device is implanted in the body physical scaring of the surrounding tissue and interaction with local blood vessels is inevitable. Thus, while a material can be non-toxic and chemically stable, it can still cause blood clotting or a severe hemorrhage because of their interaction with blood. The guideline for evaluation of the hemocompatibility of the biomaterials and devices is provided in ISO 10993-4 [7].

The standard, which was compiled from previous cytotoxicity studies, does fall short in completeness in that it targets only particulates and chemical compounds that have leached away from the material into the cell media. In this work, we present a new method, which was developed to test not only the compounds that leach out from novel biomaterials, but also test the cellular reactivity in proximity to the material under evaluation [6].

1.3. Biocompatibility of the Materials

The concept of biocompatibility is a vast topic which has been studied for a long time. Unfortunately the definition of biocompatibility means different things to different researchers typically. The capability of a biomaterial to implement its preferred function according to the medical treatment chosen, with highest efficiency in contact with the body tissue, and the absence of any unwanted local or systemic side effects, is described in the literature [8-11]. Almost all medical devices are made from various biomaterials so investigating the biocompatibility of all of the materials that were used in the prosthetic device that are in contact with tissue, or have a high risk of contact with tissue, is required. Numerous researchers continue to try to figure out the interaction of these biomaterials with the human body and how these interactions affect the performance of the implanted device [9, 10].

The human body has a complex immune system and a complex tissue regeneration mechanism. Therefore studying the biocompatibility of a material on one type of cell line or tissue is not sufficient. To figure out if a material is biocompatible, or not, the standard institutes such as ISO and ASTM established a battery of *in vitro* test standards. ISO 10993-5 is a good example of such a protocol. Although the *in vitro* tests cannot individually verify the biocompatibility of a material or device, they provide valuable data for the next steps which are ideally *in vivo* tests followed by human clinical trial. Having a reliable set of *in vitro*

biocompatibility data can result in the reduction of animal use and also help set the stage for human trials [11].

Cubic silicon carbide, more commonly written as 3C-SiC, was recognized as an alternative biomaterial for the first time by Colletti *et al.* of the USF SiC Group in 2007 [12, 13]. These results demonstrated that 3C-SiC has an advantage in biocompatibility over Si in terms of cell attachment and viability. They studied the biocompatibility of silicon and several polytypes of silicon carbide using MTT assays and fluorescent microscopy [12, 13]. Frewin *et al.* in 2009, of the same group, studied the neural / 3C-SiC interface using the same methods as well as atomic force microscopy (AFM). They suggested the application of 3C-SiC as an invasive neural implant due to its outstanding characteristics including excellent neuronal cell attachment, the absence of 3C-SiC surface degradation and excellent lamellipodia permissiveness [14, 15]. In our studies a new modified biocompatibility method is used to evaluate the biocompatibility of 3C-SiC, silicon and *a*-SiC. The results will be compared to the conventional methods of biocompatibility evaluation in chapter 3.

1.4. Hemocompatibility of the Materials

ISO 10993-4 provides test methods to evaluate blood/material interaction. Blood cell adhesion is a measure of the blood-compatibility of a material when considered in conjunction with distal embolization. Also platelet count and platelet aggregation are important for evaluating the hemocompatibility of materials [7, 16]. ISO 10993-4 suggested a static state for hemocompatibility tests, which clearly is not close to the real condition. Testing the materials in a dynamic state is a complementary test that can be done on implants that are to be used in contact with blood, which is particularly true for neural implants due to the vasculature of the human brain.

In previous studies the blood compatibility of silicon-based semiconductors and *a*-SiC was investigated [17, 18]. The results showed an outstanding blood compatibility behavior of *a*-SiC, which made it a favorable candidate for the coating of cardiovascular implants [19, 20]. Nurdin *et al.* in 2003 studied the hemocompatibility of SiC in comparison to DLC coatings [21] and Schettini *et al.* in 2009 showed the preliminary hemocompatibility of 3C-SiC based on platelet activation studies under static conditions [22]. In this dissertation evaluation of the hemocompatibility of silicon and 3C-SiC semiconductors will be evaluated in a dynamic state to support these static state tests (Chapter 4).

1.5. Chemical Simulation of the Body Environment *in vitro*

ISO 10993-14 provides methodology guidelines for the identification and quantification of degradation products from ceramics in a simulated physiological solution and also in an extreme solution [4]. The first step in the biocompatibility assessment of a material is to evaluate the chemical stability and corrosion resistance of the materials. Based on ISO 10993-14 this test consists of two parts. The first part is to test the material in a simulated solution with a pH of 7.4 ± 0.2 which is similar to human biological pH. The second part is immersion in an extreme solution of $\text{pH } 3.0 \pm 0.2$, which simulates the pH of the human body under extreme acidic conditions. Testing of the implant materials in neutral pH and extreme acidic states are necessary but not necessarily sufficient. For neural implants, which are used in the cerebral region, the pH tolerance must be around 5.9 ± 0.2 in the presence of nitrous ions. Silicon based materials, which are very common in neurological implants, are extremely sensitive to nitrous ions [23]. Therefore to test the corrosion resistance of neurological implants a complimentary test must be performed in addition to ISO-10993-14 to evaluate the corrosion resistance in the presence of

nitrous ions. When the material or device has passed the corrosion test it will then be eligible for cytotoxicity assays [4, 5].

The degradation of neurological implant materials in buffer solutions at various temperatures for several time frames was studied in the past; the effect of temperature on material degradation of polymeric biomaterials in such accelerated aging experiments was the most significant parameter and it was found to follow the time dependence of $2^{\Delta T/10}$ where ΔT is the elevated temperature above 37°C [24, 25]. In this work we seek to develop a similar relation for silicon-based semiconductor materials and, in particular, silicon carbide (SiC).

In Sella *et al* in 1993, the corrosion properties of amorphous silicon carbide (*a*-SiC) coatings was measured using potentiodynamic polarization tests in biological media, and no reaction was observed in comparison to the non-coated surface. The corrosion current was almost zero even at high potentials [26]. In our experiments we determined the corrosion resistivity of *a*-SiC in acidic and neutral solutions using the immersion method while comparing the results to control materials, which are silicon (positive control) and cubic silicon carbide (negative control). The results will be presented in chapter 2.

1.6. Cell Biology

1.6.1. Fibroblast Cell Line (L 929 Cell Line)

There are four major types of tissues in the human body and connective tissue is one of them. Collagen is the most common protein in the human body which forms a fibrous structure to realize connective tissue [27].

Ligaments and tendons consist mostly of dense connective tissues. Bones are connected to each other at the joints by ligaments, which have a rope-shaped structure. On the other hand

skeletal muscles and joints are connected to each other by tendons. In addition to these examples of connective tissue is the dermis which consists of dense connective tissue formed completely from collagen. Fibroblasts are spread among the collagen fibers in a dense connective tissue matrix and form a subunit of collagen that is called tropocollagen - they build the larger collagenous structures. Glycoproteins and polysaccharides are created by fibroblasts to form a substrate. The collagen fibers of dense connective tissue are encapsulated by this gel-like material that was produced by the fibroblasts, and formed an "extracellular matrix", which facilitates the integrity of the ligaments and tendons. All of this defines the mechanical properties of the connective tissue. In addition, due to the repair properties of fibroblasts, any tissue damage stimulates fibroblast creation [28, 29]. Therefore fibroblasts are a nearly ideal cell line with which to test the biocompatibility of new biomaterials.

Fibroblast cells vary based on their activity, size and shape. The term Fibroblast describes the activated form of these cells that are metabolically active cells, thus they have the suffix of blast in their name. For example fibrocytes cells are not active. But most of the time the term fibroblast is used to name both fibroblasts and fibrocytes. The fibroblast cells are larger in comparison to fibrocytes and also have a rough endoplasmic reticulum [30]. The mouse fibroblast cell line clone 929 of strain L, which were derived from a C3H male mouse, is the most commonly used cell line in this family of cells for cytotoxicity assays [30, 31] and is also specifically called out in ISO 10993.

1.6.2. Neuroglioma Cells (H4 Cell Line)

Neurons and neuroglial cells form the central nervous system (CNS) and they have equal share to form the CNS structure. Maintaining the homeostasis, providing support, protecting the neurons and forming myelin is the major role of neuroglia cells, which are non-neural cells of the

CNS. The glia cells also are mentioned as nervous system' "supporting cells" in the literature. The neuroglia cells have four major tasks; the structural task of these cells is to embrace the neurons and keep them in proper position; the insulation role of these cells is to surround the neurons and insulate them from each other. They also act as defending cells whereby they destroy pathogens and remove dead neurons; the last role of these cells is to provide nutrients and oxygen to the neurons [32-34].

The H4 cells are neuroglioma tumor cells from human brain neuroglia tissue. Since the neuroglial cells are the scaffold of the neurons this cell line can be used for the goals of assessing cell permissiveness on neurological implants. The adhesion of the glial cells to the surface has been used as a primary step of biomaterials testing in previous research due to its convenient comparison to actual neural cells [35-37].

1.6.3. Primary Neurons

The basic physiological performance of the neurons normally is studied by using primary neuronal cultures and neuronal cell lines extracted from rodents. In addition, they are also used to study the neuron / biomaterial interaction and effect of chemicals on neurons. The effect of released chemicals on the viability of the neurons is called neurotoxicity and is a valuable experiment that can be used in the design of neuroprosthetic implants. The protocol for culturing neurons for short-term experiments is not as difficult as the long-term culture of pure neurons. In this study 96 hours of cell culture was considered as the seeding duration [38, 39].

1.7. Statistical Theories

To have comparable results statistical analysis must be done on the data obtained from the tests. Analysis of variance (ANOVA) is a method that can be used to compare the statistical

data, such as mean and variance of several groups, to provide a statistical model for the process. By using the ANOVA method, the obtained variance in a specific variable is divided into components attributable to different sources of variation. In a simple word, ANOVA provides a statistical test so that the results of various experiments can be comparable and one can figure out if the means in several experimental groups is equal or not, and expands the t-test to more than two groups [40].

Any statistical analysis which verifies the t-distribution for the data is called t-test. The null hypothesis can be evaluated by t-test. So if the null hypothesis is correct the data has the t-distribution. In our experiment the paired t-test was used to verify the statistical significance or two groups of data, this paired test was done on all the samples, having a normal distribution in data values was the only assumption that we made [40].

1.8. Summary

The goal of this doctoral research was two-fold; first to develop a complete set of experiments that can determine all the characteristics required for the successful use of invasive neurological implants in strict adherence to ISO 10993; second, to find an alternative material for neurological implants since conventional materials have yet to show long-time durability of more than 4 years *in vivo*.

To peruse the first goal, a battery of complementary tests were conducted including the evaluation of the corrosion behavior of materials in the presence of nitrous ions, cytotoxicity evaluation of the materials considering leached ions from the materials, and the behavior of the cell/ material surface after the direct implantation of cells. This will be complimented by the

evaluation of the hemocompatibility of the materials in a dynamic flow system using the platelet activation method [41, 42].

Previous studies of 3C-SiC and *a*-SiC indicated outstanding corrosion resistance, biocompatibility and static hemocompatibility performance. The reliability of 3C-SiC, *a*-SiC or any component including these two materials as a biomaterial device were evaluated by performing further investigations and complementary tests have been suggested. This is a comprehensive materials evaluation that has not been demonstrated to date and represents a significant contribution to the field of biomaterials evaluation and development.

CHAPTER 2: CORROSION AND MATERIALS DEGRADATION

In Chapter 1 the goals of this research project were presented, which involved a coordinated battery of material stability testing followed by biological testing *in vitro*. ISO 10993 was introduced as the relevant standard that must be followed in order to see a biomedical device reach human clinical trial. In this chapter we will discuss how to faithfully follow the standard to determine the material stability requirement. To achieve the goals of this project three types of experiments have been designed. The first was to evaluate the corrosion resistance and material degradation of the materials by performing soak tests (Chapter 2), while the second was to evaluate the cytotoxicity of materials (Chapter 3) and the last involves testing the hemocompatibility of these materials under dynamic flow conditions (Chapter 4).

Corrosion tests in simulated and extreme solution were performed on both experimental controls and Si (100), 3C-SiC, α -SiC (four variant formulations), SiO₂, W and parylene C samples. For the controls gold (Au) and polyethylene (PE) served as the negative controls, while copper (Cu) and organo tin-doped polyvinyl chloride (PVC org.-Sn) served as positive controls; characterization and data analysis has been performed and is presented. The material surface changes were characterized using the scanning electron microscope (SEM), Atomic Force Microscope (AFM) and Optical Profilometer (OP) before and after soaking the samples.

2.1. Sample Preparation

Silicon substrates in the (100) orientation, 100 mm diameter, 500 μ m thick, were cleaned using the RCA cleaning method that consists of two steps [43]. In standard clean 1 (SC1) the

wafers were immersed in a 1:1:5 solution of NH_4OH (ammonium hydroxide, 27%): H_2O_2 (hydrogen peroxide, 30%): H_2O at 80°C for 10 minutes to remove any organic contamination. SC1 treatment normally results in the formation of a thin layer of oxide on the surface of the wafers. In standard clean 2 (SC2) the wafers were immersed in 1:1:6 $\text{HCl}:\text{H}_2\text{O}_2:\text{H}_2\text{O}$ at 80°C for 10 minutes to remove any trace metallic contamination, then the wafers were dipped in 5% HF acid at 25°C for 1 minute to remove the formed oxide layer. The wafers were then rinsed with DI water for 5 minutes after RCA cleaning and dried with nitrogen gas [43].

When the wafer was dried completely the desired materials were deposited on it. Metallic materials were deposited on the wafers using an electron beam physical vapor deposition (e-beam PVD) in the University of South Florida – Nanotechnology Research & Education Center (USF-NREC). The *a*-SiC film was deposited by J. register of the USF SiC Group using plasma enhanced chemical vapor deposition (PECVD) located in the USF-NREC facility (Plasmatherm 700 PECVD tool). The 3C-SiC film was grown by M. Reyes of the USF SiC Group on the Si substrate using a hot-wall chemical vapor deposition (CVD) reactor in ENB111 at USF.

After depositing the proper thin film on the silicon substrate, the 4” wafers were cut into coupons, 8×10 mm in size, using a diamond-blade dicing saw. 68 coupons of this dimension can be obtained from each 4” wafer.

The coupons were removed from the dicing saw frame and cleaned as follows: Each coupon was placed in a test tube and 5 mL of acetone (99% volume) was added. The tubes were then sonicated for 10 minutes at 25°C to remove any oily contamination and debris from the dicing process. The acetone was removed from the tubes and replaced by 5 mL of isopropanol alcohol (IPA, 96% volume) then the samples were sonicated for 10 minutes at 25°C to remove any acetone residue. The IPA was removed from the tubes and replaced by DI water and

sonicated for 10 minutes at 25°C. The samples were then retrieved from the tubes and dried using pure nitrogen gas (99% N₂) then stored in clean waffle packs in a sealed environment until they are used in the various corrosion experiments as outlined above.

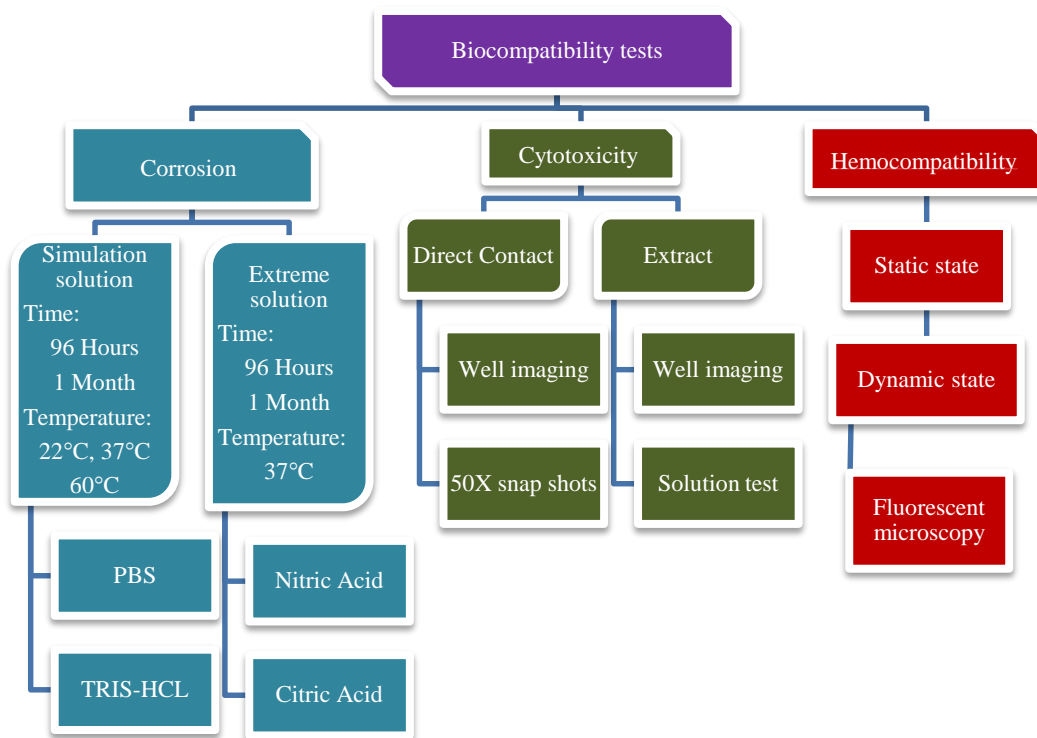


Figure 2.1: Flowchart showing the sample preparation steps and sample distribution for the material stability (Blue - Chapter 2), biocompatibility (Green -Chapter 3) and hemocompatibility (Red – Chapter 4) tests based on ISO 10993.

For the material stability study tests, such as the immersion tests (material degradation tests), the samples can be used right after solvent cleaning. But to use a sample in a biological environment to test the biocompatibility the samples must be sterilized (Chapter 3). The ceramic materials were sterilized using an autoclave at 120°C for 1 hour. The metallic and semiconductor samples were sterilized using a dry sterilizer under vacuum at 100°C. The polymer samples were sterilized using Ethylene Oxide (EtOx) at George Mason University (GMU) and shipped in sterile bags to USF for subsequent processing. The consumption of the raw materials was based on the following numbers, 9 coupons for extract tests, 10 coupons for cytotoxicity assays, 10

coupons for hemocompatibility tests, 12 coupons for degradation in simulated solution, 12 coupons for corrosion testing in extreme solutions and 10 coupons for nitric acid simulated aging testing. A total of 63 samples of each raw material are required for a complete set of experiments. Figure 2.1 shows the steps involved in sample preparation and the sample dispersal for each test.

2.2. Scientific Controls

By using a scientific control the effect of unwanted experimental variables, other than the desired one(s), can be reduced and hopefully eliminated. Therefore experiments have more reliable results when control experiments are performed [3]. Control experiments must be selected based on the primary hypothesis of the experimental method being used. For example, during corrosion testing an inert material does not have any chemical reaction with the test environment so it is an ideal negative control because of the absence of any corrosion reaction phenomenon.

Ideally, all variables in an experiment are controlled. The goal an experiment is to verify that the obtained results are because of the tested variable, so by testing on the controls and getting the expected results the correct performance of the test can be determined. The researchers are able to make a logical decision by selecting the proper scientific controls and verify the correctness of obtained data. Therefore proper selection of experimental controls is imperative and was the first task undertaken in this work.

2.2.1. Negative Control Selection

By selection of the “negative controls” the researchers verify that no reaction or effect happens on the negative control samples while doing the experiments. They are

designed/selected to ensure that there is no experimental effect when there should be no effect. To continue with the example of corrosion testing, a negative control is a material that will not react with the corrosive environment being studied. We would say that the negative control group should show a negative, or null, response during the time of the experimental study.

- Au as a negative control for corrosion and biological tests

In ISO 10993-12 polyethylene was suggested as a negative control, since this material is an insulator the necessity of having a conductor negative control is crucial. In the literature gold (Au) is the recommended conductive negative control material. Au shows good biocompatibility and is almost inert in the body. In addition it is not reactive in a corrosive environment and serves as a suitable negative control for corrosion studies as well. Pt is also a reliable biocompatible – corrosion resistant material and was also used during this work as a negative control during biological testing (Chapter 3).

The e-beam PVD equipment housed in the USF-NREC was used to deposit the metallic control thin films on 4" (100) Si wafers. A 99.99 % gold bar (Swissgold) was cut into small pieces and placed in a ceramic crucible. In order to ensure proper Au adhesion to the Si surface, Ti was used as an adhesion layer (which is also a bio-rated material). Ti pellets (99.99% Sigma Aldrich) were placed in another ceramic crucible. The Ti was melted and evaporated in vacuum using a high current electron beam (typically 100 mA). The Ti film was deposited at the rate of 10 Å/sec and the deposited film thickness was ~200 Å. Then the Au crucible was exposed to the electron beam. The molten Au is very sensitive to beam current fluctuations and if the current increases abruptly it will result in molten Au particles being ejected from the crucible, which results in film pinhole formation. The optimum deposition rate was 5 Å/sec and the deposited film thickness was ~1500 Å.

- PE as an insulator negative control for biological tests

Based on ISO 10993 polyethylene (PE) is the recommended insulator negative control material. PE shows good biocompatibility and is almost inert in the body.

PE tape (3M Transpore™ Surgical Tape) was used as the source of PE material. The samples were cut into 8×10 mm pieces under a clean hood using a surgical blade. The samples were then disinfected using a 70% ethanol solution and rinsed with DI water.

- PBS as solution negative control

Phosphate buffered saline (PBS), at the concentration of 10 mM (i.e., 1X PBS solution), is a buffer solution commonly used in biological research. It is a water-based salt solution containing sodium phosphate and, in some formulations, potassium chloride and potassium phosphate.

Table 2.1: The DI water grade requirements based on ISO-3696 [44].

Parameter	Grade 2
pH value at 25 °C inclusive range	Not applicable
Electrical conductivity mS/m at 25 °C, max.	0.1
Oxygen (O) content mg/l, max.	0.08
Residue after evaporation on heating at 110 °C mg/kg, max.	1
Silica (SiO ₂) content mg/l, max.	0.02
Absorbance at 254 nm and 1 cm optical path length, absorbance units, max.	0.01

PBS has many uses because it is isotonic and non-toxic to cells. These uses include substance dilution and cell container rinsing. PBS with Ethylenediaminetetraacetic acid (EDTA) is also used to disengage attached and clumped cells from sample surfaces.

The 1X PBS solution was prepared by dissolving 5 tablets of PBS (Invitrogen technologies) in grade 2 Deionized Water (based on ISO-10993). The pH was adjusted to

7.4±0.1 by NaOH (sodium hydroxide) – HCL (hydrochloric acid) titration. Table 2.1 shows the requirements of grade 2 DI water based on ISO-3696.

2.2.2. Positive Control Selection

The scientists use the “positive controls” to verify that the experiment has affected the sample and if that effect is what they expect. The positive controls confirm that the experiment has the result that supposed to have, by implementation of results of previous studies or scientific facts.

The experiment must be done again if the positive control did not behaved as expected, there may be a flaw with the test. Also the positive controls were used as factors that can be compared with other experiments done in the past if the investigating phenomena is complicated to evaluate.

- Cu as positive control for corrosion and biological tests

Based on ISO 10993 copper (Cu) is the recommended conductive positive control material. Cu shows no biocompatibility and is totally toxic to cells. In addition it is reactive in a corrosive environment and therefore serves as a suitable positive control for corrosion studies.

The e-beam evaporator housed in the USF-NREC was used to deposit Cu metallic thin films on the 4” (100) Si wafers. Cu pellets (99.99 % pure, Sigma Aldrich) were cut into small pieces and placed in a ceramic crucible. Ti pellets (99.99 % pure, Sigma Aldrich) were placed in another ceramic crucible (again, Ti being used as an adhesion layer). The Ti was melted and evaporated in vacuum using a high current electron beam. The Ti film was deposited at the rate of 10 Å/sec and the thickness was ~200 Å. Then the Cu crucible was exposed to the electron beam. The optimum deposition rate was 12 Å/sec and the film thickness was ~1500 Å.

- PVC as insulator material positive control for biological tests

Based on ISO 10993 organo tin-doped polyvinylchloride (PVC org.-Sn) is the recommended insulator positive control material. PVC org.-Sn shows no biocompatibility and is toxic to cells. In addition it is reactive in a corrosive environment and thus also serves as a suitable positive insulator control for corrosion studies.

Two PVC variants were used in this research. The first PVC org.-Sn used was found to be highly variable in its biological response. In order to have a better positive control F-4040-A PVC tube provided by Tygon (aka fuel and lubricant tubing, Yellow) was used as the source of the PVC positive insulator control material. The exact toxic dopant used in this material is a trade secret but we found this material to be a reliable positive control (Chapter 3). The samples were sterilized with ethylene oxide (EtOx) at George Mason University (GMU) and shipped in sterile bags to USF. The samples were cut in 2 mm pieces under a clean hood using a surgical blade. Based on calculations a 2 mm length of the tubing has the equivalent surface area of an 8×10 mm planar sample coupon. This is an important consideration since the media to material surface ratio must be constant and equal to 3 mL/cm² as stated in Chapter 1 in order for the test to be in compliance with ISO 10993.

- Citric acid as a solution positive control

Citric acid buffer solution at a pH of 3.0±0.1 is the suggested solution for positive control in ISO-10993. Citric acid is a weak organic acid with the chemical formula C₆H₈O₇. It is a natural preservative and is also used to provide an acidic or sour taste to foods and drinks. In biochemistry, the conjugate base of citric acid, citrate, is important as an intermediate in the citric acid cycle, which occurs in the metabolism of all aerobic organisms.

Citric acid is a commodity chemical, and more than a million tons are produced every year by fermentation. It is used mainly as an acidifier, as flavoring, and as a chelating agent.

Figure 2.2 shows the chemical structure of citric acid.

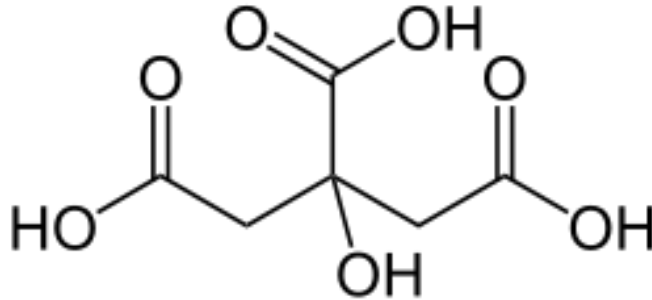


Figure 2.2: The chemical structure of citric acid $C_6H_8O_7$.

A buffered citric acid solution was prepared with a pH of 3.0 ± 0.2 at a temperature of 37 ± 1 °C as follows: 21 g of citric acid monohydrate (99.9%, ACS reagent Sigma Aldrich) was dissolved in 500 mL of grade 2 DI water in a 1 l volumetric flask. 200 mL of 1 M sodium hydroxide solution was added to the flask, then the volume was adjusted to 1000 mL using grade 2 DI water. 40.4 mL of the dilute solution was mixed with 59.6 mL of 0.1 M hydrochloric acid to obtain the desired buffered citric acid solution [4].

2.3. Test Materials

2.3.1. (100) Silicon

Silicon wafers (University Wafer, Inc.) with the crystallographic orientation of (100) and thickness of 500 μm were used as test materials. Since this type of wafer is used as the substrate for the entire semiconductor and conductor materials in this work it can be considered as a baseline material.

2.3.2. Cubic Silicon Carbide (3C-SiC)

Thin films of cubic-silicon carbide (3C-SiC) on (100) silicon were grown in the MF2 chemical vapor deposition reactor at the University of South Florida [45]. The process involves using a horizontal hot-wall, low pressure reactor at the growth rate of $\sim 5 \mu\text{m/h}$ at 1350°C for the biocompatibility, corrosion and hemocompatibility tests. In addition these films were used for SiC nanowire experiments at the University of California at Berkley (Chap. 5). The SiC growth sample number were USF2-12-147, USF2-13-012, USF2-13-018 and USF2-13-092, which is stated for reference. Quantitative analysis was performed via atomic force microscopy (AFM) using a Park Systems XE-100 AFM in tapping mode (Si_3N_4 probes).

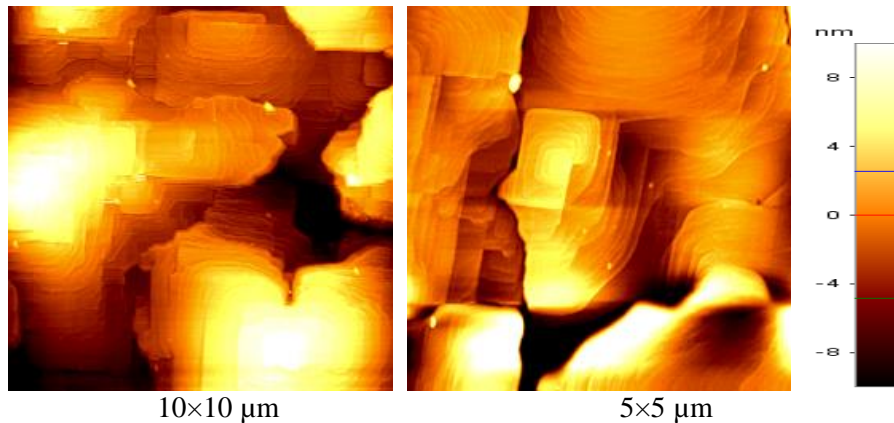


Figure 2.3: AFM micrographs of (left) 10×10 and (right) $5 \times 5 \mu\text{m}$ scans of 3C-SiC sample USF2-12-147. AFM measurement was in tapping mode with a 0.2 Hz scan rate. The micrographs are normalized to a Z height interval of (+10,-10) nm (see scale bar on the right). Note the surface displays atomic steps which is an indication of high-quality crystal growth.

The scan rate was 0.2 Hz for all of the AFM characterization reported here. A representative r_q value for the sample was $\sim 7.2 \pm 0.5$ nm RMS. Figure 2.3 shows 10×10 and $5 \times 5 \mu\text{m}$ AFM micrographs of the 3C-SiC samples, again for reference, as the sample morphology changes across the wafer but the reported RMS roughness value was ~ 7 nm across the wafer.

AFM data elaboration was performed using the XEI software (Park Systems). The 5x5 μm micrograph shown in Figure 2.3 was used for this data processing example. In these measurements the average value for the terrace width was about 41 nm and the step height was about 4.57 Å. Figure 2.4 shows this AFM data elaboration.

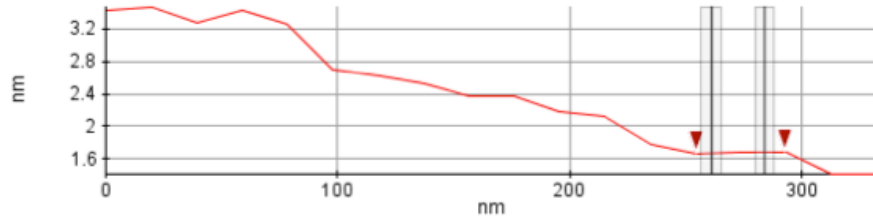


Figure 2.4: Line scan of the 5x5 μm AFM micrograph of Figure 2.3 of 3C-SiC sample USF2-12-147. The r_q value was 7.2 ± 0.5 nm RMS. From this line scan the terrace width is ~ 41 nm and the step height (not shown) about 4.5 nm

2.3.3. Silicon Carbide (*a*-SiC)

Four different variants of *a*-SiC were prepared by J. Register of the USF SiC Research Group using the USF-NREC Plasmatherm 700, plasma enhanced chemical vapor deposition (PE-CVD) tool [46]. The sequence of the deposited layers for type I was *a*-SiC on Si (100), for type II was *a*-SiC on SiO₂ on Si (100), for type III was *a*-SiC on 3C-SiC on Si (100) and for type IV was *a*-SiC on SiO₂ on 3C-SiC on Si (100). The *a*-SiC film was deposited on all substrates (Type I-IV) simultaneously in order to allow for direct comparison of the underlying material impact on the measured response. Since *a*-SiC is used as a coating on numerous materials, these four variants were selected in order to best understand the performance of the coating and influence of the underlying material. The cross-sectional view of each formulation and thickness of the deposited layers are described below.

- Type I (*a*-SiC/ Si)

A (100) silicon wafer (500 μm , University wafers) was cleaned using the RCA method [43]. The *a*-SiC thin film was deposited on a silicon wafer using plasma enhanced chemical vapor deposition (PECVD). The thickness of the *a*-SiC film was ~ 300 nm. Figure 2.5 shows the cross sectional view of the coating layers in type I *a*-SiC.

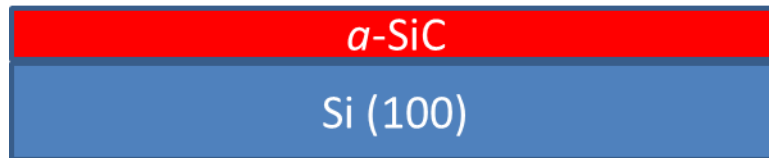


Figure 2.5: Cross-section showing the structure of type I *a*-SiC developed for testing in this research. The *a*-SiC was ~ 300 nm thick and deposited on 500 μm thick Si (100) substrate.

- Type II (*a*-SiC/ SiO₂/ Si)

The second type of *a*-SiC was deposited on a layer of PECVD-deposited 800 nm thick SiO₂ (deposited by R. Everly of the USF NREC using the Plasmatherm 700 PECVD tool) using PECVD. The SiO₂ layer was deposited on a (100) silicon wafer. The *a*-SiC thickness was ~ 300 nm. Figure 2.6 shows the cross sectional view of the coating layers in type II *a*-SiC.



Figure 2.6: Cross-section showing the structure of type II *a*-SiC developed for testing in this research. The *a*-SiC was ~ 300 nm thick, deposited on 800 nm thick SiO₂ and deposited on 500 μm thick Si (100) substrate.

- Type III (a -SiC/ 3C-SiC/ Si)

The third type of a -SiC was grown on a layer of 3C-SiC film using PECVD. The 3C-SiC was grown on a (100) silicon wafer using hot wall CVD by Dr. M. Reyes of the USF SiC Group [47]. The a -SiC thickness was ~ 300 nm. The 3C-SiC thickness was ~ 6.2 μm . Figure 2.7 shows the cross sectional view of the coating layers in type III a -SiC.



Figure 2.7: Cross-section showing the structure of type III a -SiC developed for testing in this research. The a -SiC was ~ 300 nm thick, deposited on ~ 6.2 μm 3C-SiC and grown on 500 μm thick Si (100) substrate.

- Type IV (a -SiC/ SiO₂/ 3C-SiC/ Si)

The fourth type of a -SiC was deposited on a layer SiO₂ film deposited using PECVD, which previous had been deposited on a layer of 3C-SiC. The 3C-SiC was grown on a (100) silicon wafer using hot wall CVD. The a -SiC thickness was ~ 300 nm.



Figure 2.8: Cross-section showing the structure of type IV a -SiC developed for testing in this research. The a -SiC was ~ 300 nm thick, deposited on 800 nm SiO₂, deposited on ~ 6.2 μm 3C-SiC and grown on 500 μm thick Si (100) substrate.

The thickness of oxide layer was 800 nm. The 3C-SiC thickness was measured to be ~6.2 μm . Figure 2.8 shows the cross sectional view of the coating layers in type IV *a*-SiC.

2.4. Corrosion Testing in Simulated Solution

The material coupons, 8×10 mm in size, were solvent cleaned and rinsed with DI water according to the protocol that was mentioned in the sample preparation section of this chapter. The goal of these experiments was to determine the degradation of materials in a simulated solution which has similar pH, temperature and chemical composition to the human body. The samples were placed in pyrex screw cap test tubes (sigma aldrich), 1.6 mL of filtered 10 mM PBS (phosphate buffer saline to have electrolyte to surface area ratio of 1 mL/cm²) was added and the cap was closed loosely to avoid any internal pressure increase inside the tubes. A 2 μm particulate filter used for PBS filtration. The pH of the solution was monitored 24/7 using a PC controlled SPER scientific pH meter. The pH was maintained at 7.4±0.1 and the tests performed at 37°C and 60°C for 4 days and 30 days, respectively. This was done to allow for accelerated aging effects to be studied during this work which is also in compliance with the ISO standard. The tests were repeated for 6 treatments of each material studied.

Artificial cerebrospinal fluid (ACSF) is another alternative for a simulated solution when the implant is used in a neurological environment. Another alternative is artificial plasma, which is useful for blood environment simulated testing. Cu was used as the positive and Au as the negative controls for conductive materials. For polymer materials PVC (tygon) was the positive control and PE was the negative control. Scanning electron microscopy (SEM) and optical microscopy (OM) were used for the qualitative evaluation of materials degradation. Atomic force microscopy (AFM) was used for nanometer-scale surface feature observation and optical profilometry (OP) was used for large-scale surface characterization.

2.4.1. Scanning Electron Microscopy

The Hitachi SU-70 and Hitachi S-800 scanning electron microscopes housed at the USF NREC facility were used to determine the surface morphology changes qualitatively. The SEM was used in field emission mode at 25 kV acceleration voltage using the secondary electron detection mode. The samples were imaged at a tilt angle of 45° at 100, 1000, 5000, 10000 and 50000X magnifications. The magnification and tilt angle were selected based on feature size and surface roughness values of the samples.

Figure 2.9 shows the SEM micrographs of the Au negative conductor control samples used in corrosion tests. When the SEM results of samples after soaking in 1X PBS at 37 and 60 °C for 24 hours, 96 hours and 30 days were compared to the SEM micrograph of the Au baseline surface, no surface degradation was observed. Having no reaction with the chemical environment confirms the role of Au as a negative control, as was expected.

Figure 2.10 shows the SEM micrographs of the Cu samples as the positive conductor control samples in the corrosion test. When the SEM result of samples after soaking in 1X PBS at 37 and 60 °C for 24 hours, 96 hours and 30 days were compared to the SEM micrograph of the Cu baseline surface, a significant surface degradation can be seen. By comparing the SEM micrographs of the Cu samples soaked for different time frames, it can be understood that Cu oxide crystals were grown in size after passing longer periods of time. Having a complete reaction with the chemical environment confirms the role of Cu as a positive control, again as was expected.

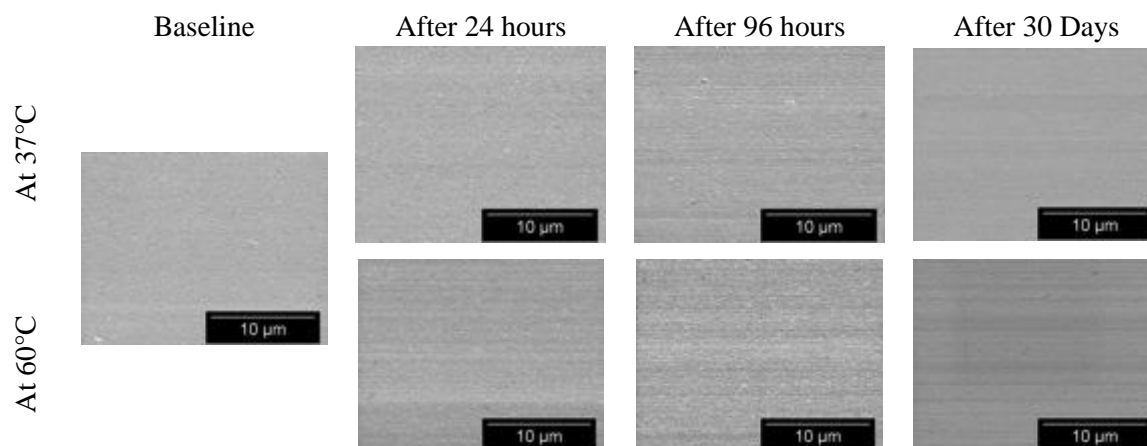


Figure 2.9: The SEM micrographs of Au samples at 60° tilt angle, 25 kV acceleration voltage and 5000X magnification after soaking in 1X PBS at 37 and 60°C. No change in surface morphology was observed confirming that Au is a suitable negative control material.

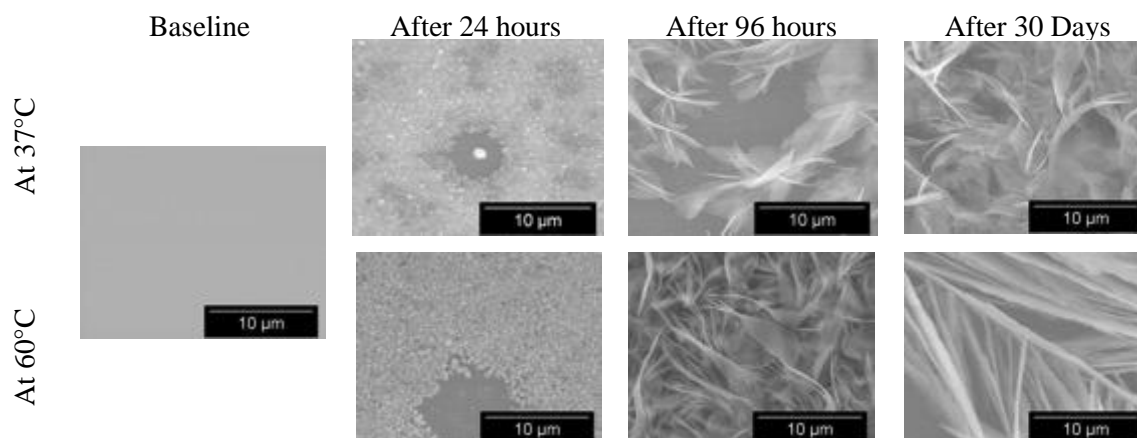


Figure 2.10: The SEM micrographs of Cu samples at 60° tilt angle, 25kv acceleration voltage and 5000X magnification after soaking in 1X PBS at 37 and 60°C. Significant changes in morphology observed confirming that Cu is a suitable positive control material.

Figure 2.11 shows the SEM micrographs of the PE samples used in the corrosion test. When the SEM result of samples after soaking in 1X PBS at 37 and 60 °C for 24 hours, 96 hours and 30 days were compared to the SEM micrograph of PE baseline, a slight surface degradation can be detected. By comparing the SEM micrographs of the PE samples soaked for 30 days to the rest of the samples, it can be understood that the PE samples could not tolerate the high temperatures for longer periods of time. Having a complete partial reaction with the chemical

environment rejects the PE sample as a negative insulator control for corrosion tests. Therefore a more suitable insulator negative control material is required to properly follow the ISO standard. Since parylene-C is a standard negative control for biological testing, this material was evaluated (see Fig. 2.13) and found to be a suitable negative control for corrosion testing as well, as described below.

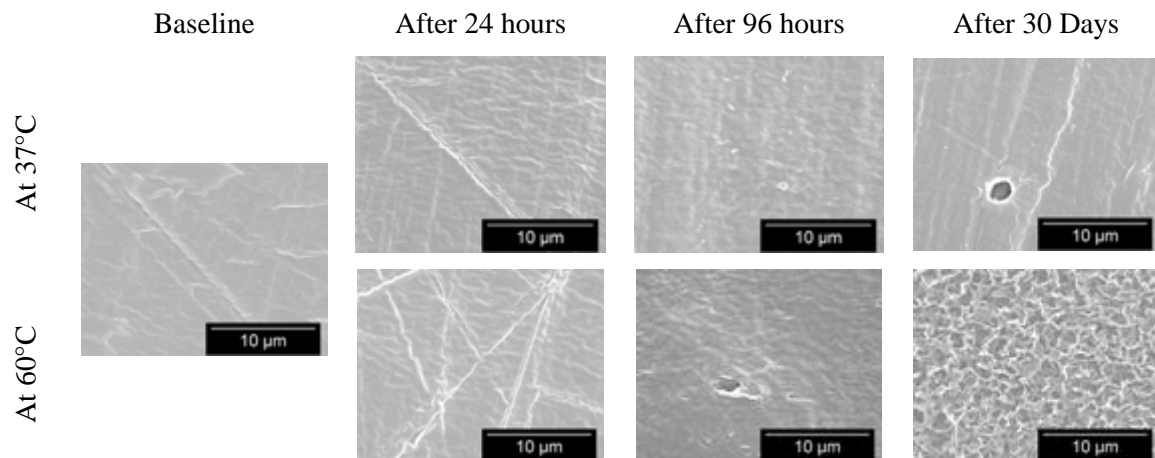


Figure 2.11: The SEM micrographs of PE samples at 60° tilt angle, 25kv acceleration voltage and 5000X magnification after soaking in 1X PBS at 37 and 60°C. Changes in surface morphology were observed which invalidate PE as a suitable negative control material.

Figure 2.12 shows the SEM micrographs of the PVC (Tygon) samples as the positive conductor control samples used in the corrosion test. When the SEM result of the samples after soaking in 1X PBS at 37 and 60 °C for 24 hours, 96 hours and 30 days were compared to the SEM micrograph of PVC baseline, a significant surface degradation can be seen. By comparing the SEM micrographs of the PVC samples soaked for different time frames, it can be understood that the surface degradation increased after passing longer periods of time at higher temperatures. Having a complete reaction with the chemical environment confirms the role of PVC as a positive control as it was expected.

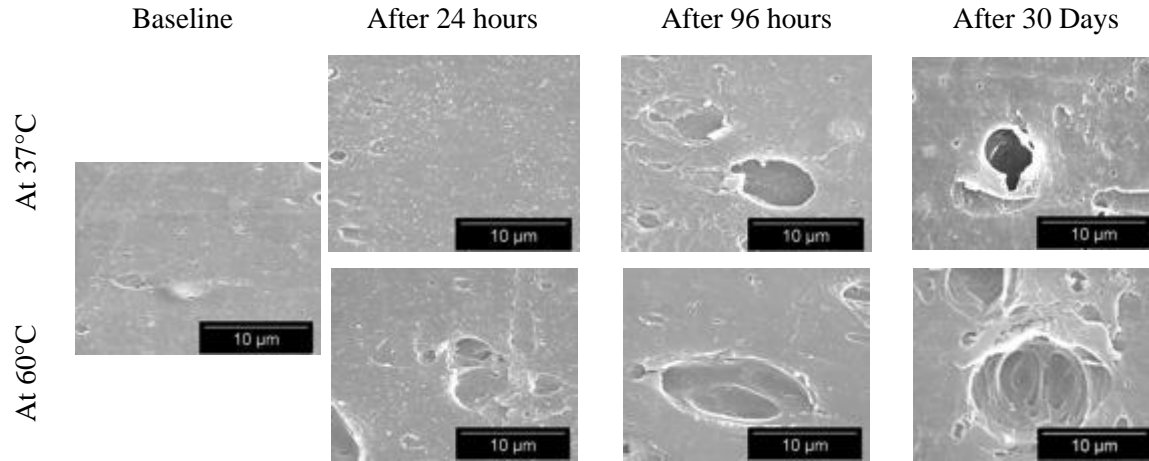


Figure 2.12: The SEM micrographs of PVC samples at 60° tilt angle, 25kv acceleration voltage and 5000X magnification after soaking in 1X PBS at 37 and 60°C. Significant changes in surface morphology were observed confirming that PVC (Tygon) is a suitable positive control material.

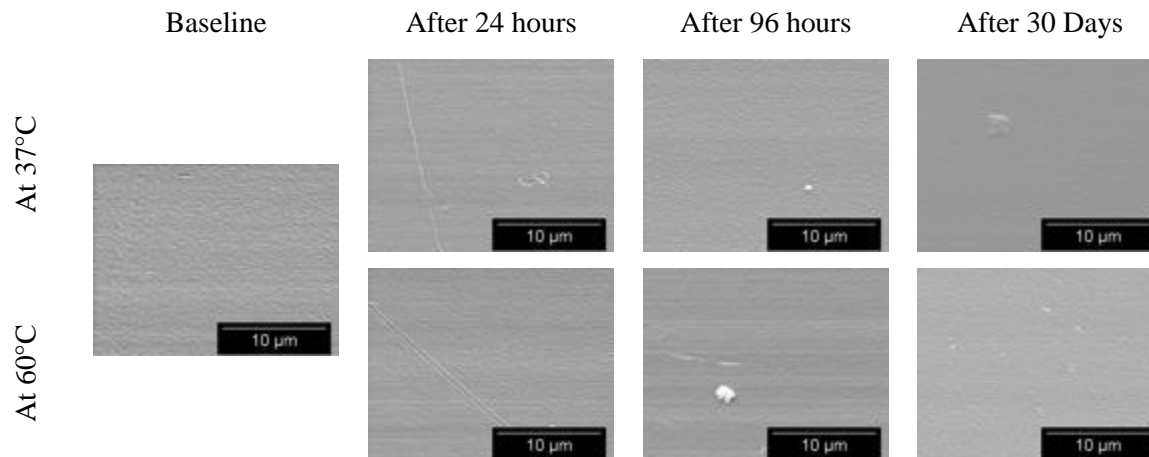


Figure 2.13: The SEM micrographs of parylene C samples at 60° tilt angle, 25kv acceleration voltage and 5000X magnification after soaking in 1X PBS at 37 and 60°C. No change in surface morphology was observed confirming that parylene-C is a suitable negative control material.

Figure 2.13 shows the SEM micrographs of parylene-C samples which were evaluated for use as a negative insulator control sample in the corrosion test since PE failed the test. When the SEM result of samples after soaking in 1X PBS at 37 and 60 °C for 24 hours, 96 hours and 30 days were compared to the SEM micrograph of parylene-C baseline, no surface degradation can be seen. Having no reaction with the chemical environment confirms the role of parylene-C as a negative control, as was expected.

2.4.2. Atomic Force Microscopy

The USF SiC Group atomic force microscope (XE-100 Park systems) was used to determine the surface roughness of the samples. The optimum performance range of the AFM with the current set up is ± 200 nm in surface topology (i.e., z variation). So this machine was only used for samples with a smooth surface morphology. A Wyko 100322 optical profiler (OP) was used to evaluate samples that displayed a higher surface roughness. AFM and OP are two methods that quantitatively characterize the surface roughness of planar samples. Surface roughness quantitative data, accompanied by SEM qualitative data, can give us a valuable interpretation from the material's degradation after soaking in various temperatures and for various time durations.

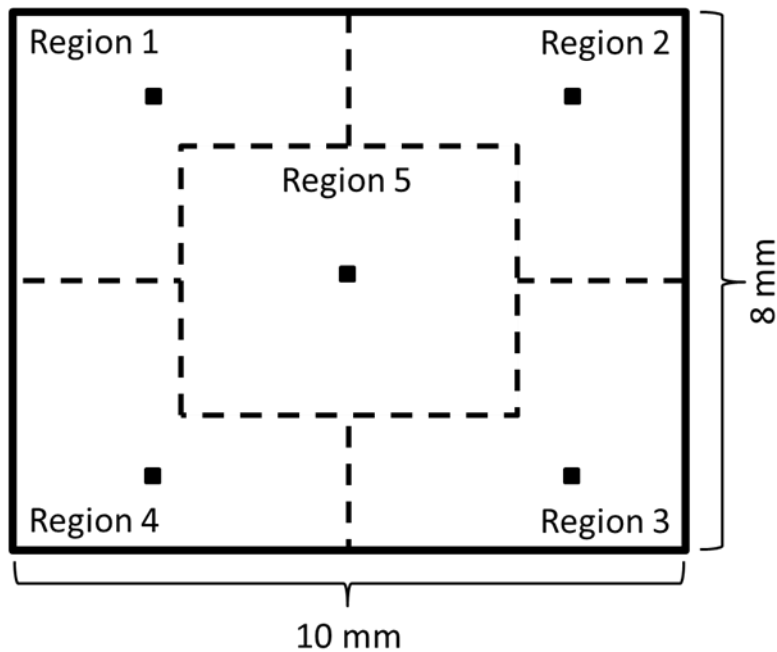


Figure 2.14: Sample map showing the position of the patches in 5 regions studied for each sample and their corresponding designation. Each patch has a rough dimension of 500 by 500 μm . The patches evaluated were randomly chosen in order to save time and data analysis. Each sample had a minimum of 3 patches of each sample evaluated and since 10 samples were tested for each experiment proper statistical methods were used to properly average the data.

The AFM was used in tapping mode using non-contact tips from Budget Sensors® and the samples scanned for 5×5, 10×10 and 45×45 μm scan sizes. Each sample was scanned in three randomly selected regions from 5 major regions. Figure 2.14 shows the location of the test regions on the test samples.

2.5. Material Stability Tests on Silicon

In a previous investigation by C. Frewin of the USF SiC Group [14], it was observed that Si had surface damage after cell culture, but the exact source of this damage was unknown [12, 14, 15]. Goodwin *et al.* in 1997 and Pocock *et al.* in 2001 indicated in their work that the cultured of hippocampal microglial cells could release nitric oxide [48, 49]. Wink *et al.* in 1998 provided evidence about the role of nitric oxide in the biochemistry of neurological systems [50, 51]. The release of nitric oxide in the extracellular fluid within the brain by inflammatory cells can result in the formation of nitrous and nitric ions which act as corrosive agents for silicon. ISO 10993 suggests a set of corrosion tests prior to any *in vivo* application of the implantable materials and devices [4, 5]. In this experiment, we devised a method, based off of the ISO standard, to identify the source of the surface modifications seen after cell culture on Si. The surface morphology of (100)Si was examined using samples cultured with H4 neuroglioma (from H4 ATCC ® HTB-148™) cells against samples soaked in Dulbecco's modified eagle medium (DMEM) and artificial cerebrospinal fluid (ACSF) [52].

A series of *in vitro* tests were designed to study the stability of silicon to cell media, cell media plus H4 cells, and artificial cerebrospinal fluid (ACSF). Si(100) coupons, 8 x 10 mm in size, were immersed in these solutions for 96 hours at 37°C.

Table 2.2: Cleaning methods description

Cleaning method	Step 1	Step 2	Step 3	Step 4	Step 5	Step 6
Solvent cleaning	Rinsing with DI water flow for 5 minute	Immersion in Acetone for 10 minutes in ultrasonic bath	Rinsing with DI water flow for 2 minutes	Immersion in iso-propanol for 10 minutes in ultrasonic bath	Rinsing with DI water flow for 2 minutes	Drying with N ₂
Piranha Cleaning	Solvent cleaned	Rinsing with DI water flow for 5 minutes	Immersion in Piranha solution for 10 minutes	Rinsing with DI water flow for 10 minutes	Drying with N ₂	
HF Cleaning	Piranha Cleaned	Rinsing with DI water flow for 5 minutes	Immersion in HF solution for 10 minutes	Rinsing with DI water flow for 10 minutes	Drying with N ₂	

After the immersion test the samples were cleaned individually under a flow of deionized water for 10 minutes to remove any residue from the biological solutions. Then the samples were kept in dry sample holders to await analysis.

Table 2.2 shows an overview of all three cleaning methods that were used in these experiments. This step was performed since the cleaning method itself could serve as the source of the observed surface degradation. Therefore it was important to understand the role, if any, of the cleaning method used on the observed surface morphology after *in vitro* testing.

The cleaning methods may be different from other references. In this set of experiments, as indicated in the table, the samples were solvent cleaned before piranha cleaning; also they have been piranha cleaned before HF cleaning.

2.5.1. Solvent Cleaning of Immersed Samples

The samples were rinsed with DI water flow for 5 minutes. Then the samples were individually sonicated in acetone for 10 minutes. To remove any residual solvents they were rinsed with DI water for 2 minutes after that. Then the samples were sonicated in isopropanol for 10 minutes. Quantitative analysis was performed using the AFM (Park systems XE-100) in tapping mode. Figure 2.25 (A-C) shows the AFM results of solvent cleaned samples for a scan area of 45 x 45 μm . 5 x 5 μm and 10 x 10 μm scans were also recorded to reveal more detailed surface features.

Table 2.21 shows the AFM data elaboration for all of the samples. The surface roughness and peak-to-valley values for all of the samples are recorded in Table 2.5.

The Hitachi S800 SEM at the USF NREC was used for qualitative surface analysis. Magnifications of 100X, 500X, 1000X and 5000X were used during this investigation. Figure 2.22 (A-C) shows the SEM micrographs of the samples after solvent cleaning at 1000X as a representation of all of the scans. Sample surface tilting angle of 45° was also used to reveal more features on the surface.

2.5.2. Piranha Cleaning of Immersed Samples

Piranha solution (1:2 H_2SO_4 : H_2O_2) was prepared in the ENB111 laboratory at USF. The temperature of the solution was approximately 80-85°C. The samples had been solvent cleaned and rinsed with DI water previously, then they were immersed in piranha for 10 minutes. After 3 samples were cleaned a new solution was prepared so as to have a consistent cleaning step for all samples studied. After piranha cleaning the samples were rinsed with DI water for 10 minutes. The samples were then dried and kept in cleaned sample holders.

Quantitative analysis was performed using the AFM Park Systems XE-100 AFM in tapping mode. Figure 2-21 (D-F) shows the AFM results of solvent cleaned samples for a scan area of $45 \times 45 \mu\text{m}$. $5 \times 5 \mu\text{m}$ and $10 \times 10 \mu\text{m}$ area scans were recorded to reveal more detailed features.

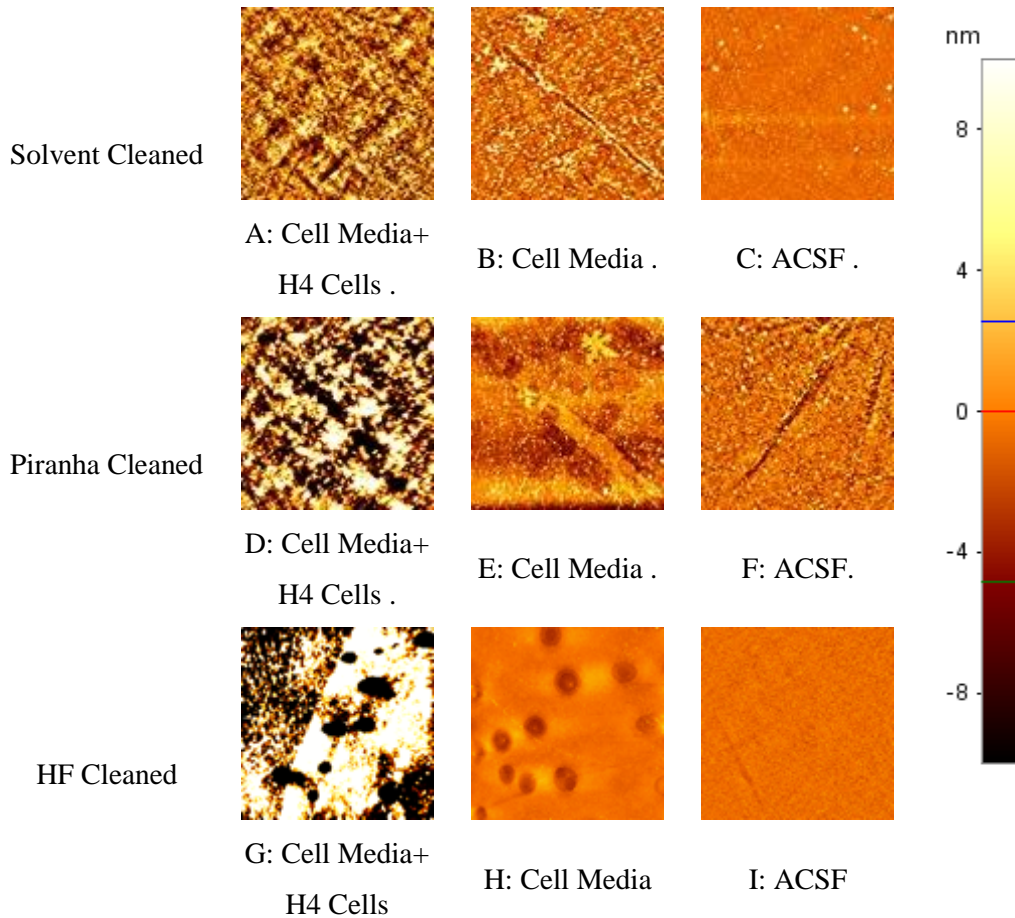


Figure 2.15: $45 \times 45 \mu\text{m}$ area AFM micrographs of silicon samples immersed in Cell Media+ H4 Cells (left column) , Cell Media (center column) and ACSF (right column) for 96 hours at 37°C . Cleaned with Solvents, solvents + Piranha and Solvents + Piranha + HF, respectively. The micrographs are normalized to a Z height interval of $+10, -10 \text{ nm}$, permission obtained from [52], presented in appendix A [52].

The Hitachi S800 SEM at the USF NREC was used for qualitative surface analysis. Magnifications of 100X, 500X, 1000X and 5000X were used during this investigation. Figure 2.22 (D-F) shows the SEM micrographs of the samples after Piranha cleaning at 1000X as a

representation of all of the scans. Sample surface tilting angle of 45° was also used to detect more features on the surface.

2.5.3. Hydrofluoric (HF) Acid Cleaning of Immersed Samples

Hydrofluoric acid (HF) is an extremely strong acid, used for removing oxides on the surface of samples. The samples were previously solvent and piranha cleaned. Then the samples were immersed in buffered HF for 10 minutes. After cleaning the samples were rinsed with DI water to remove any residue. The samples were then dried and kept in cleaned plastic sample holders.

Quantitative analysis was performed using the AFM (Park Systems XE-100) in tapping mode. Figure 2.21 (G-I) shows the AFM results of HF cleaned samples for a scan area of 45 x 45 µm. 5 x 5 µm and 10 x 10 µm area scans were recorded to reveal more detailed features.

The Hitachi S800 SEM at the USF NREC was used for qualitative surface analysis. Magnifications of 100X, 500X, 1000X and 5000X were used during this investigation. Figure 2.22 (G-I) shows the SEM micrographs of the samples after HF cleaning at 1000X as a representation of all of the scans. Sample surface tilting angle of 45° was also used to detect more features on the surface.

To separate the major factors that may have caused the surface degradation of Si, the samples were tested in three distinct environments consisting of: the presence of H4 cells in DMEM, DMEM in absence of the cells, and ACSF, an artificial formulation of biological cerebral-spinal fluid which is suggested in ISO 10993.

From Figure 2.22, the original surface of the silicon sample was very smooth and flat due to chemical mechanical planarization (CMP) processing by the wafer manufacturer.

Consequentially, no particulates or depressions can be seen on the surface of the untested material. Based on our observation from the SEM micrographs in Figure 2.22 and AFM micrographs in Figure 2.21, miniscule surface modifications occurred across the surface of the samples in the presence of DMEM and ACSF. Before cleaning, this surface change was more significant, but was considerably reduced after cleaning the samples with piranha and HF, indicating the presence of organic particulates or solidified salts to likely be the source of the observed surface features. Anisotropic etching, or chemical etching, of (100) Si produces a distinctive pyramid shape due to faster etching rate of the (100) plane as compared to the (111) plane [11]. As the SEM and AFM micrographs did not display the presence of the typical pyramid shaped pits, we have no indication of the chemical etching of (100)Si from the cell media/ACSF only.

Table 2.3: AFM data extracted from *in vitro* tests

Cleaning method	Data	Cell Media+H4 Cells	Cell Media	ACSF
Solvent cleaned	Surface roughness, R_q (RMS)	4.859 nm	4.392 nm	2.550 nm
	Peak to valley :	69.276 nm	78.378 nm	102.217 nm
Solvent + Piranha Cleaned	Surface roughness R_q (RMS)	10.315 nm	3.377 nm	2.669 nm
	Peak to valley :	146.975 nm	75.099 nm	56.719 nm
Solvent + Pirhana +HF cleaned	Surface roughness R_q (RMS)	30.305 nm	789.180 pm	808.417 pm
	Peak to valley :	348.478 nm	14.865 nm	7.438 nm

Alternatively, the morphology of the Si samples exposed to the presence of H4 cells in cell media displayed a significant surface modification. This surface change was also seen and increased in size through the various cleaning stages, with the largest effect noticed after HF cleaning. As HF removes SiO₂, this would indicate that the surface was partially oxidized by the biological environment

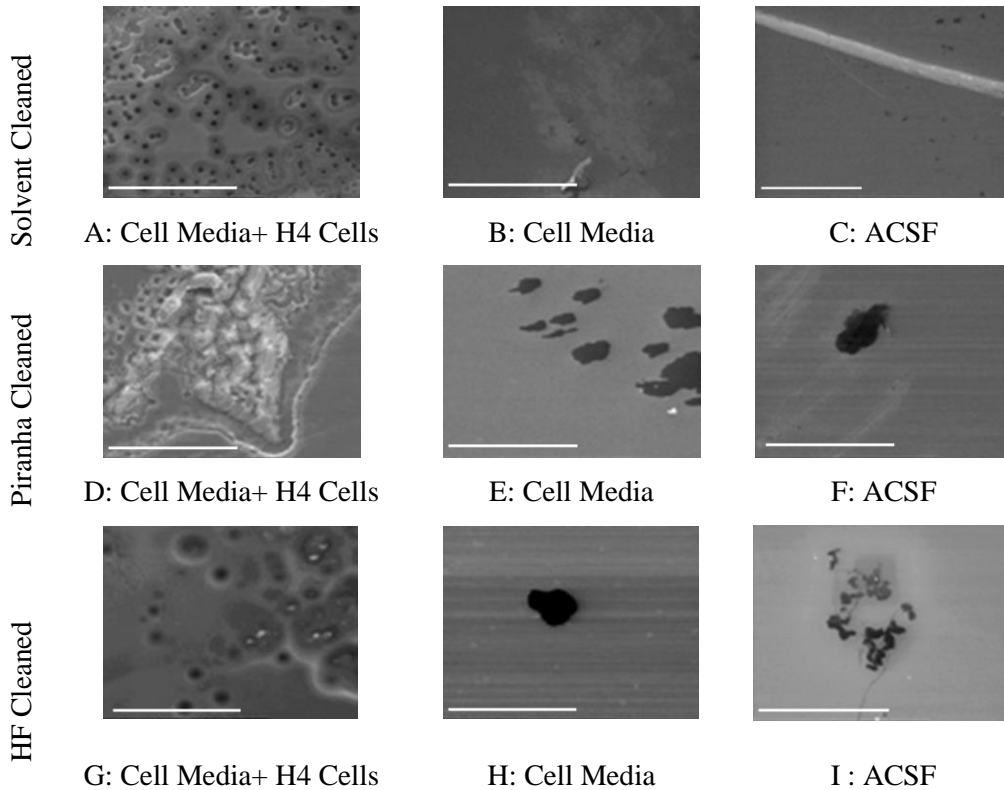


Figure 2.16: SEM micrographs of silicon samples immersed in Cell Media+ H4 Cells, Cell Media and ACSF; for 96 hours at 37°C. Cleaned with Solvents, the acceleration voltage was 25 kV, working distance was 5 mm and sample surface tilting angle was 0°, gold palladium coating were not used for these scans. Magnification 1000X. The scale bars' length is 50µm in all the micrographs, permission obtained from [52] presented in Appendix A.

The qualitative results from SEM and AFM analysis verify the presence of multiple pyramid shaped pits on the surface of this type of material, as seen in Figure 2.23. The average pit depth was 57 ± 8 nm with average width of 4600 ± 70 nm. The deepest pit that was observed had the depth of 138 nm. Due to the absence of these features on the soaked samples, we theorize

that the cells are the most likely source of the surface etching. Inflammatory cells have been shown to release chemicals during frustrated phagocytosis to dissolve the invading material [53]. Furthermore, it has been reported that neural inflammatory cells, like microglia, produce large amounts of nitric oxide, NO, a free radical which is used in signaling and cellular defense, and hydrogen peroxide, an oxidizing agent. NO in aqueous environments can chemically react to produce numerous species, one of which is nitric acid (HNO_3), a known anisotropic etchant of Si [50, 51, 54]. These chemicals could be the source of the oxidation and subsequent etching as revealed by the HF, but we will need to use alternative measurement techniques, like mass spectroscopy, to exactly quantify the chemical factors involved. Furthermore, we need to evaluate if this effect is particular to the H4 glial derived immortalized cell line, or if it is characteristic of all cells. To accomplish this aim we will use immortalized mouse fibroblasts, L929, and primary derived rat neurons as a comparison.

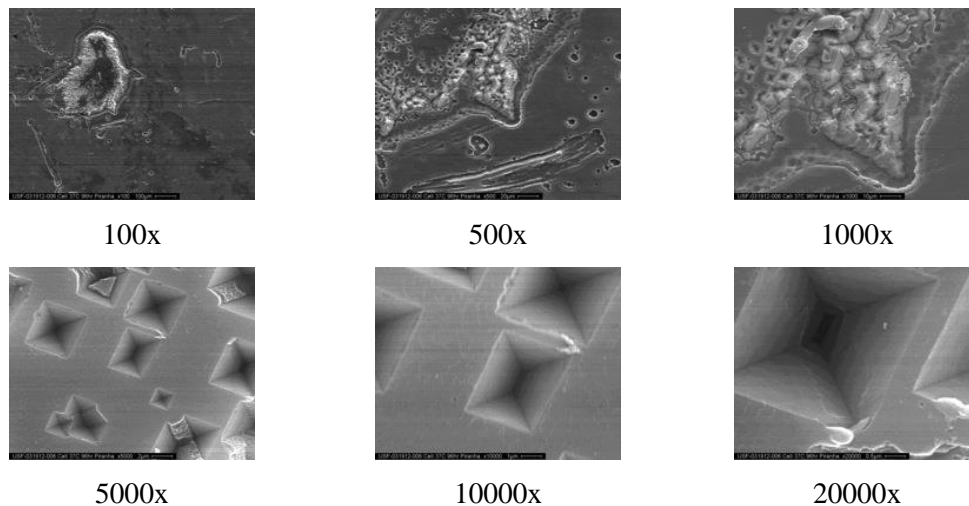


Figure 2.17: SEM results of silicon after in vitro testing. Clear changes to the Si surface are observed indicating that Si, a known cytotoxic material, is not chemically stable in physiological environments and suffers increased degradation in the presence of plated cells (H4 human neuroglioma cells).

2.6. Surface Degradation of *a*-SiC and 3C-SiC

Corrosion resistance of the four variant formulation of *a*-SiC was evaluated in PBS at 20 °C, 37 °C and 60 °C the results were compared to 3C-SiC, SiO₂ and Si (100). Figure 2.18 shows the effect of temperature on the surface degradation of the Cu and PVC after 30 days. As it can be seen the obtained data fits the empirical model that mentioned in the section 1.5. The proportional surface roughness change was considered as surface degradation data.

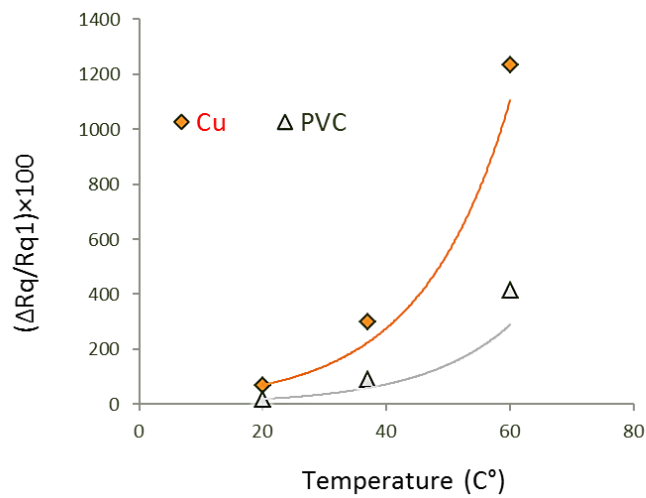


Figure 2. 18: Surface degradation of positive controls. Cu as conductor positive control and PVC as insulator positive control.

The surface degradation for the silicon based semiconductor materials also evaluated and effect of temperature was observed. In figure 2.19 the quantitative data collected with AFM before and after corrosion test in PBS after 30 days for *a*-SiC, 3C-SiC, SiO₂ and Si was shown. As it can be seen in this figure the average surface roughness has not been changed for 3C-SiC and all four types of *a*-SiC after 30 days and even by increasing the temperature to 60 °C. But the surface degradation for Si and SiO₂ increased by increasing the temperature. The slope of fitted line for Si was larger than SiO₂.

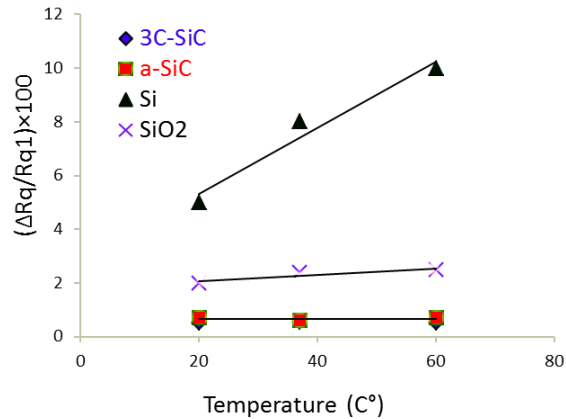


Figure 2. 19: Surface roughness change of *a*-SiC, 3C-SiC, SiO₂ and Si (100).

2.6. Summary

As described in Chapter 1 the first evaluation that devices and biomaterials must pass is the materials stability test. In this chapter two of the methods that are specified by the ISO, namely ISO 10993-14 and ISO 10993-15 [4, 5], were used to determine the degradation of the materials for both reaction controls and test materials.

Corrosion tests in PBS and HCL-Tris at 37°C and 60°C for 96 hours and 30 days were performed at the pH = 7.4 ± 0.2 based on ISO 10993-14 [4]. The control materials were selected based on ISO 10993-12 [3], polyethylene as the insulator negative control, Cu and PVC as the positive controls. But the ISO gave the freedom to the researcher to select the conductive negative control. To select the best conductive negative control, a variety of materials such as W, Pt and Au were tested for the degradation experiments. The only material that satisfied all the requirements of the stability test in a simulated solution was Au. Thus for the rest of experiments Au was used as conductive control material. In all the experiments including neutral and extreme solutions 3C-SiC, *a*-SiC, SiO₂ and Si (100) were tested as semiconductor materials. All of the

semiconductor materials passed the corrosion test in neutral solution at 37 °C and 60 °C except for Si (100) which showed minor surface damage at 60 °C after 30 days of soaking.

There are two goals in doing the corrosion test in a neutral environment; the first goal is to eliminate the materials that cannot stand the natural environment, a material that is not stable enough to tolerate the pH= 7.4 ± 0.2 definitely cannot resist in the harsh environment of the human body. So those materials would be eliminated to avoid a waste of further time and resources. The second goal of this experiment was to determine the effect of temperature as an acceleration factor. By checking the micrographs for positive controls it can easily be seen that the samples tested at a higher temperature faced more degradation, as expected. In the literature this acceleration factor was formulated as $2^{\Delta T/10}$. For our experiments, the surface roughness change ($\Delta r_q / r_{q1}$) was used as the quantitative value to verify this formula in our experiments for the positive control materials in neutral solutions. The most important factor that was ignored by previous studies reported in the literature is the liquid volume to surface area ratio. As specified in ISO 10993-15 section 7.2 this value for all of the soak tests, including tests in simulated solutions and extreme solutions, must be 1 mL / cm² [5].

After elimination of weak materials by testing in neutral environment, testing of the samples in the extreme environment of citric acid at a pH of 3.0 ± 0.2 is suggested by ISO 10993-14 [4]. The test was performed at 37 °C for 96 hours and 30 days. The temperature was not elevated for the acid test due to safety purposes. The same control materials that were used in the neutral solution were used in this experiment. No surface degradation was observed on Au but the surface of the positive controls had severe damage. Also all of the semiconductor samples, including 3C-SiC, *a*-SiC, SiO₂ and Si (100), passed the experiment without any

degradation. It can be concluded that temperature is more effective for design of acceleration tests in comparison to pH.

The last set of experiments was performed in acid solutions and base solution; various concentrations of HNO₃ (1 μM, 1mM and 0.1 M) at 37 °C for 96 hours and 30 days were used as the acid solution; also KOH in various concentrations (1 μM, 1mM and 0.1 M) at 37 °C for 96 hours and 30 days was used as the basic solution. The data is under preparation and will be included in the final version of dissertation.

By doing the materials degradation test the researcher can determine the stability of their products so that they can consider it in their fabrication process. The next step of pre medical evaluation of biomaterials and biodevices is to evaluate their *in vitro* cytotoxicity; First to eliminate the number of animals that would be sacrificed for *in vivo* experiments, and second to reduce the number of materials that need to be tested *in vivo* to save the time and resources.

CHAPTER 3: BIOCOMPATIBILITY OF THE BIOMATERIALS

In Chapter 1 the minimum requirements of a premedical evaluation of a biomaterial was described. In Chapter 2 materials stability as the first step in the design of a biodevice was presented. The materials that have passed the stability test will then be evaluated from a toxicity point of view based on ISO 10993-5 [6]. In this chapter the biocompatibility evaluation of the materials based on the ISO standard will be presented.

In modern biomedical devices the goal is distributed sensors that are able to record patient biological activity, such as vital signs, and ideally provide therapeutic pathways via treatment or the dispensing of medicine based on the measured parameters. In most cases it is absolutely essential that there be at least a component of the device that performs its function *in vivo*. One example of where traditional medicine is not able to provide assistance to patients is when they suffer the loss of a body part, such as limbs and joints. Then prosthetics become necessary and a plethora of examples are now common place – knee and hip replacements, dental implants, etc. One of the grand challenges of our time is both understanding how the brain functions and restoring lost cognitive functionality after trauma or disease. For example patients with Parkinson's disease or severe injury in the nervous system can recover all or part of their functionality via the use of brain machine interfaces [14, 53]. Diabetic patients can be treated by implantable biological microelectromechanical systems (BioMEMS) for drug delivery [54] and patients with arthritis or movement disorders can be cured by joint replacement [55]. To be able to use a device in contact with the human body it must satisfy several requirements such as

corrosion resistance, biocompatibility, hemocompatibility and durability in the physiological environment of the human body for the desired time period which is, in general, application specific.

ISO 10993 provides a guideline to evaluate the biocompatibility of biomedical devices and biomaterials. All the devices that are interfacing with the human body, including implants and external devices, must not cause irritation or any disturbance of human body physiology. ISO 10993 consists of several parts which describe sample preparation and reference (i.e., control) materials selection [3], biomaterial chemical stability [4, 5], *in vitro* tests such as cytotoxicity [7] and hemocompatibility evaluation [6, 16]. For a device to be selected for clinical trial strict adherence to ISO 10993 is a minimum requirement, hence it is critical to fully understand the standard and how to properly implement it in the laboratory.

ISO 10993-5 recommends the following methods to evaluate the cytotoxicity of the biomaterials and devices: testing via cell media extract, direct contact cell seeding and MTT (3-(4 5-dimethylthiazol-2-yl)-2 5-diphenyltetrazolium bromide) assay as an appendix [6]. ISO 10993-5 has been used as a baseline for that purpose in research activities by a lot of groups around the world for various applications of biomedical devices. For example it was used in the evaluation of materials for the construction of neural implants [56], implantable biosensors [57], drug delivery implants [2] and even for the evaluation of biodegradable implants such as Mg alloy bone scaffolds [58]. In many cases the method that was used, while originally based on ISO 10993, has deviations from the original protocol, which could result in inconsistency of the data and therefore comparison of results from different laboratories becomes very difficult. The common deviations from the protocol, as introduced in Chapter 1, are in the following parameters: surface area to volume ratio, the use of agitation, and especially the selection of

correct control materials and proper sterilization methods. For example, Green *et al.* used *in-vitro* testing with the extract and direct contact tests as an evaluation of cytotoxicity of microelectrode arrays (MEAs). While the surface area was mentioned in the extract preparation part of the paper the reason for avoiding agitation was not mentioned. In addition for the direct contact assays performed the cells were grown on top of the specimens which is a deviation from the protocol and an indicator of cell permissiveness not cytotoxicity [59]. Cell permissiveness was used in some cases including our previous work [12-15]. Although cell attachment to the surface of some materials is an important factor in biomaterials selection, it must not be mistaken with cytotoxicity [12, 14]. In another case Meric *et al.* used ISO 10993 as a method for cytotoxicity evaluation of silica-glass fiber composites for dental applications but preparation of the extracts in a non-sterilized environment, the absence of agitation of the samples, and the use of test tubes as the carrier of the extracts were deviations which can affect the reproducibility of the experiments [60]. The extract method shows promising results for the cytotoxicity evaluation of materials but it should be considered that testing with extracts only is valuable for degradable materials and it can result in misleading results when it is used for robust materials with lower biocompatibility. Also the absence of essential proteins such as albumin in the extract test could be critical since albumin can increase the materials degradation by a factor of 4, which can result in an increase of harmful corrosion products in the extracts [61]. To have a complete verification of biocompatibility for implantable materials a series of cytotoxicity assays, or a method that includes all of their criteria, is necessary. In this chapter we present such a methodology that is in strict compliance with ISO 10993 and it is our hope that this chapter will serve as a practical guide to how to perform these highly critical biomaterial and biodevice compatibility assessments.

There are basically three (3) methods for conducting the *in vitro* cytotoxicity assays, as illustrated in Figure 3.1. The first method (Figure 3.1. left), the extraction method, involves the transfer of cell media that was exposed to the material under test (including controls) to a cell culture well that has living L929 cells present. One then observes the response of these cells to the addition of this extract. The next two methods are based on a direct testing approach. In the direct method (Figure 3.1. center) the material under test (including controls) is placed above the cells that have been cultured in the well and the reaction of the cells to the presence of the material is evaluated. One issue here is the mass of the sample and the likely probability that this will cause a mechanical effect on the cells rather than only a chemical effect. In the seeding method (Figure 3.1. right) the goal is to plate the cells on the material under test and study the resulting cell behavior.

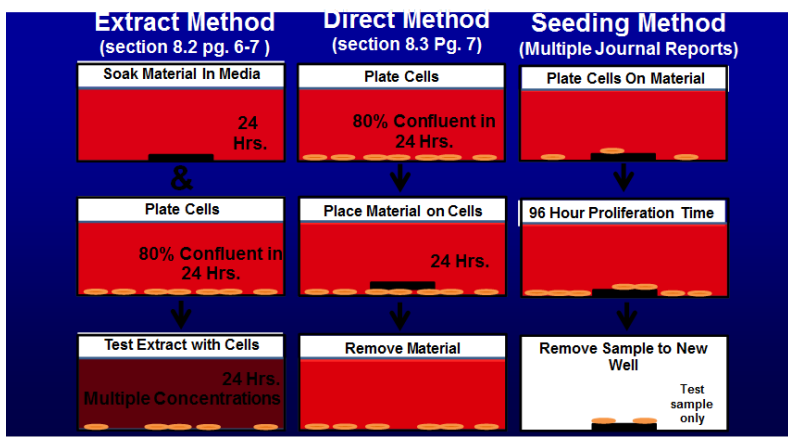


Figure 3.1: The schematic of material/ cell orientation in: Extract test based on ISO 10993-5 section 8.2 (left)[6], Direct test based on ISO 10993-5 section 8.3 (center)[6] and Seeding test (right)[12-15].

3.1. Sample Preparation

The test materials used in this set of experiments consisted of both materials under test and the proper control materials as per ISO 10993 and as described in Chapter 2. The materials

under test were coupons diced from the following materials: (100) Si 100 mm wafers (ID 1910 obtained from University wafer); SiO₂ deposited on (100) Si 50 mm wafers in a plasma enhanced chemical vapor deposition (PECVD) system with an oxide thickness of 1500 nm; Ti/W deposited on (100)Si 100 mm wafers using electron beam physical vapor deposition - EB PVD (1500 Å of W deposited on 200 Å of Ti which serves as an adhesion layer). The Control materials consisted of: Ti/Cu deposited on (100)Si 100 mm wafers using EB PVD (1500 Å of Cu deposited on 200 Å of Ti); Ti/Au deposited on (100)Si 100 mm wafers using EB PVD (1500 Å of Au deposited on 200 Å of Ti); Polyethylene tape (1534-3, 3M™ Transpore™); polyvinyl chloride doped with organotin (PVC-org. Sn) and polyvinylchloride (F-4040-A, Tygon®).

All of the wafers were cut into 8×10 mm coupons using a dicing saw with a diamond-coated blade. The PE tape and the PVC tube were cut to have 80 mm² of exposed surface area. After dicing the metallic and semiconductor samples, the samples were cleaned in acetone, isopropanol and deionized water ($\rho > 16 \text{ M}\Omega \text{ cm}$) for 10 minutes using an ultrasonic bath to remove any organic residue and debris from cutting. The PVC was sterilized via EtOx at George Mason University. The metallic and semiconductor samples were sterilized in a dry heat sterilizer at 120 °C for 60 min in the presence of N₂ gas. The PE tape was disinfected by 70% ethanol solution as sterilization of this material, in the form tested, was not possible.

3.2. Cell Culture

The entire cell plating activity was performed in a disinfected environment under a sterilized biological hood. 30 minutes prior to cell culture activity the UV light inside the hood was turned on to disinfect the hood chamber. The glass door of the hood remained closed and the operator left the room while the UV light was on. After UV sterilization the hood chamber was disinfected using a 70 % (volume %) ethanol solution. Clean lab coats and disposable nitrile

gloves (powder free Touch N Tuff ® Ansell) were worn by the operator to avoid any contamination.

The following materials and supplies were used for cell culturing. One T-75 flask (CytoOne), six sterile 10 mL serological pipets (USASCIENTIFIC), one sterile 15 mL conical screw cap centrifuge tube (USASCIENTIFIC), one sterile 50 mL conical screw cap centrifuge tube (USASCIENTIFIC), one sterile 200 µL centrifuge tube (USASCIENTIFIC), a Motorized Pipet Filler/Dispenser (Fisher Scientific), a 200 µL manual pipetter (Digital Adjustable-Volume Pipetter, Fisher Scientific), 1X sterile PBS solution, and finally a 6-well plate which contained the mounted coupons as described above. The required supplies for cell culturing were sprayed by the 70% ethanol solution and were placed in the bio hood prior to assay processing.

ISO 10993-5 suggests the use of a Mice fibroblast cell line (NCTC clone 929, strain L) for cytotoxicity assays, which is commonly known as L929 [6]. In this set of experiments the L929 cells, purchased from American type culture collection (ATCC® CCL-1™), were used. The cell culture media consisted of Dulbecco's Minimum Eagle Medium (DMEM) (Life Technologies™ #10313-021), infused with 10% fetal bovine serum (FBS) (Life Technologies™ #16000-044), 2.2mM l-glutamine GlutaMAX-1 (Invitrogen #35050-061), and 1% antibiotic / anti mycotic solution (Sigma #P4458-100ML). The L929 cells were cultured in 75 cm² tissue culture flasks (CytoOne T-75 filter cap; USAScientific, Ocala, FL) in a water jacketed incubator at 37°C, 95% relative humidity and 5% CO₂. The L929s received fresh media every 72 hours by replacing 50% of the existing media. The cells remained in the flask until they were used for cytotoxicity assays; otherwise they were passed to a new flask when they exceeded 90% confluence level, to avoid any over population.

The cell culture media and trypsin 1x (gamma irradiated, SAFC bioscience) were placed in a water bath at 37°C and allowed to reach the proper temperature. This temperature adjustment must be done to avoid any thermal shock to the cells.

The most confluent flask of cells was selected from the incubator. The flask was disinfected with 70% ethanol and placed in the hood. The 50 mL conical centrifuge tube was marked as trash, and then the old cell culture media was removed from the flask using a 10 mL serological pipet and disposed of in the trash tube. 5 mL of sterile 1X PBS was added to the cells in the flask, the flask cap was closed and the flask was tilted to wash the cells completely and then the contaminated PBS was disposed of. Next 4 mL of warm trypsin was added to the cells to scrape the cells from the walls of the flask. The cap was closed and the flask was tilted to cover all the cells with trypsin. The flask was then stored in the incubator for 10 minutes. The cell-trypsin mix was agitated using the pipette to remove any cell agglomerations. Next the cell-trypsin mix was added to a 15 mL conical centrifuge tube and 8 mL of fresh cell media was added to that which was agitated again by the pipette to form a uniform solution.

Next 30 μL of the cell mixture was extracted using the digital pipette and placed in the 200 μL centrifuge tube. Then 30 μL of trypan blue solution (0.4%, sigma life science) was added to tube and was agitated to have a uniform liquid after which 15 μL of the cell mix was placed in a hemocytometer (Bright-Line TM Sigma-Aldrich) and a glass cover slide placed on top. The cells in 4 corner regions of the hemocytometer and the central region were then counted using the optical microscope (ZEISS - image.M2m) in the bright field mode. The area of each square is 1 mm^2 and the height is 0.1 mm so when we count the cells in each square it means we count the cells in 0.1 mm^3 . The hemocytometer was used to calculate the cell population prior to seeding on the specimens. Figure 3.2 shows the hemocytometer being loaded with the cell mix.

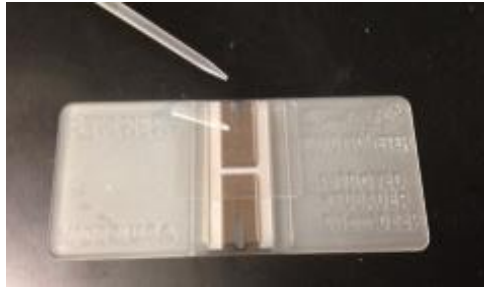


Figure 3.2: Photograph of the hemocytometer used for counting the cell concentration. Shown is a pipette which is used to transfer the cell mix to the hemocytometer for analysis. A glass cover slide is placed (not shown) prior to microscope observation.

To number of cells present per microliter is calculated based on the number of counted cells, n , via the following formula [62]:

$$\#Cells/\mu l = \frac{n \times 2 \times 10}{5}$$

Where n is the number of cells in a large square (cells per 1 mm x 1 mm x 0.1 mm), 2 is the dilution factor of trypan blue, 5 is used to calculate the average number of cells per 0.1 mm³, and 10 is used to calculate the number of cells per 1 mm³ (or 1μL).

Because we counted five regions and we added them up we must divide the “ n ” by “5” to have the average number of cells in the regions. Also the dilution factor with trypan blue was two so we must multiply the average by “2” and to get cells per 1 mm³ we must multiply the number by 10. The number of cells per microliter was recorded for each material tested in order to check the repopulation behavior of the cells.

3.2.1 Cell Plating

Before plating the cells on the test coupons and control surfaces, 2 mL of cell culture media was added to each well. Knowing the concentration of cells, as described above, the proper number of cells can now be plated on the test materials in the 6-well plate. The proper

number of cells is the number of cells which, when plated, will yield 80% confluency after 96 hours of cell incubation.

After cell plating the 6-well plate was placed in an incubator (fisher-scientific) at 37°C, 95% relative humidity, 5% CO₂, for 96 hours and the cells monitored periodically for cell growth and infection.

To make sure that we have cells for the next experiments we need to pass some cells to a new flask. Based on the plan for future experiments the quantity of cells that were seeded in the flask varies. Normally 2×10^6 of cell mix was placed in a new T-75 flask, after which 10 mL of fresh media was added. The generation number, passage date, cell type, operator's initials and the volume of added cell mix were recorded on the flask. By doing this procedure we maintain the cell line for future experiments.

All waste was disposed of in the biohazard bin and the hood disinfected with 70% ethanol solution after this step. The test was repeated 5 times to achieve N=10 for each test material.

3.3. Extract Method

As described in Section 3.1, to evaluate the effect of leached ions from a material under test on the cells ISO 10993-5 recommends a protocol under the name of extract test. Figure 3.1 (left) shows an illustration of this method. The L929 cells were seeded on a 96-well plate (CytoOne; USAScientific, Ocala, FL), with nine wells used for each assay. Each well received 1.5×10^4 of L929 cells to reach 80% of confluence, followed by the addition of cell media to adjust its volume to 100 µl total volume. The cells were incubated for 24 hours at 37°C, 95% relative humidity and 5% CO₂. To obtain the extracts each sample was placed into a well of a 24-

well plate then the cell culture media was added until 3 cm²/mL exposed surface area to media ratio was achieved (as specified by the ISO). The 24-well plate containing the materials was carefully sealed with parafilm and placed on a shaker at 1 Hz frequency for 24 hours at 37°C. The 96-well plate was retrieved from the incubator and the media replaced by extracts of various percentages (100%, 70% and 50%). The assays consisted of a triplicate of 100%, 70% and 50% extract replacement. The assays were repeated three times for the test materials, controls and polystyrene wells which served as the baseline. The 96-well plate that included the added extracts was incubated for 24 hours at 37°C, 95% relative humidity and 5% CO₂. After 24 hours of incubation the old media was removed and the wells were stained by ethidium homodimer-1 (EthD-1, life technology) and calcein, AM (to detect live cells) and the fluorescence tagged cells were then imaged using a fluorescence microscope (Zeiss image.M2m) at 5X and 50X magnification.

Selection of controls were discussed in Chapters 1 and 2. Polyethylene was selected as the negative control for insulator materials as it was mentioned directly in ISO 10993-12 Appendix A [3]. But since no negative control material for conductors was suggested by the ISO standard, platinum [63] and gold [64], which are conventional biomaterials that have been used in the human body and are known as inert materials, were used as the conductive material negative controls. The positive controls were copper for conductive materials and PVC doped with organo-tin (PVC-org. Sn) for insulator materials as these were mentioned in Appendix A of ISO 10993-12 [3]. A fluorescence microscope was used in order to have a qualitative and quantitative evaluation of cell behavior in the presence of the various materials. Calcein was used as a fluorescence dye to detect cell viability, which has the ability to penetrate through the cell membrane. When this happens the esterases enzyme of the cell removes the acetomethoxy

group from the calcein am, which results in a green fluorescence. It can only happen in live cells so the presence of green fluorescence means that the cells are alive [65]. A second dye, ethidium homodimer, was used as the second fluorescence dye and this dye was used to detect dead or dying cells. Under normal circumstances the ethidium cannot penetrate the cell through the membrane but when the cell is dead or dying the stain can enter the cell and react with the DNA of the cell. Under the fluorescence microscope the dying or dead cells will appear as dark orange or red spots [65]. Figure 3.3 shows the fluorescence micrographs of the Au and Cu control materials, which are used to verify if the test was working properly.

The effect of the concentration of leached ions from the extracts was evaluated by replacement of various quantities of old media by material extracts. Figure 3.3 a) shows fluorescence micrographs after replacement of 50% of old media by Au extract. As expected all the cells emitted green light, which means all the cells are alive and no toxic reaction happened between cells and the extracts from our negative control. When the concentration of the extract was increased to 70% and even to 100% for Au specimens the cells passed the minimum required viability, Figure 3.3 c) shows the cells after replacement of 100% of old media with Au extract at 50X magnification. Figure 3.3 b) illustrates qualitative evaluation of cell viability in the presence of Cu extracts after replacing 50% of old media with extracts. As can be seen in this micrograph most cells are dead (orange fluorescence) and the few living cells, which appear to be unhealthy, are present and clearly dying. When the concentration of Cu extract was increased to 70% and 100% no live cells were seen, as shown in figure 3.3 d).

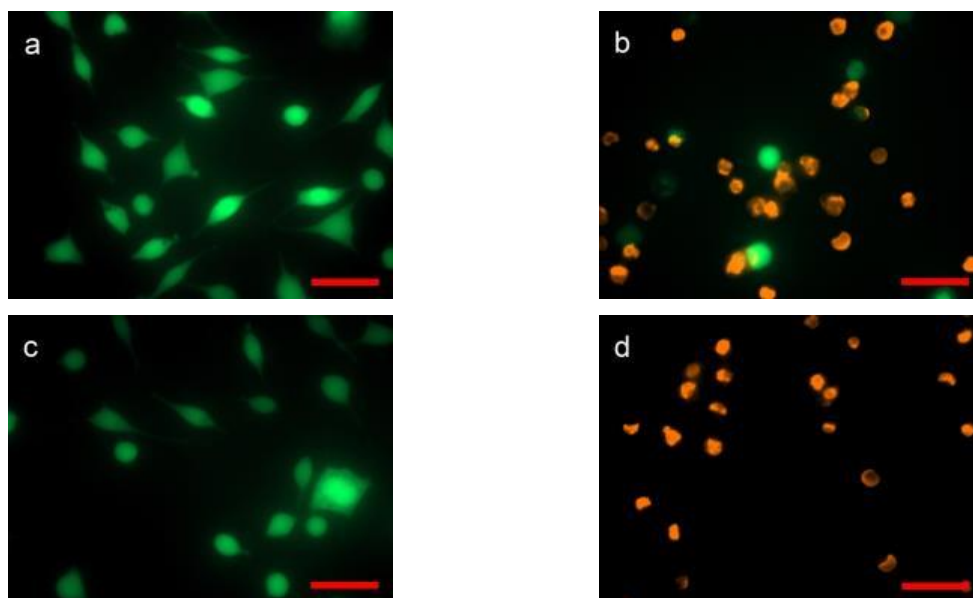


Figure 3.3: Live/ dead cell assay data. Fluorescence micrographs of control materials: a) 50% of media replaced by Au extract; b) 50% of media replaced by Cu extract; c) 100% of media was replaced by Au extract; and d) 100% of media was replaced by Cu extract. The size of the scale bars is 50 μm . Green fluorescence signifies live cells while orange/red dead cells.

Figure 3.4 contains a histogram of L929 cell viability in the presence of the control material extracts at three various concentrations from the 100 %, 70 % and 50 % of extracts. The conductor controls and PE, the negative insulator control, behaved as expected but the PVC org.-Sn, which is supposed to be a positive control, did not have a toxic reaction with the cells. We believe that the toxic elements, which were present in this product, were removed at the time of material fabrication so that this material does not have the expected toxic effect. In order to have a more reliable positive reaction control the PVC org.-Sn was replaced by another type of PVC known as Tygon. The exact toxic element(s) in the second type of PVC is unknown due to confidential fabrication method but for the test performed on this material a strong toxic reaction occurred between the extract and the cells. Application of Tygon as a positive control was reported by Charkhkar *et. al* [21] as well as Hooper and Cameron [66]. As can be seen the cell

viability increased by decreasing the concentration of extracts of Au and Cu but a logical trend was not found for the insulator controls.

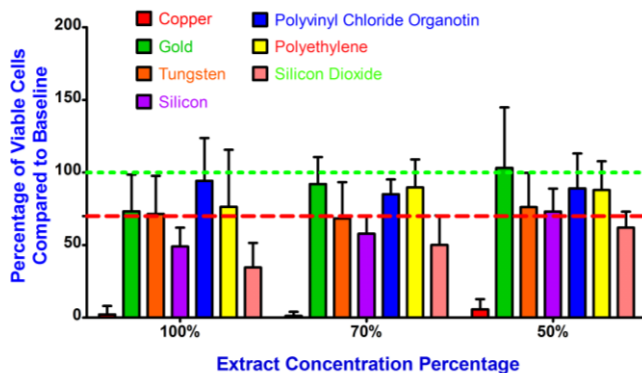


Figure 3.4: Quantitative data of control materials Au, Cu, PE and PVC done with extract method on L929 cells. For reference 100% and 70% threshold are shown with dashed lines. Materials who fall below 70% have, by ISO 10993 definition, failed the test. Cu, as expected, failed the test but unfortunately PVC org.-Sn did not. Based on these results the positive control was switched to Tygon which proved to be a reliable positive reaction control (not shown).

3.4. Direct Contact Method

As was mentioned in Section 3.1 of this chapter to study the direct material/ cell interaction ISO 10993-5 suggests the Direct Contact method. It is illustrated in Figure 3.1 (center) that the cells were seeded in the well plate and then the test materials were placed above them. The L929 cells were seeded on a 6-well plate (CytoOne; USAScientific, Ocala, FL). Each well received 2 mL of fresh cell culture media and 1.8×10^5 of L929 cells to reach 80% of confluence. The well plate was incubated for 24 hours at 37°C, 95% relative humidity and 5% CO₂. After one day the cells were checked under the microscope to verify their sub confluence status. The old media was replaced by 2 mL of fresh media. The sterilized samples were then placed in the center of each well and it was verified that at least a monolayer of cells were covered by the sample. The plate was incubated for another 24 hours at 37°C, 95% relative

humidity and 5% CO₂ [7]. After 24 hours the materials were removed and the wells imaged using the fluorescence microscope.

Figure 3.5 illustrates the fluorescence micrographs of Au as the negative conductor control material to verify the performance of the test. As can be seen in Figure 3.5 a) the number of live cells close to the material, and where the material used to be, is zero. But as can be seen in figure 3.5 b) at a location far from the material the cells behaved normally. Since this behavior happened for all materials, including the negative controls, it can be assumed that the decrease in cell viability could be a result of mechanical force applied by the weight of material to the cells rather than the toxicity of the materials. It can be clarified better if we recall Figure 3.1 (center) where the cell/material orientation was illustrated. As it can be seen the material is on top of the cells so if the material is heavy it can put pressure on the samples and kill them.

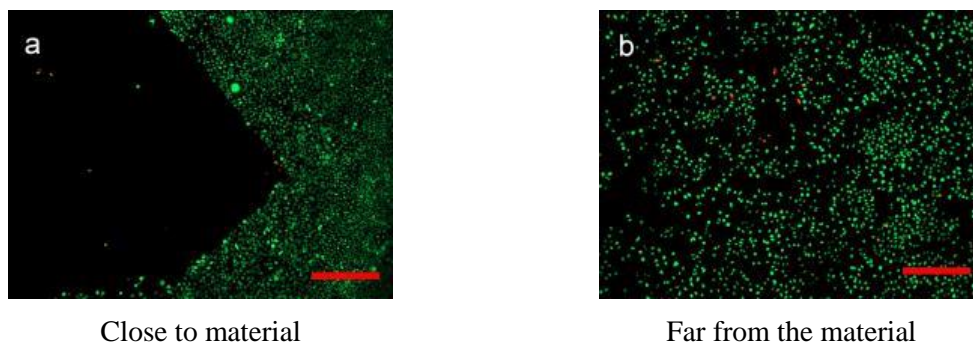


Figure 3.5: Fluorescence micrographs of Au as negative control material after performing direct contact method with L929 cells. The size of scale bars is 500 μm . Note the lack of cells at/near where the material was located but normal cell population observed far from the sample position. This data indicates that the direct contact method can cause cell death due to mechanical, and not cytotoxic, effects.

In Figure 3.5 b) the fluorescence micrograph of the well that included the gold sample shows that the cells are alive as expected for gold samples. Also in the case of light materials the specimens were floating on the surface of the media and did not sink properly to get in contact

with the cells, which is another reason why the direct contact method suggested by ISO 10993 may not be the best method to use for cytotoxicity testing.

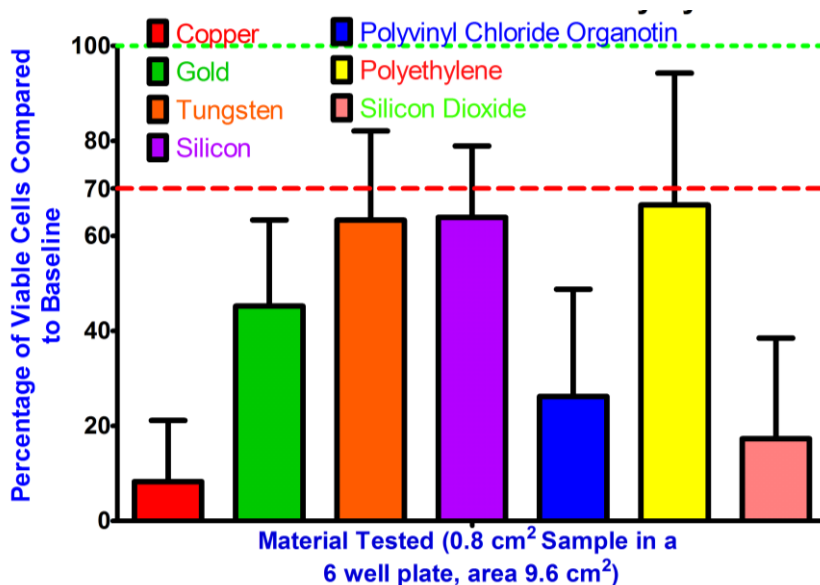


Figure 3.6: Quantitative analysis of the direct contact test on control materials. Note all materials failed the test, which is an unexpected result and provides evidence that mechanical damage from the test material may be masking the cytotoxicity results which were as expected for the extract method (see Fig. 3.4).

Figure 3.6 shows the quantitative analysis of the direct contact test on the aforementioned control samples using the L929 cells. All data was normalized to culture treated polystyrene well plates. Surprisingly the cells did not behave as expected. Although the number of live cells was significantly higher in the negative control cultures to the positive controls, as expected, they should have displayed a viability of more than 70% to be considered as nontoxic materials. However they failed the test which we believe is a result caused by test coupon mechanical damage and not a cytotoxic effect.

3.5. Seeding Method

In section 1 of this chapter a second method that has been reported in the literature to study the cell/material interaction was discussed. In this method samples were placed in the well

plate and the cells were plated on top of them. Figure 3.1 (right) illustrated the position of the cells and material. The samples were placed in the center of the wells in the 6-well plate. The L929 cells were seeded to the well plate and each well received 1.1×10^5 of L929 cells to reach 80% of confluence and 2 mL of fresh cell culture media. The plate was incubated for 96 hours at 37°C, 95% relative humidity and 5% CO₂ [7]. The materials were then removed carefully and imaged using the fluorescence microscope.

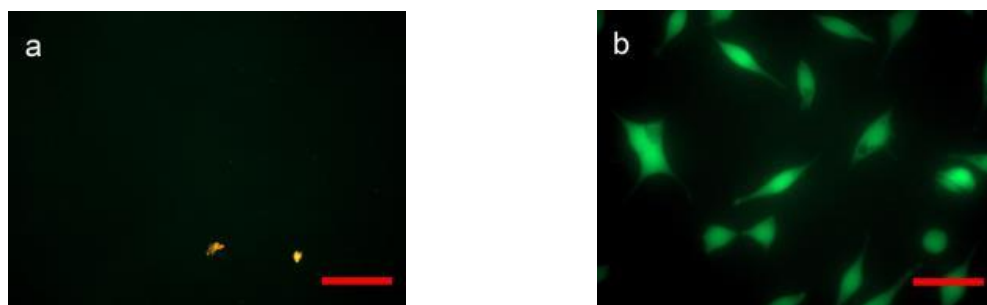


Figure 3.7: Fluorescence micrographs comparing PE after (a) direct surface seeding method, with b) the extract method with 100% media replacement. The size of scale bars is 50 μm . Note that the PE failed the direct seeding test while it passed the extract test (not shown), thus showing that proper selection of the proper cell assay under ISO 10993 is critical.

As mentioned in ISO 10993-12, and based on other tests that were performed, PE is supposed to be a negative insulator control which means no toxic reaction with the cells. But as can be seen in Figure 3.7 a), which shows cell permissiveness after testing PE with the surface seeding method, no cells were attached to the surface. Also to verify the nontoxicity of PE, Figure 3.7 b) is included for comparison; in this figure the fluorescence micrograph of PE after 100% replacement of media with the extract is illustrated. One explanation of this observation can be the effect of surface wettability, surface roughness, etc., which can affect the cell attachment but are not necessarily caused by material toxicity.

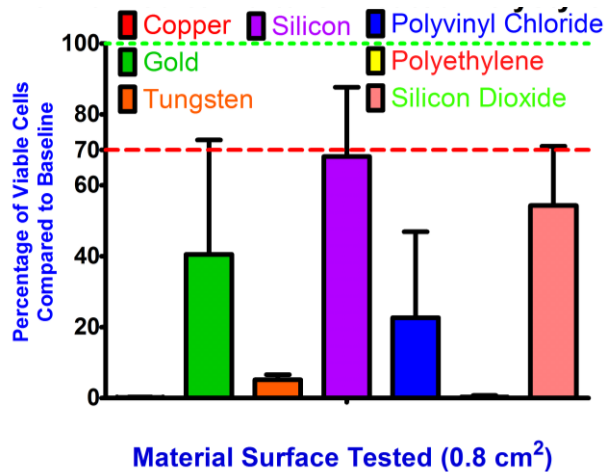


Figure 3.8: Qualitative analysis of the control materials (Au, Cu, PE and PVC) using surface seeding method. Note that all materials, including the negative controls, have failed the test as per the ISO definition of 70% viability. This method assesses material permissiveness and this result was not expected and requires further study.

Figure 3.8 shows the quantitative results of the surface seeding method. All the results were normalized to cell culture treated polystyrene. The cells did not attach to the PE samples, which could be a result of the surface properties of that material and not a cytotoxic effect, since PE easily passed the extract test. But even for Au samples the cell permissiveness did not reach 70% in comparison to the baseline so clearly some systematic error in the implementation of this variation of the cell cytotoxicity assay is present and must be better understood.

3.6. Direct Cell Plating (BAMBI Method)

In the recent sections we have outlined the methods specified in the ISO standard, namely the extract, direct contact and cell seeding methods. One of the important observations of this work was that a more elegant solution should be possible that both adheres to the ISO standard while optimizing the information that can be gained about a material under test. In this section a direct cell plating method, which we have called the BAMBI method for Biocompatibility of Advanced Materials for Brain Interfaces (DARPA project title that funded this research), is

presented. This work has indeed resulted in a very efficient method to follow the ISO standard and gain as much insight into the behavior of a material under test by basically combining the cell seeding and extract methods all in one test. We now describe how this was accomplished.

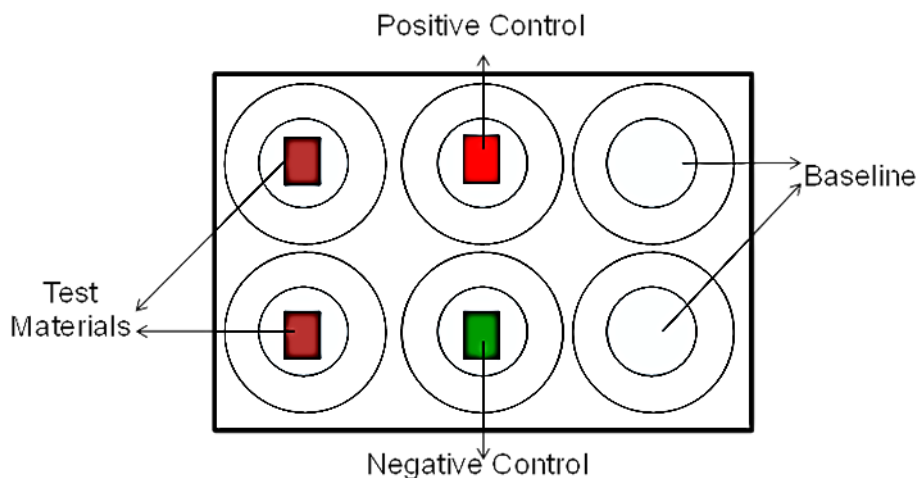


Figure 3.9: BAMBI method sample placement schematic showing the orientation of samples in the 6 well cell culture plate containing 2 coupons of test material, 1 coupon of positive control, 1 coupon of negative control, and 2 CTPC samples used as baseline.

Test material coupons, 8×10 mm in size, were mounted on tissue culture treated (CT), 22 mm diameter, round polycarbonate (PC) cover slides, using Hystoacryl® glue. The coupons + CTPC slides were mounted within 6-well TC plates (CytoOne®, USASIENTIFIC). The 6-well plate was sealed using the parafilm tape and cured for at least 72 hours at 37 °C allowing the glue solvent to evaporate completely so as not to affect the cytotoxicity results, one hour before using the 6-wll was placed under the sterilized bio hood and the seal was opened, rinsed with sterilized DI water and left there to degas and water to be removed.

Figure 3.9 shows top view of how the materials were mounted within the 6-well plate.

Figure 3.10 shows how the cells were plated on the combination of the PC slide and the samples.

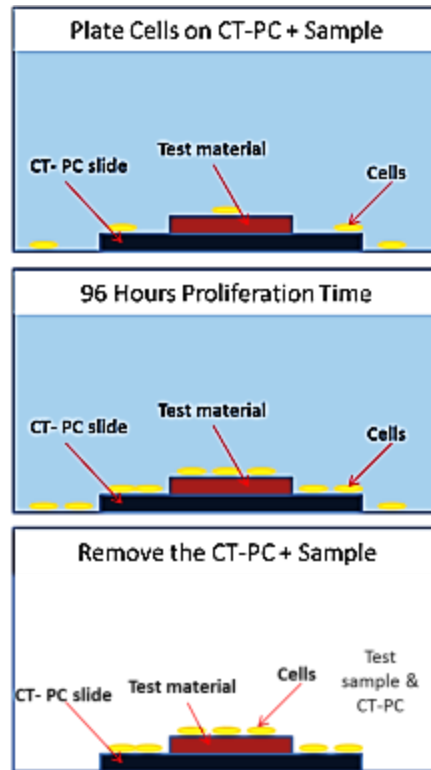


Figure 3.10: Illustration of BAMBI method sample mounting on a cell treated polycarbonate slide and the cells seeded above them versus time. After 96 hours the mounted sample is removed and the cell population, both on the test material and the baseline polycarbonate disk, evaluated thus combining the extract method (evaluation of cell population on the disk) and direct seeding method (evaluation of the cell population on the test material, which is a measure of material permissivity).

After 96 hours of cell culture the sample/slide combination was carefully removed from the well. The dye was added to the cells to provide a fluorescence tag with which to determine the live or dead status of the cells. The fluorescence dye consists of 10 mL of 10 mM PBS diffused with 5 μ L of 1 mg/mL calcein dye (1mg/mL in anhydrous DMSO, Life Technologies) to detect live cells and 7.5 μ L of 2 mM ethidium homodimer-1 dye (EthD-1,2mM solution in 1:4 DMSO/H₂O, invitrogen) to detect dead cells.

The fluorescence microscope (ZEISS image.M2m) was used for qualitative and quantitative evaluation of the live/dead behavior of the cells. The quantitative evaluation of live/dead behavior of the cells was obtained by taking images at low magnification but from a

whole population of the cells on the material and CTPC. The qualitative analysis of cell attachment to the surface of the material can be determined by imaging at higher magnifications such as 50X.

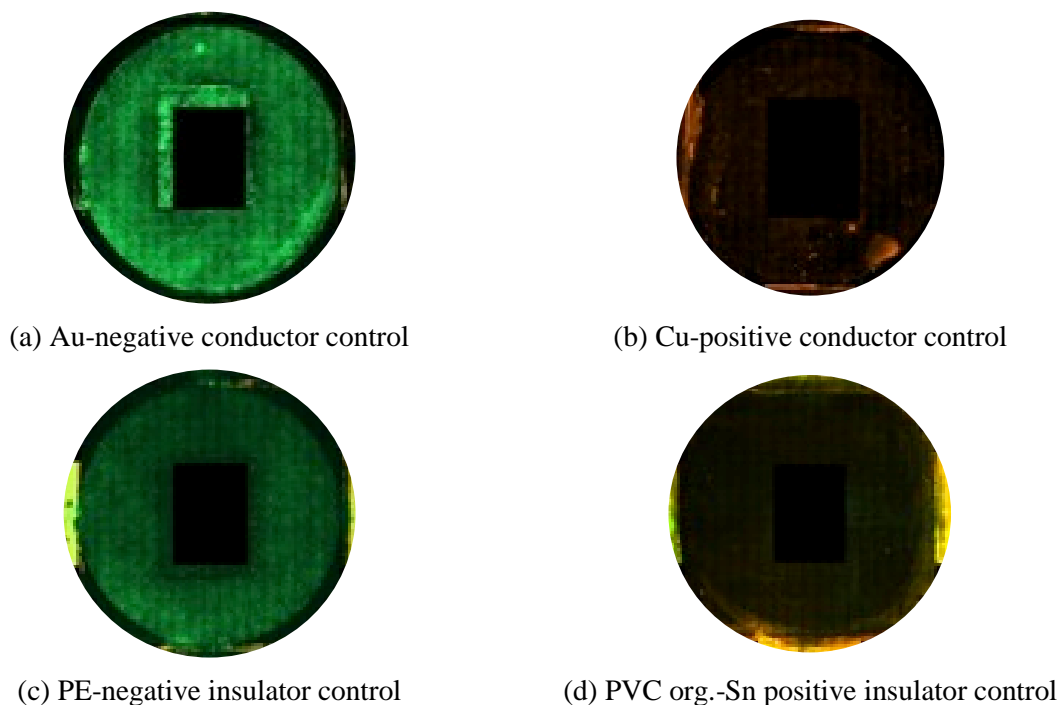


Figure 3.11: BAMBI method fluorescence micrographs, at 10X magnification, of the wells that included the control materials (a) Au, (b) Cu, (c) polyethylene and (d) PVC organo-Sn. Cells present on the test materials are out of focus and thus appear black in the image (see Fig. 3.12 for cell images from the test materials).

Figure 3.11 shows the fluorescence micrograph of the wells that included the control materials. The 10X magnification micrograph shows the whole cell population, which is useful for statistical analysis of live/dead assays.

Based on the fluorescence microscope images in Figure 3.11 the population of live cells is totally dominant for the negative controls, as expected. The cells are alive in the PE and Au wells indicating that there was no leaching of toxic ions to the cell media so the role of these two materials as negative controls were verified. Figure 3.11 shows no live cells in the Cu and PVC org.-Sn wells indicating that toxic materials leached from the materials and reacted with the

cells. The leached ions from Cu and PVC org.-Sn caused the death and absence of cell attachment to the wells.

Based on the fluorescence microscope images from the surface of the control materials at 10X magnification, the Au and PE controls showed a large population of attached cells and they are healthy and alive. The 50X magnification micrographs of the Au and PE confirm that the cells are attached perfectly to the surface and are healthy. So an absence of a reaction with the cells means the negative materials behaved as expected. We can see the opposite behavior for the Cu and PVC org.-Sn samples, no cells were present on the surface of the samples and also the 50X magnification images showed the absence of healthy live cells on these materials. Having the reaction of toxic material with the cells verifies the role of Cu and PVC org.-Sn as positive controls. Figure 3.12 shows the 10X and 50X magnification micrographs of the control material surface cell population.

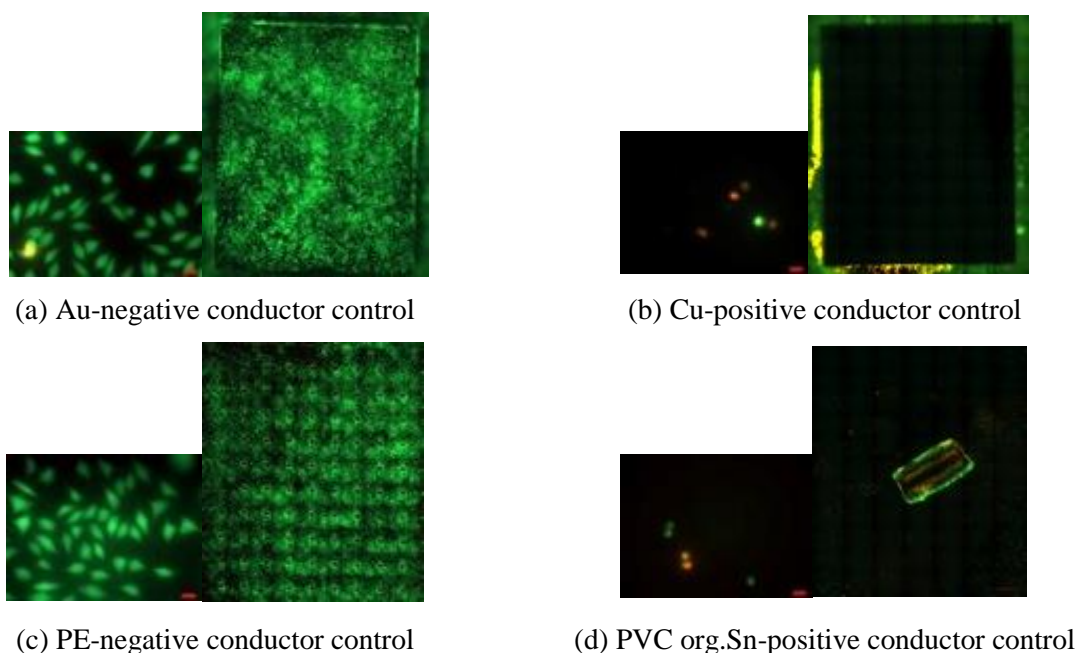


Figure 3.12: BAMBI method fluorescence micrographs, at 10X and 50X magnifications, of the materials that included the control materials (a) Au, (b) Cu, (c) polyethylene and (d) PVC organo-Sn. (See Fig. 3.11 for well images corresponding to this data).

Figure 3.13 shows the wells that contained the 3C-SiC samples as the test material. By comparing the micrographs with the control and baseline images, the complete absence of any reaction between the 3C-SiC samples with the cells in the well is obvious. So we can understand that 3C-SiC behaves more like a negative control. The quantitative analysis can verify this hypothesis. In the next session the statistical analysis will be discussed.

The statistical analysis of the live/dead cell biocompatibility tests quantitatively verified the fluorescence microscopy micrographs in the previous section. All the results were normalized to the corresponding CTPC slide, so the results not only can be compared to the controls but also they can be compared to each other.

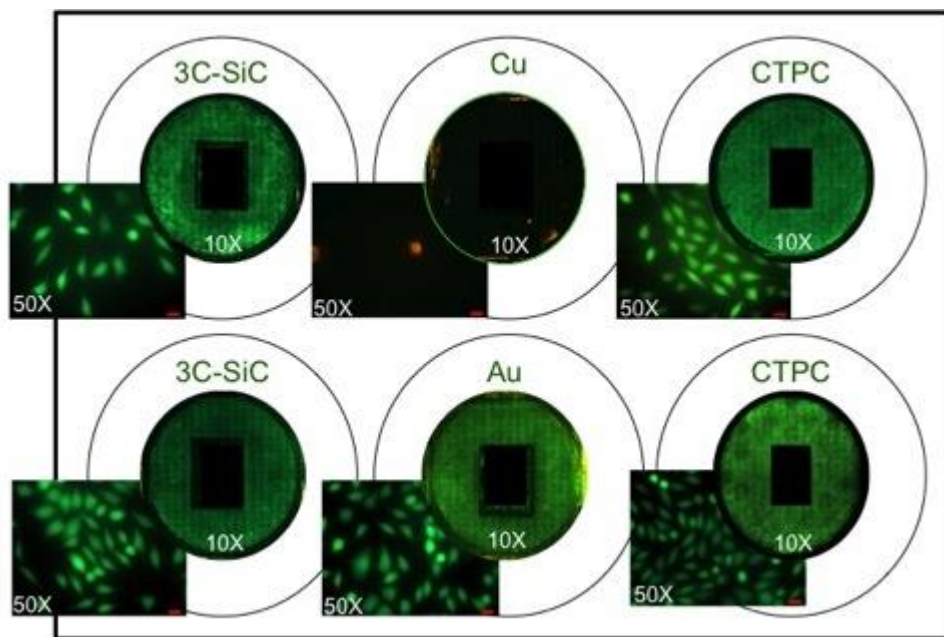


Figure 3.13: BAMBI method fluorescence micrographs of 3C-SiC, Cu as positive control, Au as negative control and 2 CTPC as baseline samples, from the wells at 10X and 50X magnification. Note that 3C-SiC displays outstanding in-vitro performance thus motivating the use of 3C-SiC as a negative control for additional experiments.

Figure 3.14 shows the quantitative statistical analysis of the live/dead assays for the control materials and test materials. The negative controls such as PE, Au and Pt had more than

90% of live cells in total (well + material), as expected. Also the positive controls such as Cu and PVC org.-Sn had less than 2% live cells in total.

The test results for 3C-SiC and type I *a*-SiC (500 nm of *a*-SiC on Si (100), same material as described in Chapter 2) are also presented. 3C-SiC grown on Si (100) shows an outstanding number of live cells and the results are comparable to the negative materials such as Au or Pt. But *a*-SiC showed 80% live cell viability which passes the test but less than the 3C-SiC viability results. More statistical data and discussion about the four types of *a*-SiC will be presented here.

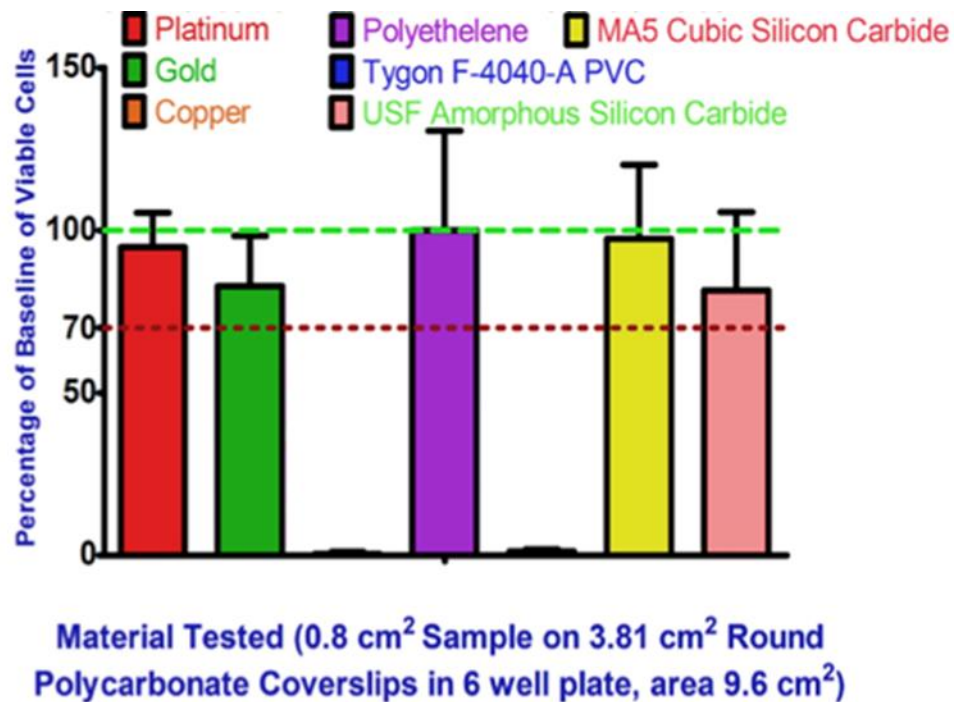


Figure 3.14: BAMBI method statistical analysis of control materials (Cu, Au, PVC org.-Sn, PE) and test materials (3C-SiC and *a*-SiC). Note that 3C-SiC and *a*-SiC pass the test with 3C-SiC having comparable behavior to the negative controls.

3.7. Summary

ISO 10993 provides a general protocol for testing the biocompatibility of materials. While this method is one of the best currently existing methods for testing materials it could not

solely fulfill all the demands for the biomaterials testing and it requires some complementary methods, one of which has been introduced in this chapter – the BAMBI method.

In this chapter first the extract test, which is a part of ISO 10993-5, was used to evaluate the cytotoxicity of the control materials including PE, Au as a negative control and PVC and Cu as positive controls; and test materials including Si (100), SiO₂, *a*-SiC, 3C-SiC and W. Although the extract method showed promising results we must consider that this method evaluates the indirect effect of leached chemicals on the cells and does not give any information about cell/material direct interaction.

In section 8.3 of ISO 10993-5 a method was introduced as the direct cell test. This method was also tested on control materials and the results were not as expected for these materials. Since the material was placed above the cells, the cells cannot tolerate the weight of the material and will die eventually, and since the material is placed face down it is not clear that the cell died due to the leaching of the ions from the deposited film or from the substrate material itself, which was fully exposed in this method.

In the literature a method was introduced that uses direct cell seeding on the sample to evaluate the cytotoxicity, and this method was described as seeding method in this chapter. The cells on the material were analyzed after 96 hours. Although this method is a better method to study the cell/ material interaction, we have to consider that in this test we study the cell/ material permissiveness and not the cytotoxicity. As was shown in this chapter the PE sample (insulator negative control) that was introduced by ISO as inert material; did not show any cell attachment but we know from the ISO standard and other experiments that PE is an inert non-toxic material. So the necessity of the design of a method that has all the advantages of ISO method became apparent and was undertaken.

Due to this concern a method, named the BAMBI method, was developed at USF to evaluate the cytotoxicity and cell permissiveness at the same time and was shown to overcome all of the drawbacks of the other methods in ISO 10993. The results of BAMBI test were checked with the already published results of other tests, and no contradiction observed. Indeed direct seeding and extract tests were separately performed and the data completely correlated with the BAMBI method (except for the issue described above for the direct seeding method and the mechanical cell damage observed).

By testing a material from both a stability and biocompatibility point of view the premedical tests are almost completed as specified in ISO 10993. But we must consider that these two characteristics are required but they are not sufficient. In addition to stability and nontoxicity the biomaterial must have a good interaction with blood. It is obvious that a material cannot be implanted in the body and not contact with any blood vessel. Since the biomaterials are implanted to improve the quality of life for the patient and not increase their suffering the implant material must not cause any blood coagulation. In Chapter 4 the hemocompatibility of the materials for pretrial *in vivo* will be discussed thus completing the battery of tests required by ISO 10993 to qualify a biomedical device for clinical trials.

CHAPTER 4: HEMOCOMPATIBILITY OF BIOMATERIALS

In the last two chapters the chemical stability of materials in physiological environments and the cytotoxicity of these same materials were reported. In addition to those characteristics implantable materials must be compatible with blood. To emphasize the importance of hemocompatibility, just in the brain alone there are 500 miles of blood vessels [67], so when a prosthetic device is implanted in brain tissue interaction with a vascular vessel is not only probably but inevitable.



Figure 4.1: Human brain and neck blood vessel network (i.e., brain vasculature) [67] showing how dense is the brain vasculature. Clearly any neural implant will subtend a blood vessel thus making the hemocompatibility of biomaterials an important property of implantable devices. Image Copyright belongs to © to-BBB, permission obtained from © to-BBB and presented in appendix A.

The brain vasculature system is illustrated in Figure 4.1. It can be seen that the network of blood vessels is packed densely so any foreign object which is implanted in a patient's head must not cause any thrombosis when it contacts a blood vessel [68, 69]. As a part of the premedical evaluation of implantable biomaterials and devices performing a test that can determine the blood compatibility (i.e., hemocompatibility) is necessary. Embolic problems with catheters, failure of biosensors due to thrombus accumulation and platelet activation on long-term implants are just a few examples of the problems that may occur if an implantable biomaterial is not hemocompatible [70].

In the literature, which has been focused on the topic of blood compatibility, researchers try to answer the following questions:

- How can blood compatibility be measured?
- What materials can be called 'hemocompatible'?
- What is the biological basis of the reaction of materials with blood [70]?

Based on these questions, in this chapter the focus is on both a hemocompatibility methodology and materials evaluation. The minimum requirements for hemocompatibility measurements are mentioned in section four of ISO 10993. Based on ISO 10993-4 we describe an experiment we designed to evaluate the blood compatibility of the materials both in the static and dynamic state.

The first step was to understand the thrombosis model, then to develop the experimental methods and finally to select the experimental controls based on the current information present in the ISO. Statistical data (mean value, standard deviation, 95% confidence interval) must be the experimental outcome of any hemocompatibility assessment. Tests have to be performed with a

minimum delay of usually 2 hours since some properties of blood change rapidly following collection. Various conditions (depending on the wall shear rate) were simulated within the circulation system (i.e., dynamic testing). The qualities and aspects of hemocompatibility that can be analyzed are platelet activation, oxidative burst, hemolysis, fibrinolysis, fibrin formation, generation of thrombin, contact activation, and complement activation [18]. In this chapter the major focus is on platelet activation in the dynamic state. The results were entered non-dimensionally into a non-dimensional score system, where 0 points stand for the best and 100 points for the worst experimental outcome. The goal was to find a good correlation between the total platelet activation score in the high shear stress system. Before explanation about the circuit design some basic flow dynamics phenomena about human physiology must be explained [16, 22].

4.1. Flow Dynamics

The blood flow in veins, arteries and capillaries can be considered as a laminar flow which is consisted of parallel streamlines in the rigid tubes. Since the blood flow is considered as a laminar flow the thin blood layer which is in contact with the blood vessel can be considered as a steady layer without any velocity. The velocity in the center of the blood vessel has the highest value. Figure 4.2 shows the flow gradient within a blood vessel. A flow which has a velocity lower than the critical velocity is called the laminar flow and if the velocity is equal or higher than the critical value it is called the turbulent flow. The turbulent flow normally generates sound on the other hand the laminar flow is silent, the sounds created by the turbulent flow is called a bruit and is so useful in medical sciences.

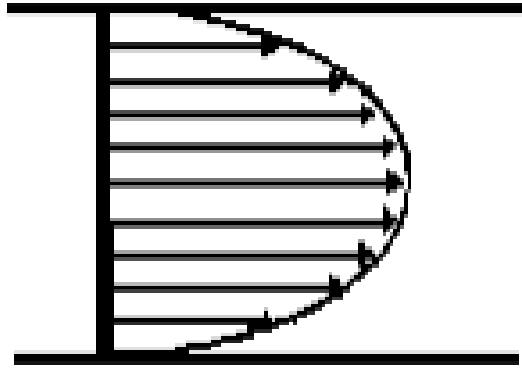


Figure 4.2: Velocity vector distribution of a laminar flow pattern in a tube geometry. Zero velocity occurs on the blood vessel walls and a maximum flow occurs in the blood vessel center, as shown.

There are two parameters that affect the probability of turbulence flow occurrence first is the radius of the tube and second is the viscosity of the blood. The mathematical relation of the inertial ratio to viscous forces is a unit-less number called Reynolds number which can specify the probability of having a turbulence flow [20, 71]. The magnitude of the Reynolds number has a direct relation with the probability of turbulence; the increase in value of the number will result in increase of value of probability.

In humans, by the time of constriction in the artery and when the maximum systolic ejection occurs the blood flow becomes a turbulence flow and the velocity value is more than critical velocity value [17, 72]. In the patient with anemia due to lower blood viscosity the Reynolds number increases so the probability of the turbulence flow increases and they will have systolic murmurs [17].

At the time of study the flow dynamic recognizing the difference between the velocity that is defined as displacement in unit time (e.g., m/s), and the flow, which can be defined as moved volume per unit time (e.g., cm^3/s). The value of the flow (Q) is equal to Velocity (V) multiplied by cross-sectional area of the tube (A), the following equation is showing the value:

$$V = Q/A.$$

In the tubes network such as human vascular system the total cross-sectional area of the blood vessels has an inverse effect on the average blood velocity at that specific point. For example the average blood velocity in the aorta is higher than the capillaries which has the slowest velocity due to a larger total cross sectional area. It must be kept in mind that the diameter of an individual capillary is smaller than the aorta but the total cross section of the capillaries is 1000 times larger than the value for the aorta and in blood flow the total cross section is considered not the individual cross section. When the blood enters the veins the velocity increases but it is not as fast as the aorta.

The average velocity of blood is 40 cm/s in the aorta, also the maximum velocity occurs in systolic state which is 120 cm/s and the same value but with opposite direction happens in diastolic state.

4.2. Chandler's Loop

A useful test configuration was developed by Chandler in 1958 to measure blood-clotting times [7]. The Chandler's loop system consisted of a tube that was filled 70% of its capacity with blood and connected with a silastic collar to close the loop, the circuit was tilted at 45°. The tube was rotating till the blood clot in the tube, the time that requires to form a blood layer on the surface and form the blood clot was the goal of his initial study [73].

In recent years, the Chandler loop system has been modified for anti-coagulated blood to measure biomaterial-induced platelet activation [8]. The most noticeable modification in the chandler's loop is the increase of surface-area-to-blood-volume ratio which will result in the reduction of background noise. Even with the modifications in the Chandler's loop the presence

of air bubbles which cause blood-air interface is a major drawback in this method of evaluating the hemocompatibility of the materials. Presence of blood-air interface could result in protein aggregation which will result in platelet activation. In the empirical experiments presence of even microscopic air nuclei resulted in increase of platelet adhesion and activation of them afterwards [42].

4.3. Current Design

These experiments were designed to use a modified Chandler's loop. The loop consists of a peristaltic pump, 0.2" (5.08 mm) diameter S-50-HL PVC Medical Surgical Tubing, Clear (Tygon) tubing (the surgical grade PVC provided by Tygon is different from the fuel PVC tubes that contain organo-tin and used as positive control in chapter 3), a sample holder, polymeric gasket and a vacuum system as shown in Figure 4.3 below. The circuit was placed inside a 1 m³ polyethylene chamber including an electrical heater which maintains the temperature at 37±1 °C. The system is housed in the Pathology & Cell Biology Laboratory of Dr. K. Muffly, USF Morsani College of Medicine.

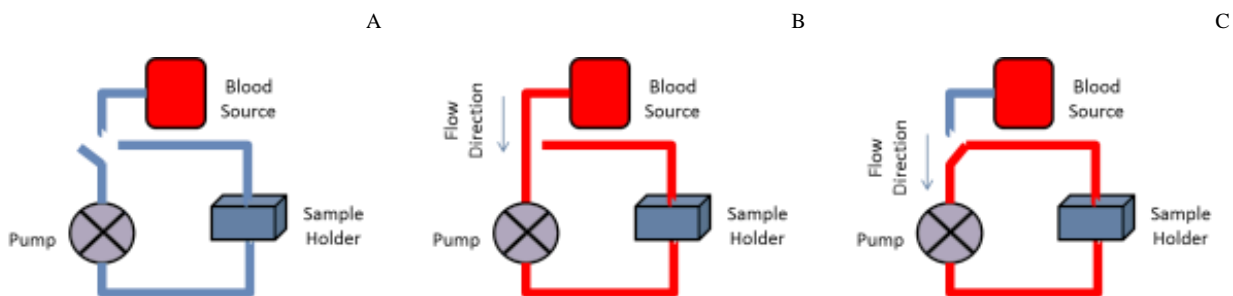
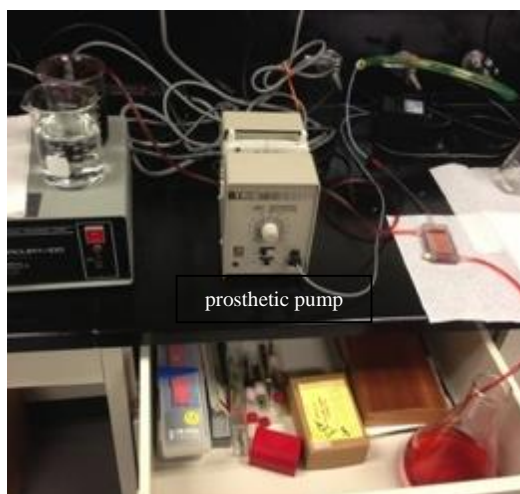


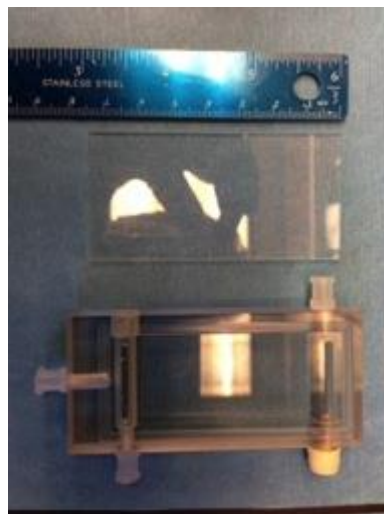
Figure 4.3: The schematic of the modified Chandler's circuit design in A) stage 0, the circuit is open and the tubes were rinsed with PBS B) stage 1 the circuit is still open but the blood source is connected and C) stage 2 the circuit is closed and the tubes are completely filled with PRP.

The sample size was originally 50 x 75 mm. A new sample holder was designed using solid works and printed using the USF SiC Group 3D printer (using nylon). The sample size

from the new design is 10 x 30 mm which was done to conserve area and reduce materials cost, especially for the SiC samples. Once the new system passed the leaching test it replaced the old one. Figure 4.3 (right) shows the initial sample holder.



Test set up in USF College of medicine



Sample Holder

Figure 4.4: The current dynamic hemocompatibility test set up in Dr. Muffly's lab in the USF College of Medicine (left). The original sample holder, which can accommodate large 50x75 mm samples (right).

Figure 4.4 shows the new sample holder design. The left figure shows the 3D-printed sample holder, the center figure is the solid works™ design and the right one is the sample holder which was machined out of Teflon. Due to surface roughness issues, which disturbed the fluid flow during prototype testing, it was decided to machine a block of Teflon instead of using the 3D printed nylon cell. The Teflon cell will be used for all subsequent experiments presented in this chapter.

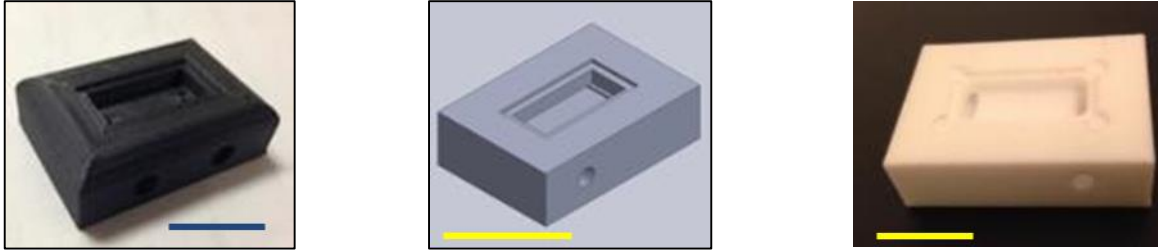


Figure 4.5: Design and fabrication of a new, more cost-effective sample holder. USF SiC Group 3D printed nylon cell (Left), solid-works schematic (center), the sample holder machined out of Teflon by the USF engineering machine shop (right). The scale bars have the length of 2 cm in all the images.

4.4. Method and Materials

The test materials were: Si (100) from University wafers Lot 567434, 3C-SiC grown in University of South Florida SiC Group hot-wall CVD reactor MF2 (sample ID USF2-14-28), *a*-SiC deposited via PECVD on Si in the USF NREC, Polyethylene (as negative control) and PVC (tygon) (as positive control).

4.4.1 Platelet Rich Plasma (PRP) Preparation

Farm pig blood was provided by the University of South Florida's Center for Advanced Medical Learning and Simulation (USF-CAMLS) labs under Institutional Animal Care and Use Committee (IACUC) certification (protocol ID: T IS00000216). The blood was collected post mortem by the CAMLS lab technician in blood bags including acid citrate dextrose (ACD) as an anticoagulant (1:9 ACD: blood volume ratio). The blood bags were stored in a portable refrigerator at 4°C and transported to the IDRB 313 Lab using a portable refrigerator at 4°C. Next 50 mL ACCUSPIN™ centrifuge tubes were filled with 45 mL of whole blood. The tubes were centrifuged at 4°C for 10 min at 1000 g. As shown in Figure 4.6.a the blood consists of three phases after centrifuge, 55% of total blood is the plasma which will be above the other layers due to its lower density; the buffy coat which includes leukocytes and platelets form 1% of

whole blood and is located between the plasma and Erythrocytes layers; the Erythrocyte layer has the highest density and will be the under the two other layers after centrifuge. In Figure 4.6.b the whole blood sample after centrifuge is shown. Due to the presence of the membrane in the ACCUSPIN™ the plasma, leukocytes and platelets phases were not mixed with the Erythrocytes and form a type of media that had a high concentration of the platelets. The PRP was collected in the 50 mL conical centrifuge tubes and stored in the refrigerator at 4°C. The concentration of platelets in the PRP was measured using a hemocytometer and it was found to be ~150,000 platelets per 1 μ l.

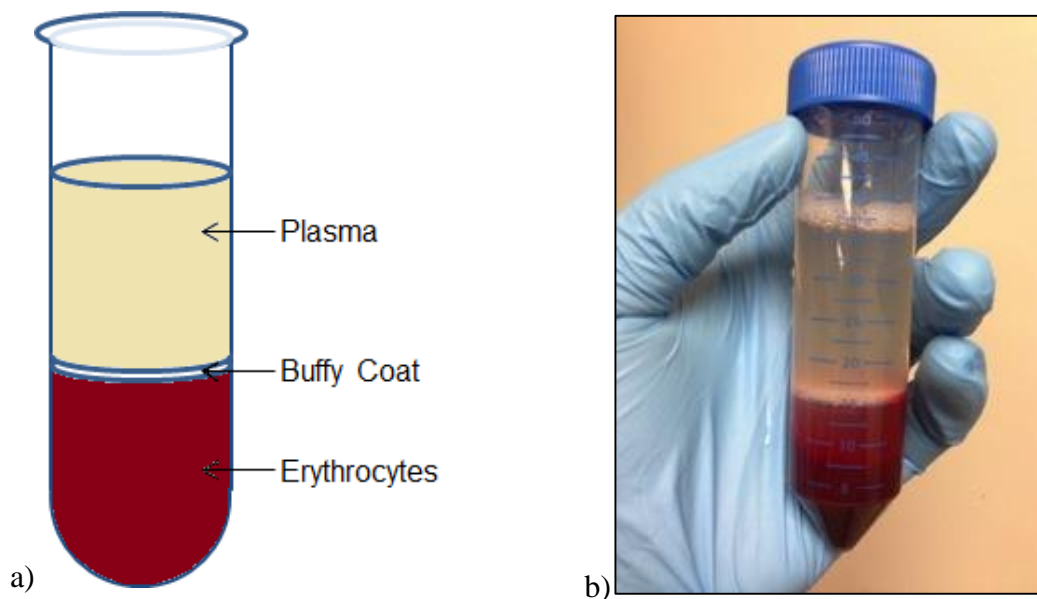


Figure 4.6: Formulation of PRP for hemocompatibility testing. a) Schematic that shows the three phases of the blood after centrifuge b) The 50 mL ACCUSPIN centrifuge tube including the separated PRP and Erythrocytes phases. The PRP is the nearly clear liquid layer on top of the two red layers below.

The PRP was then transported to the Pathology & Cell Biology Laboratory of Dr. K. Muffly, USF Morsani College of Medicine (transit time ~20 min) where it was used to test the platelet interaction with various materials as outlined above.

We can determine the PRP velocity directly from equation (4.1) (i.e., $V=Q/A$). By measuring the flow Q and knowing the cross-sectional area the velocity V can be determined. Based on the velocity we can control the flow to be laminar or turbulent.

The flow rate was measured right before and after the sample holder. The tube area is 0.2 cm^2 , so the flow must be less than $8\text{ cm}^3/\text{s}$. So we have adjusted the pump in a way that the flow that enters the sample holder is equal to the flow that exits the sample holder and is less than $8\text{ cm}^3/\text{s}$. When we did this measurement, the PRP was replaced with 100 mL of fresh PRP, the flow cell tubing filled, and the flow initiated with a syringe by hand. When the tube was filled and air bubbles were minimized the two ends of the tube were connected to have a closed loop flow system (Fig. 4.3 b). The pump ran for 15 min and the sample under test retrieved for platelet fixing and subsequent microscope analysis.

Platelet activation was evaluated by using fluorescence microscopy as described by N. Schettini of the USF SiC Group during her static hemocompatibility tests of SiC materials [22]. Her sample preparation involved $1\text{ }\mu\text{L}/\text{mL}$ Rothamin solution in 1X PBS which was used as the fluorescent dye, and the micrographs were analyzed using image J analysis software. Surface changes were evaluated using SEM and AFM analysis after platelet removal and sample cleaning. In that work it was demonstrated that 3C-SiC had superior hemocompatibility to 4H- and 6H-SiC, as well as Si, via the observation of significantly lower platelet adhesion and activation [74]. Indeed the work reported by Schettini was the basis for the dynamic work reported here, as a more realistic model of the physiological environment is a more reliable measure of a materials compatibility with blood.

4.5. Static Hemocompatibility Experiment

The hemocompatibility of semiconductor materials and specifically silicon carbide in the static state was studied by Schettini in 2009 [22] and 3C-SiC showed a promising result in those experiments. So in this set of experiments the hemocompatibility of Si (100), 3C-SiC, SiO₂ and *a*-SiC were evaluated when the flow rate was equal to zero cm³/s to achieve two goals: first to study the platelet adhesion to the surface when the shear forces are not present, and second to have a comparable result to the previous studies.

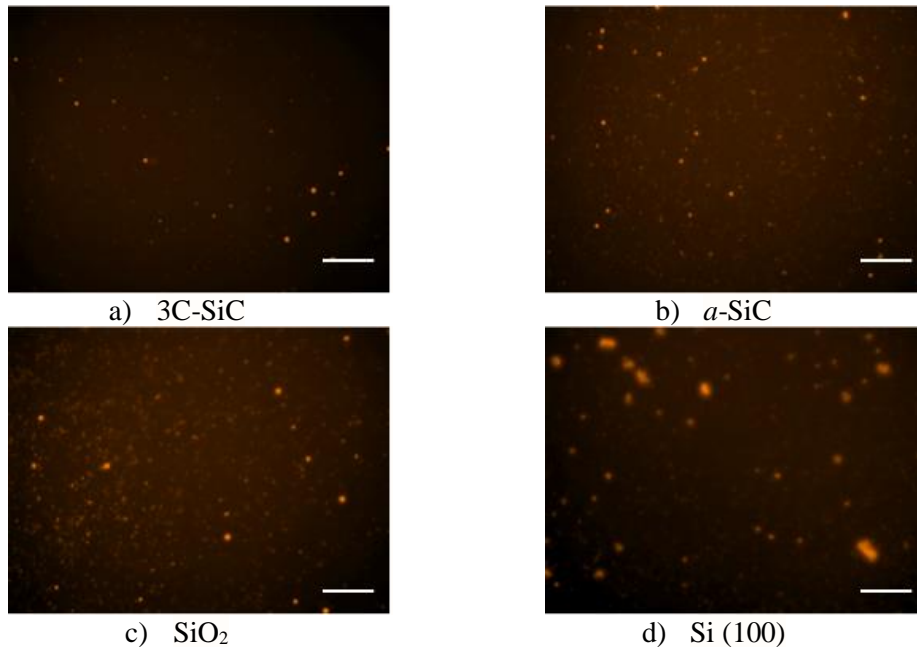


Figure 4.7: Static hemocompatibility test fluorescence micrographs using Rothamin as a fluorescence tag at 50 x of magnification. a) 3C-SiC b) *a*-SiC, c) SiO₂ and d) Si (100). Scale bar is equal to 100 μ m.

As shown in Figure 4.7. a) the 3C-SiC fluorescence micrograph shows little platelet activation. By comparing this result with the *a*-SiC micrograph in 4.7. b) and Si (100) in 4.7. d) it can be concluded that 3C-SiC showed an acceptable hemocompatibility in comparison to the other two silicon based material that are already used in prosthetic devices. Also SiO₂ was tested as positive control and to show that the test is working. As it can be seen in Figure 4.7. c), the

platelets were completely activated on the surface of SiO₂ which verifies the role of glass as a positive control for blood compatibility.

The statistical analysis was performed on the results of hemocompatibility test. The bar chart including the standard deviation as the positive error bar is illustrated in Figure 4.8. The ANOVA analysis showed the value of 4.1 for “F” which is higher than the 3.4 value for F_c. This means that the samples behaved significantly differently. Also by doing the paired t-test on the results we can conclude that 3C-SiC showed the lowest platelet activation, *a*-SiC had more platelet activation than 3C-SiC and Si (100) showed higher values in comparison to the first two samples. The SiO₂ showed the highest value of platelet activation among the tested materials.

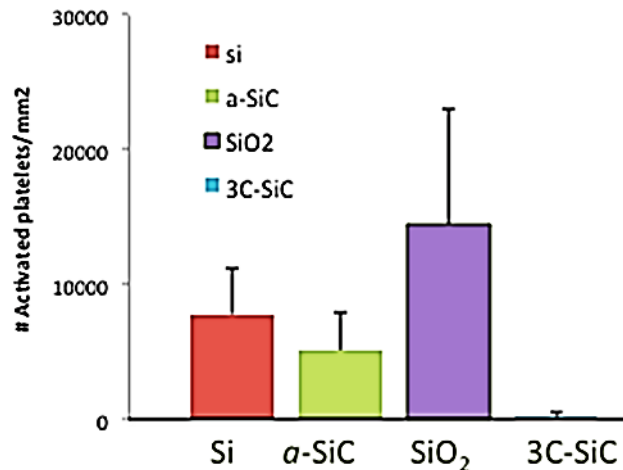


Figure 4.8: Static hemocompatibility histogram of platelet activation of the Si, a-SiC, SiO₂ and 3C-SiC in static hemocompatibility test using standard deviation as the error bar. Activated platelets per mm² used to evaluate the hemocompatibility of the materials.4.6 Dynamic Hemocompatibility Experiments.

The hemocompatibility of the biomaterials were tested in a dynamic state to simulate the real conditions of the *in vivo* environment. Tests in a static state showed a promising result but to verify the performance of a device for biomedical applications it must be tested in more realistic

environment. Applied shear forces to the blood proteins could alter the platelet adhesion to the surface of implanted samples. Therefore a study of the effect of various flow rates and exposure time on platelet binding and activation is very important. The samples for the dynamic experiment were 3C-SiC, α -SiC, Si (100) and SiO₂ thin film.

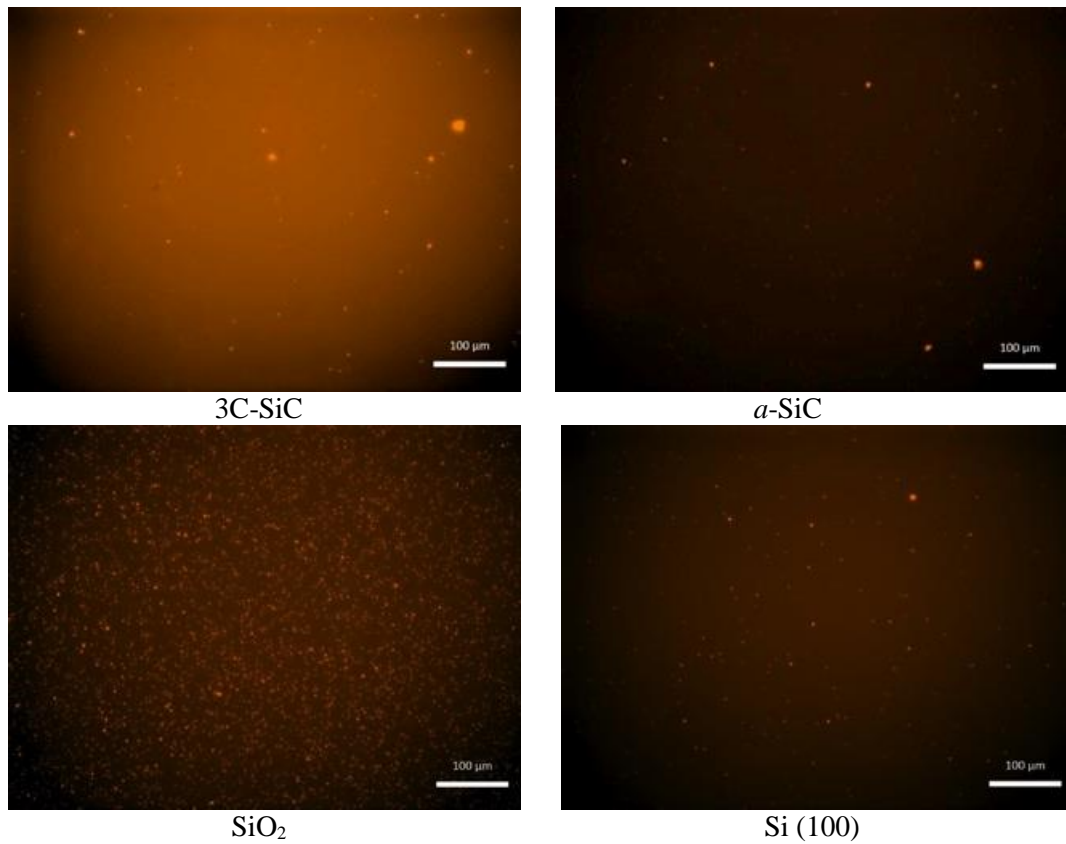


Figure 4.9: Static hemocompatibility test fluorescence micrographs using Rothamin as a fluorescence tag at 50 x of magnification. a) 3C-SiC b) α -SiC, c) SiO₂ and d) Si (100). Scale bar is equal to 100 μ m.

Figure 4.9 a shows the fluorescence micrograph of 3C-SiC after dynamic hemocompatibility testing with the rate of less than 8 cm³/s for 15 minutes. As can be seen in the figure the 3C-SiC samples showed the lowest platelet activation. The platelet activation was

higher on α -SiC in comparison to 3C-SiC and also Si (100) (Figure 4.9.d) which showed higher platelet activation in comparison to the first two type of materials.

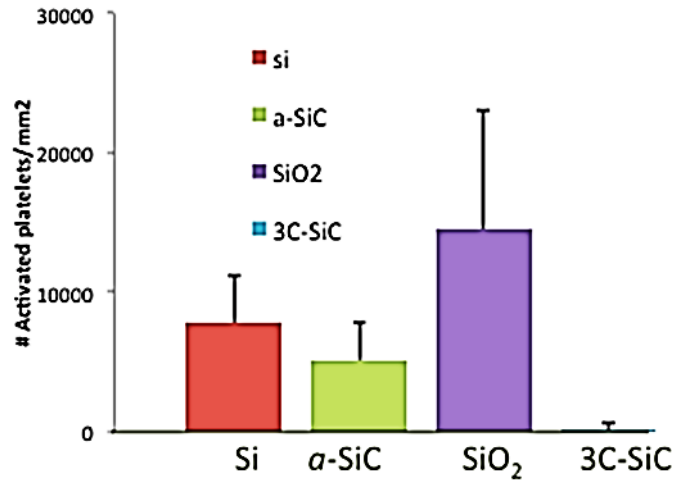


Figure 4.10: Dynamic hemocompatibility histogram of platelet activation of the Si, α -SiC, SiO₂ and 3C-SiC using standard deviation as the error bar. Activated platelets per mm² used to evaluate the hemocompatibility of the materials.

The qualitative data of Figure 4.9 can be more meaningful when statistical analysis was performed on the obtained data. Figure 4.10 shows a histogram including the data standard deviation as error bars. Two important points can be understood from the statistical analysis of dynamic test. First, the platelet activation decreased when a shear force was applied to the cells in the flow even for the laminar flow conditions of the test. The activation of the platelets decreased by a factor of 9% when the materials were tested under laminar flow. Second point that can be understood from Figure 4.10 is the performance of the materials. The materials behaved the same way in the dynamic test as they behaved under a static state.

4.7 Summary

In the last two chapters the stability and cytotoxicity of biomaterials were studied. In this chapter the blood compatibility of biomaterials under the static state and under laminar flow

using PRP was studied. A modified Chandler's loop was used as the blood circuit. The platelet activation as a measure of hemocompatibility was studied using fluorescence microscopy. The data obtained from the static test verified the previous work reported using the same method by Schettini in 2009 [22]. That is that 3C-SiC showed lower platelet attachment and activation in comparison to conventional implant materials such as Si (100), α -SiC and SiO₂. The obtained result from dynamic testing under laminar flow had the same performance as the samples in static state, but 9% lower platelet attachment, on average, for almost all samples tested. While this preliminary dynamic flow data is encouraging we need to study the performance of the materials in various flow rates and time frames to fully understand the hemocompatibility of a particular material (see Chapter 6 Future Work).

CHAPTER 5: SILICON CARBIDE NANOWIRES AS A BIOMATERIAL

We have discussed the preclinical evaluation of biomaterials and prosthetic devices in the last four chapters where we have outlined a methodology fully consistent with ISO 10993 and also suggested an alternative method (i.e., the BAMBI method), which can be used as a complement to ISO 10993. In this chapter we will study the biological properties of silicon carbide nanowires (SiCNWs) as a new biomaterial. In chapter 2 we have shown that SiC, both in cubic and amorphous crystallographic forms, has adequate corrosion resistance and chemical stability. In Chapter 3 we saw that SiC specimens (3C-SiC and *a*-SiC) passed the ISO 10993 cell viability requirement. So by knowing that SiC is a chemically stable material with a high degree of biocompatibility, the SiCNWs could be a new candidate for device fabrication, since it has all the advantage of SiC and also has enormous surface area in comparison to planar samples.

The goal of this chapter is to study the cytotoxicity and cell permissiveness of various types of SiCNWs and compare it to the results obtained from testing other materials. These tests give us the ability to determine the potential applications of SiCNWs to record from and stimulate neurons, as well as its potential use in biosensors. .

5.1. Silicon Carbide Nanowire Properties

Silicon carbide nanowires (SiCNWs) have become popular because they not only have the outstanding properties of silicon carbide, but also due to their small dimension, they can be used in applications where a high surface area to weight ratio is required. Silicon carbide under specific circumstances solidifies in various crystallographic structures called SiC polytypes [75].

One of the hexagonal polytypes, named 6H-SiC, is the most stable structure among the SiC polytypes from a thermodynamic equilibrium aspect. But the cubic form of SiC, 3C-SiC, is the most stable during low temperature growth; Thus 3C-SiC is the most abundant SiCNW structure. After SiCNW growth a thin layer of oxide and a carbon rich phase normally form on the surface of the wires [79]. Since the nanowire is a 1-dimensional structure enclosed in a continuous outer structure it can be considered as a nanocable rather than a nanowire. However the nanowire coating is a native oxide that does not have any effect on the properties of the material and can be removed by HF etching [76].

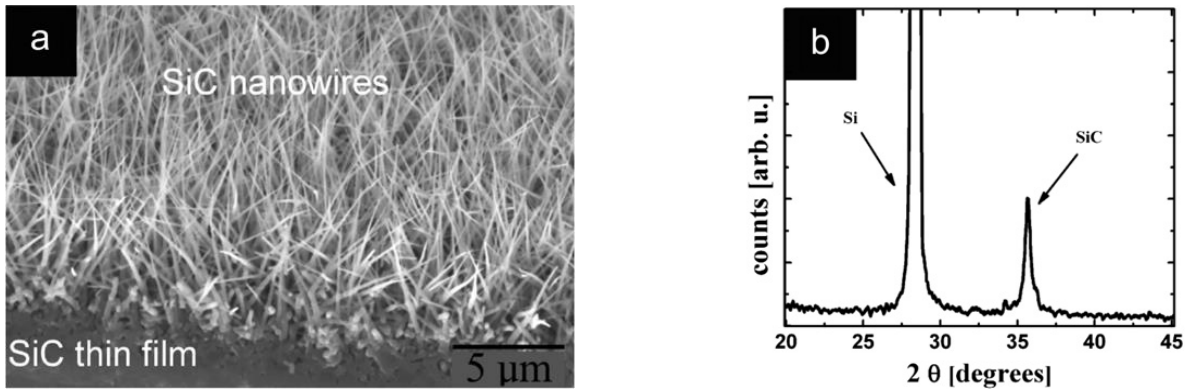


Figure 5.1: 3C-SiC NWs grown in UC Berkeley: a) SEM micrograph of Si(100)/3C-SiC substrate b) XRD spectrum of Si(100)/3C-SiC. The 3C-SiC on Si substrate [75]. Image copyright permission obtained from [75] and presented in appendix A.

Scanning electron microscopy is the most common method used to study the surface properties of the grown SiCNWs. Figure 5.1 a) shows some representative SEM micrographs of SiCNWs grown at UC Berkeley by J. Alper and L. Luna on a Si (100)/3C-SiC substrates. The SiCNWs were grown using the solid-liquid-solid growth method with Ni as the catalyst [77]. The SiCNWs have a straight structure with random orientations and small dendrites can be seen on the main stem of the wires. As can be seen in Figure 5.1 b) the presence of both silicon carbide phase and Si in the XRD spectrum is specified [75, 77, 78].

Another type of SiCNW is shown in Figure 5.2, which shows a curved structure of long wires attached to the surface of a Si (100) substrate. These wires were grown by P. Lagonegro of the Italian National Research Center, IMEM-CNR, affiliated with University of Parma via solid-liquid-solid method using Fe as a catalyst [79]. The average diameter of this type of nanowire was 20 ± 5 nm and the average length of 5000 ± 100 nm.

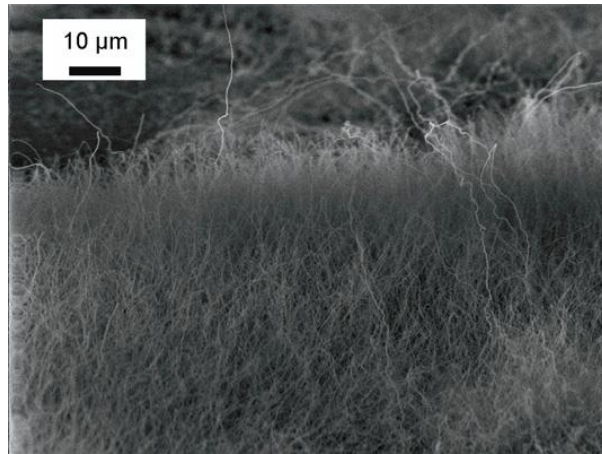


Figure 5.2: SEM micrograph of $\text{SiO}_2/\text{SiCNWs}$ grown directly on (100)Si in the IMEM-CNR laboratory, Parma, Italy, copyright permission obtained from [80] and presented in appendix A.

High-resolution SEM was used in the literature not only for evaluating the dimension of the SiCNWS but for determining the growth mechanism. This was done by inspecting the tips of the SiCNWs for the presence of the catalyst metals. As shown in Figure 5.3 a) the structure of SiCNWs transformed to a hexagonal prism and in Figure 5.3. b) a bamboo shape structure just by changing the reaction temperature from 1470°C to 1550°C and 1630°C , respectively. The results have been explained in terms of equilibrium shapes at each temperature [81-83].

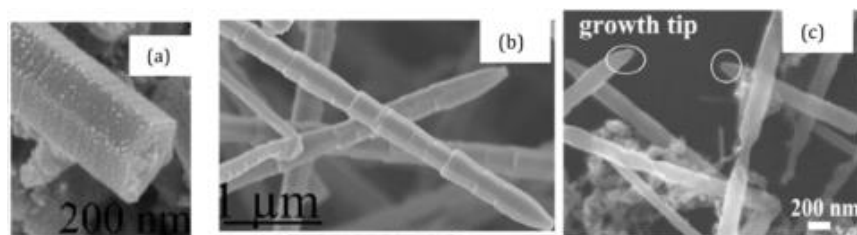


Figure 5.3: High resolution SEM micrographs of various structures of individual SiCNWs. a) hexagonal prism NWs, b) bamboo-like NWs, c) conical growth tips of cylindrical NWs. Copyright permission obtained from [81-83] and it is presented in appendix A.

5.2. SiCNW Fabrication Methods

In this section the methods that have been used to fabricate the SiCNWs will be discussed. Traditionally 3C-SiC nanowires were grown in the 1990's via the decomposition of organic silicon compounds, carbothermal reduction of silica and reaction between silicon halides and CCl_4 . Most of the conventional SiCNWs were thicker than 500 nm in diameter which made them less suitable for micro/nanoelectronic applications [76].

5.2.1 Conversion of C or Si 1D Structures to 3C-SiC

The first method of SiCNW fabrication that will be discussed here is the conversion of 1-D carbon fibers to SiCNWs. In this method carbon nano tubes (CNTs) were exposed to a Si-rich vapor formed by evaporation of SiI_2 or SiO with the result of the gas/solid reaction being the formation of SiCNWs. This method was used for the first time by Zhou and Seraphin [84] in 1994. The only drawback in this method is the large size of the SiCNWs, as described by Dai *et al.* with the diameter and length of these NWs being larger by one order of magnitude in comparison to CNTs [85]. But this problem was solved by them and they were able to produce SiCNWs identical to CNTs with a diameter of 2-30 nm [85].

Conversion of 1-dimensional Si structures to SiCNWs is the second method that will be discussed in this section. Growing 3C-SiC on Si by heating the Si substrate in the presence of a

carbon rich gas is very common but there are two factors that increase the presence of defects in this film: first there is the difference in thermal expansion coefficient of Si and C, and second there is the lattice constant mismatch between Si and 3C-SiC [86]. The accumulated strain can be released through lateral relaxation for SiCNWs so there is less concern about that in NW growth compared to thin film growth. Growth of SiCNWS from silicon nanowires (SiNWs) was reported by Zhang *et al.* in 2000 as a side effect when they were trying to form CNTs on SiNWs [87].

5.2.2. SiCNW Growth Based on the Vapor–Liquid–Solid (VLS) Mechanism

The VLS method process is the most developed process to grow the SiC nanowires. In the VLS method liquid phase catalyst is used to form an alloy with the substrate by increasing the temperature the alloy forms a supersaturated vapor phase which results in growth of the nanowirestructure. The only drawback in fabrication using VLS method is presence of catalysts on the tip of nano wires. Various growth configurations using the VLS mechanism have been employed for the SiCNW growth. In this work the silicon carbide nanowires grown in University of Parma used the VLS method using $\text{Fe}(\text{NO}_3)_3$ as liquid catalyst which formed an Fe-Si alloy on the surface and the islands for nucleation and growth of SiC nanowires [88].

5.3. Cytotoxicity Evaluation of SiCNWS

The SiC nanowire and SiO_2 nanowires samples provided by P. Lagonegro (of University of Parma- IMEM-CNR laboratory) were tested using the extract method, as described in Chapter 3. Figure 5.4 shows the assay results for the test materials. 100% of the media was replaced by the extract from the samples. Based on ISO 10993-12 the volume to area ratio for the thin films tested with less than 0.5 mm thickness is $6 \text{ cm}^2/\text{mL}$ and for the specimens with complicated

shape or porosity the ratio is 0.2 g/ mL. Using material mass instead of surface area for samples with a complex shape is reasonable since precise surface area measurement methods, such as Brunauer–Emmett–Teller (BET) method [3], are not available in most laboratories, so the ISO organization simplified the test and allows the use of mass / volume ratio in this specific exceptional case. So the first ratio 6 cm²/mL was used for the planar Si, SiO₂, *a*-SiC and 3C-SiC samples; and the 0.2 g/mL ratio was used for the nanowire samples.

As can be seen in Figure 5.4. the lowest cell viability was observed for the Si and SiO₂ samples, which is not unexpected since the presence of SiO₂ in a liquid for long times results in the formation of a weak acid called silicic acid [53]. This acid, even in low concentration, can cause cell death. To verify the formation of an acid in the presence of SiO₂ and Si, an independent experiment was performed. The samples were placed in the media for 4 days under the same conditions of the extract test but in a chemical hood, the pH was monitored continuously, the initial pH of 7.2±0.2 DMEM dropped to 6.7±0.2 after one day and to 6.4±0.2 after four days in the presence of the Si sample. The pH value for the SiO₂ sample was even lower and the pH after one day was 6.5±0.2 and after four days it was 5.9±0.2. Also a blank test tube including just the DMEM was monitored all the time and the pH was 7.3±0.2 after one day and 7.4±0.2 after four days, thus discounting any degradation in pH with time and temperature of the liquid media.

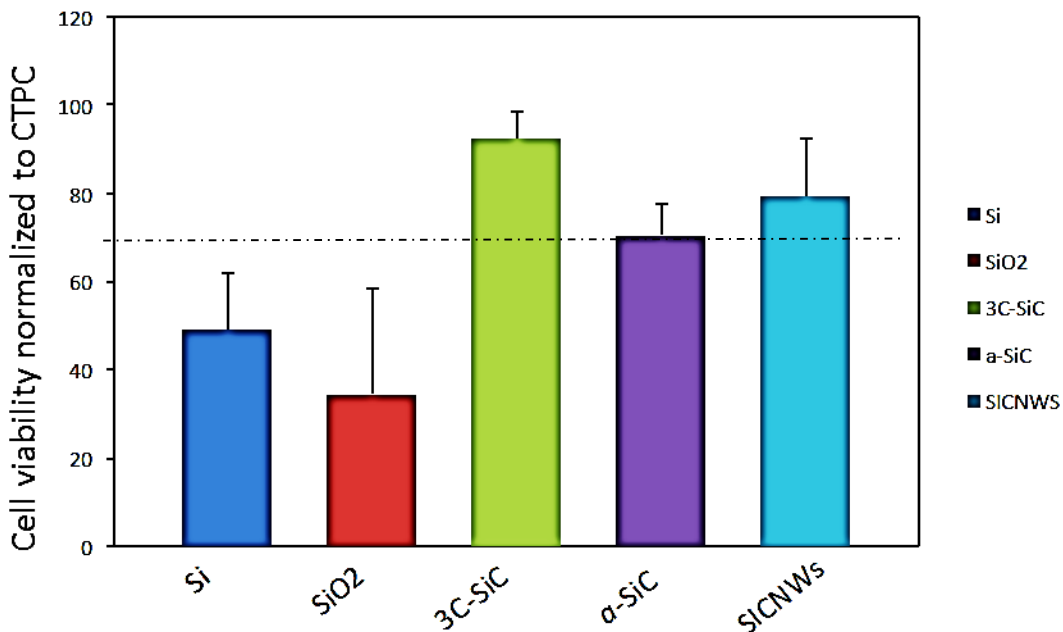


Figure 5.4: Histogram of the quantitative evaluation of semiconductor materials via extract method based on ISO 10993-5, after 24 hours on L929 fibroblast cells. Volume to area ratio for the thin films was 6 cm²/mL and for the NW specimens 0.2 g/ mL as specified in ISO 10993. The SiC NWs tested were provided by P. Lagonegro of University of Parma. In this data all SiC-based materials passed the test while Si and SiO₂ failed (less than 70% cell viability).

The cell viability for the SiCNWs is lower than 3C-SiC but it is higher than *a*-SiC. Since the expected structure of SiCNWs is the cubic form, ion release is not expected to be the reason for lower cell viability. Instead in the recipe for SiCNWs growth the presence of Fe as a catalyst is noticeable, so the lower cell viability may be the influence of the growth catalyst. But since it is chemically and crystallographically the same as 3C-SiC, a more stable structure is expected from it in comparison to *a*-SiC samples. A more likely explanation is that there may be residue in the NW matrix that was difficult to remove completely during NW sample cleaning.

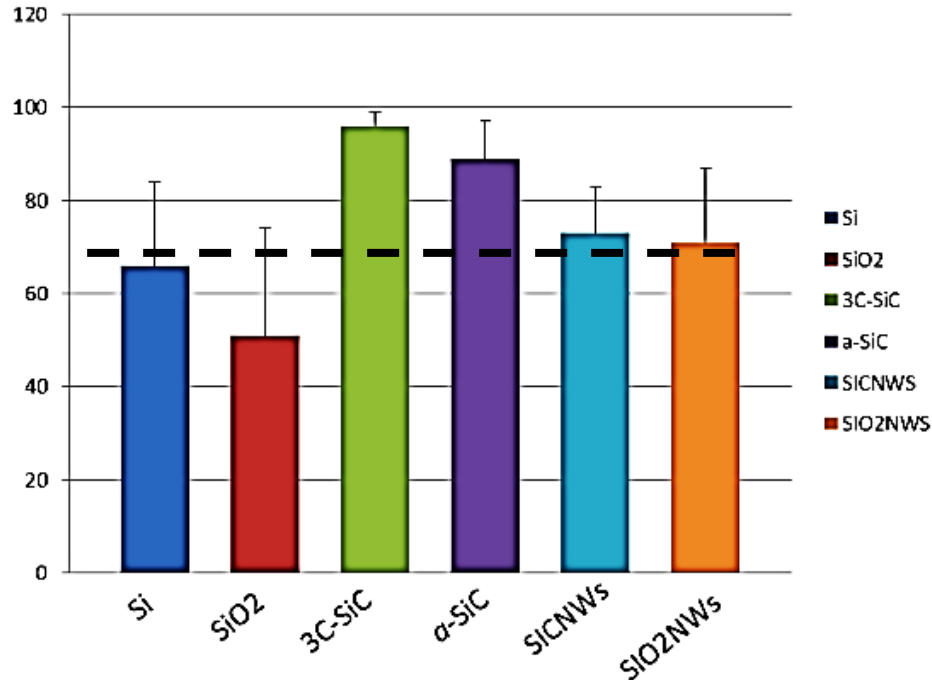


Figure 5.5: Histogram of the quantitative evaluation of semiconductor materials via MTT assays based on ISO 10993-5. This data is consistent with the extract method data (Fig 5.4) in that all SiC materials passed the test and planar Si and SiO₂ failed. It is indeed interesting that the SiO₂ coated SiC NWs passed the test, an observation under further study.

As an additional measurement MTT assays were performed on the wells that included the cells previously plated on the test samples. The cell culture time was 24 hours and 6×10^4 L929 cells were seeded on the materials. As it can be seen in Figure 5.5 Si and SiO₂ have the lowest cell viability among the tested samples and it can be explained the same way that was mentioned previously in the extract section. But since there was no shaking in this method the quantity of released ions and the concentration of formed acid is lower, so likely more cells survived the MTT assay.

5.4. Cell Adhesion on SiCNWS

Seeding cells directly on the material and the study of the adherence mechanism on them is the method that we used for studying the cell permissiveness on SiCNWs. Both L929 fibroblast cells and H4 Neuroglia cells were used to study the cell/material surface interaction.

The behavior of the cells on the control materials was reported in the previous sections. In this section the cell adhesion on Si, SiO₂ (film), 3C-SiC, *a*-SiC, SiCNWs and SiO₂NWs will be presented. Sample preparation and cell culturing was performed exactly as described in Chapter 3.

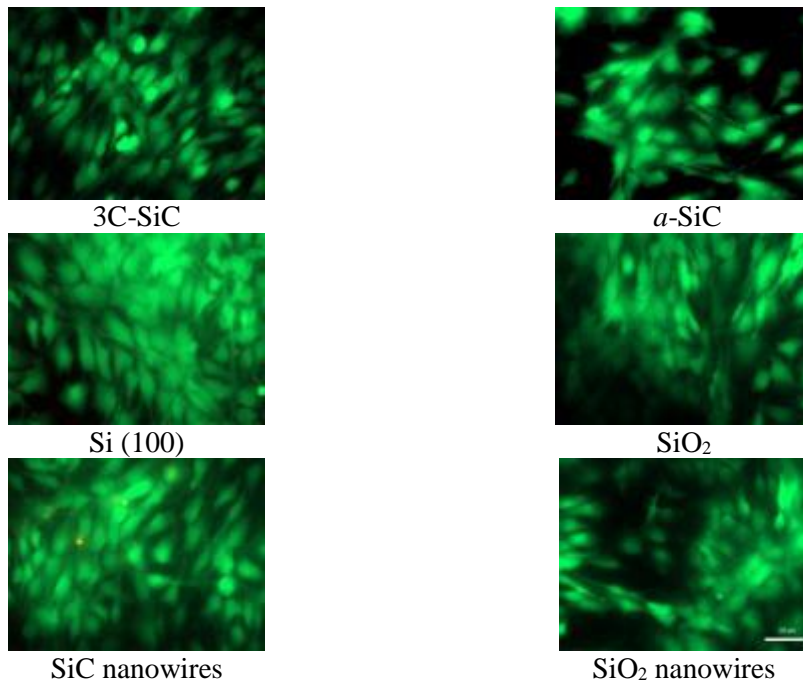


Figure 5.6: Fluorescence micrographs of H4 neuroglioma cell adhesion on a) 3C-SiC, b) *a*-SiC c) Si(100), d) SiO₂ , e) SiC nanowires f) SiO₂ nanowires.

The samples were extracted and analyzed via fluorescence microscopy. Generally the cell adhesion on silicon-based semiconductor materials is good, but we want to study this aspect within this type of semiconductor material family and find an alternative for Si, since Si showed less chemical stability in comparison to 3C-SiC and *a*-SiC.

Figure 5.6 shows fluorescence micrographs of H4 cells plated on various semiconductor materials. The cell adhesion on Si is shown in Figure 5.6 a). As can be seen the cells are attached very well to the surface but the cells are not confluent in comparison to the cells shown in figure 5.6 c) that shows the 3C-SiC samples. The SiCNWs in Figure 5.6 e) show good

adhesion but, due to the structure of the SiCNWs, there seem to be present an agglomeration of cells. This may be due to the cells being trapped in the network of the wires and not having any place to move to and grow. The agglomeration also can be seen in Figure 5.6 f) as well but cells on this surface had a lower survival rate due to presence of SiO₂.

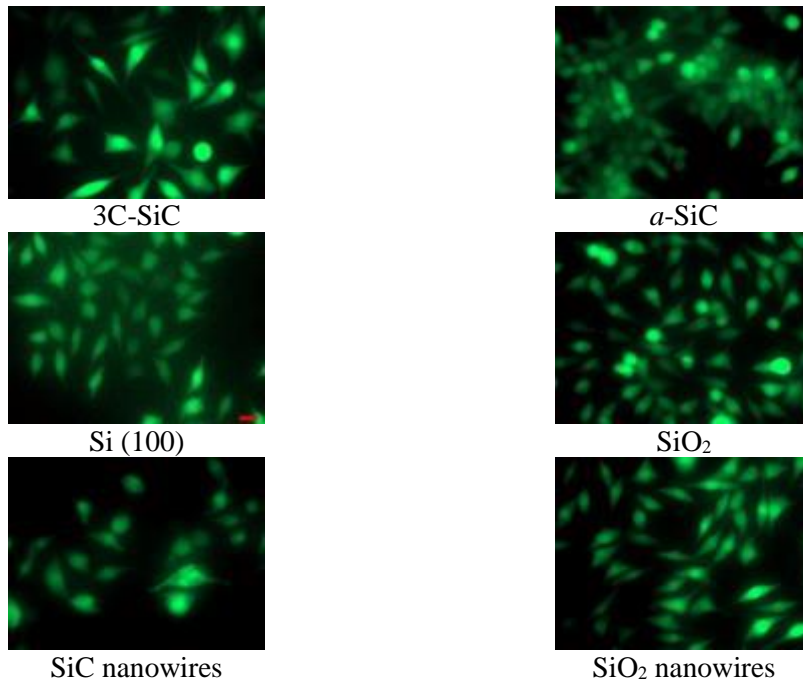


Figure 5.7: Fluorescence micrographs of cell permissiveness on semiconductor materials using L929 fibroblast cells. a) 3C-SiC, b) *a*-SiC c) Si(100), d) SiO₂, e) SiC nanowires f) SiO₂ nanowires.

In Figure 5.7 L929 cell permissiveness is shown, since one of suggested applications of the nanowires could be a tissue scaffold culturing fibroblast cells. The number of cells on Si was low, as expected, but the number of cells on the flat SiO₂ film was relatively high which was surprising. However if the micrographs are studied closely it can be seen that most of the cells have a round shape that can tell us the cells are actually dying, in our opinion due to the better hydrophilicity of the oxide layer in comparison to the bare silicon surface the number of cells attached to that surface is higher but when the samples start to release ions and silicic acid cell

survival is reduced. The better understanding of cell adhesion mechanism on the SiC nanowires requires further investigation.

In Figure 5.7 c) and d), it can be seen that 3C-SiC and *a*-SiC showed almost the same L929 cell permissiveness. In Figure 5.7 e), the fibroblast cells seem to not attach to the surface of SiCNWs, which is not expected but by studying the micrograph closely the cells appear to be healthy, the writer assumes that the stiff structure of SiCNWs network perhaps did not let the L929s form a colony and start to grow, because the fibroblast cells need to be in contact with each other to grow properly. On the other hand since the SiO₂NWs have a weaker structure so the cells can move around and find each other to grow better, which can be seen in Figure 5.7 f).

5.5. Summary

In this dissertation and also previous studies by our group, 3C-SiC showed great material stability, biocompatibility and hemocompatibility. In this chapter the biocompatibility of SiCNWs which have exactly the same chemical composition and almost the same crystallographic structure as 3C-SiC were tested.

The SiCNWs, due to their enormous surface area, can be useful in the design of sensors that require both high surface area and biocompatibility. The biocompatibility results using the extract and MTT methods for SiCNWs were compared to flat 3C-SiC, *a*-SiC, Si (100) and SiO₂. The SiCNWs showed higher biocompatibility in comparison to *a*-SiC, Si (100) and SiO₂ but lower biocompatibility in comparison to 3C-SiC. The decrease in biocompatibility can be due to small quantity of residues of Fe which was used as the catalyst during the growth of nanowires, or more likely the incomplete removal of chemical residues due to the intricate structure of the 3D NW matrix.

Further studies on the extract liquid that was in contact with the NWs should help to shed some light on the observed findings. Rinsing with 0.1 HCl after growth can be an alternative for removal of the remained catalysts, and other methods can be employed to further understand these very preliminary results. Nonetheless the observed cytotoxicity assays show that SiC NWs did indeed pass the ISO 10993 tests which are very promising for this material system.

CHAPTER 6: SUMMARY AND FUTURE WORKS

6.1. Summary

The challenge of modern implantable biomaterials is the long-term functionality in-vivo whereby both the device is able to continue functioning while the surrounding biological material is not affected. The difficulty is two-fold for this ambitious goal – to realize truly bio- and hemo-compatible materials, and to have the proper means to assess the performance and predict long-term performance. The goal of this research was to develop the proper methodology to address the second issue, while helping to further provide evidence that 3C-SiC, and its associated materials, meet the first issue.

To state it differently, we are trying to achieve two goals by doing these experiments. First to develop an experimental methodology that can determine all the characteristics required for the invasive neurological implant; second, to continue to evaluate 3C-SiC, *a*-SiC (four formulations) and SiCNWs as alternative materials for neurological implants since conventional materials do not show long-time durability with a maximum reported in-vivo operation of 4 years reported to date in the literature.

The immersion test in a simulated electrolyte mimicking the neutral pH of 7.4 ± 0.2 in 1X PBS, Tris-HCl, ACSF and Artificial Plasma (including the albumin) for 96 hours and 30 days at 37°C and 60°C was done on control materials, 3C-SiC, *a*-SiC, Si (100) and SiO₂. The AFM and SEM data sets were completed for all of these materials. The test materials, which failed to resist

the neutral pH, were eliminated and the test was continued with the chemically stable materials. The citric acid challenge was conducted based on ISO 10993-15 and as described in the text in Chapter 2. The failed materials were screened and the last acid challenge, which was nitric acid resistivity, were done on them.

Based on previous works that have done by the USF SiC group since 2007, 3C-SiC showed promising biocompatibility and hemocompatibility, the MTT cytotoxicity assays were done by Colletti *et al.* in 2007 [12], direct cell plating done by Frewin *et al.* in 2009 [14] and hemocompatibility evaluation was done by Schettini in 2009 [22]. During the last two years the live/dead assays based on the extract method and the new BAMBI method were performed on control materials and 3C-SiC samples. These results verified previous works of the USF SiC group. Complementary tests on Si (100), tungsten and 4 types of *a*-SiC based on the extract and new BAMBI method were done to complete the experiments. Also hemocompatibility tests were performed in a dynamic state on the materials, which had passed all of the chemical tests and biocompatibility tests. This is the first time that a fully comprehensive battery of tests have been performed on an important material system, namely material stability, biocompatibility (both cytotoxicity and material permissivity) and hemocompatibility. 3C-SiC and *a*-SiC passed all tests with flying colors which, once again, demonstrates the potential of this important material system for advanced biomedical devices.

6.2 Future Works

Materials degradation was discussed in Chapter 2 of this manuscript. The most important test to evaluate the degradation of a material is the potentiodynamic test. By knowing the primary information about the degradation of a material; a complementary potentiodynamic test can be used to evaluate the corrosion current, passive potential and break down potential of the

material, and can thus give us valuable information. First to determine the corrosion resistance, second to evaluate the material for possible use as a biosensor. Testing the impedance and also open circuit potential can be helpful as well. Also the potentiodynamic test can be done in the presence of albumin which is the most common protein in human body. For a more in-depth understanding of material stability in-vivo it is recommended that potentiodynamic tests be performed so that feedback can be provided to the material developer to improve their material performance.

The cytotoxicity assays have shown that some materials were releasing ions, which cause toxic effect on the cells. But the identity of these ions is, at present, unknown. In addition the critical concentration for each ion that can cause the death of the cells is also unknown. Study of the leached liquid from the materials with chemical methods such as inductively coupled plasma mass spectrometry (ICP-MS) and attenuated total reflection- Fourier transform infrared spectroscopy (ATR-FTIR) could be valuable as well and should be considered for especially promising biomaterials.

In Chapter 4 we determined the hemocompatibility of some candidate materials using Platelet Rich Plasma (PRP) by studying the platelet activation on surfaces exposed to PRP in a dynamic flow condition. To have a realistic evaluation of the hemocompatibility a study of whole blood, or perhaps a more complex blood solution containing PRP as the main component, can be studied.

Study of the neurotoxicity on the materials and devices should be done for materials that have potential application as neuroprosthetics. Therefore specific neurological environment testing, both in terms of material stability (Chapter 2), biocompatibility (Chapter 3) and hemocompatibility (Chapter 4) should be undertaken for particularly promising neuroprosthetic

candidate devices/materials. Indeed this can be achieved by following the methodology developed here and altering the test solutions to better mimic the neural environment.

REFERENCES

- [1] L. G. Donaruma and D. F. Williams, Ed., "Definitions in biomaterials," *Journal of Polymer Science Part C: Polymer Letters*, vol. 26, pp. 414-414, 1988.
- [2] G. Kotzar, M. Freas, P. Abel, A. Fleischman, S. Roy, C. Zorman, "Evaluation of MEMS materials of construction for implantable medical devices," *Biomaterials*, vol. 23, pp. 2737-2750, 2002.
- [3] I. O. f. Standardization, "ISO 10993-12:2004," in *Biological evaluation of medical devices Part 12: Sample preparation and reference materials*, ed, 2004.
- [4] I. O. f. Standardization, "ISO 10993-14:2001," in *Biological evaluation of medical devices -- Part 14: Identification and quantification of degradation products from ceramics*, ed. Switzerland: ISO copyright office, 2001.
- [5] I. O. f. Standardization, "ISO 10993-15:2000," in *Biological evaluation of medical devices -- Part 15: Identification and quantification of degradation products from metals and alloys*, ed, 2000.
- [6] I. O. f. Standardization, "ISO 10993-5:2009," in *Biological evaluation of medical devices -- Part 5: Tests for in vitro cytotoxicity*, ed, 2009.
- [7] I. O. f. Standardization, "ISO 10993-4:2002," in *Biological evaluation of medical devices -- Part 4: Selection of tests for interactions with blood*, ed, 2002.
- [8] J. Black, *Biological Performance of Materials: Fundamentals of Biocompatibility, Fourth Edition*: Crc Press-Taylor & Francis Group, 6000 Broken Sound Parkway Nw, Ste 300, Boca Raton, Fl 33487-2742 USA, 2006.
- [9] J. M. Anderson, "Biological responses to materials," *Annual Review of Materials Research*, vol. 31, pp. 81-110, 2001 2001.
- [10] S. C. Gad, "Standards and methods for assessing the safety and biocompatibility of biomaterials," in *Characterization of Biomaterials*, M. Jaffe, W. Hammond, P. Toliias, and T. Arinzeh, Eds., ed: Woodhead Publ Ltd, Abington Hall Abington, Cambridge Cb1 6ah, Cambs, Uk, 2013, pp. 285-306.
- [11] U. Muller, "In vitro biocompatibility testing of biomaterials and medical devices," *Med Device Technol*, vol. 19, pp. 30, 32-4, Mar-Apr 2008.
- [12] C. Coletti, M. J. Jaroszeski, A. Pallaoro, A. M. Hoff, S. Iannotta, S. E. Sadow, "Biocompatibility and wettability of crystalline SiC and Si surfaces," in *Engineering in Medicine and Biology Society, 2007. EMBS 2007. 29th Annual International Conference of the IEEE*, 2007, pp. 5849-5852.

- [13] C. Coletti, "Silicon carbide biocompatibility, surface control, and electronic cellular interaction for biosensing applications," Doctor of Philosophy, Electrical Engineering, University of South Florida, Tampa, FL.
- [14] C. L. Frewin, M. Jaroszeski, E. Weeber, K. E. Muffly, A. Kumar, M. Peters., "Atomic force microscopy analysis of central nervous system cell morphology on silicon carbide and diamond substrates," *Journal of Molecular Recognition*, vol. 22, pp. 380-388, 2009.
- [15] C. L. Frewin, C. Locke, S. E. Sadow, E. J. Weeber, "Single-crystal cubic silicon carbide: An in vivo biocompatible semiconductor for brain machine interface devices," in *Engineering in Medicine and Biology Society, EMBC, 2011 Annual International Conference of the IEEE*, 2011, pp. 2957-2960.
- [16] U. T. Seyfert, V. Biehl, J. Schenk, "In vitro hemocompatibility testing of biomaterials according to the ISO 10993-4," *Biomolecular Engineering*, vol. 19, pp. 91-96, 8// 2002.
- [17] L. Muthusubramaniam, R. Lowe, W. Fissell, L. Li, R. Marchant, T. Desai, "Hemocompatibility of Silicon-Based Substrates for Biomedical Implant Applications," *Annals of Biomedical Engineering*, vol. 39, pp. 1296-1305, 2011/04/01 2011.
- [18] R. K. Roy, H. W. Choi, J. W. Yi, M. W. Moon, K. R. Lee, D. K. Han, "Hemocompatibility of surface-modified, silicon-incorporated, diamond-like carbon films," *Acta Biomaterialia*, vol. 5, pp. 249-256, 2009.
- [19] A. Bolz, "Coating of Cardiovascular Stents with a Semiconductor to Improve Their Hemocompatibility," 1996.
- [20] B. A. Weisenberg and D. L. Mooradian, "Hemocompatibility of materials used in microelectromechanical systems: Platelet adhesion and morphology in vitro," *J Biomed Mater Res*, vol. 60, p. 8, 2002.
- [21] N. Nurdin, P. François, J. K. Y. Mugnier, M. Moret, B.-O. Aronsson, P. Descouts¹, "Haemocompatibility evaluation of DLC and SiC coated surfaces " *European Cells and Materials*, vol. 5, 2003.
- [22] N. Schettini, "Hemocompatibility Assessment of 3C-SiC for Cardiovascular Applications," PhD, Electrical Engineering, University of South Florida, Tampa, FL, 2009.
- [23] D. A. Wink and J. B. Mitchell, "Chemical biology of nitric oxide: insights into regulatory, cytotoxic, and cytoprotective mechanisms of nitric oxide," *Free Radical Biology and Medicine*, vol. 25, pp. 434-456, 9// 1998.
- [24] M. Celina, K. T. Gillen, R. A. Assink, "Accelerated aging and lifetime prediction: Review of non-Arrhenius behaviour due to two competing processes," *Polymer Degradation and Stability*, vol. 90, p. 10, 2005.
- [25] D. W. L. Hukins, A. Mahomed, S. N. Kukureka, "Accelerated aging for testing polymeric biomaterials and medical devices," *Medical Engineering & Physics*, vol. 30, pp. 1270-1274, 2008.

- [26] C. Sella, "Corrosion resistance of amorphous hydrogenated SiC and diamond-like coatings deposited by r.f.-plasma-enhanced chemical vapour deposition," *Surface and coating technology*, vol. 60, p. 7, 1993.
- [27] K. K. Sanford, "The growth in vitro of single isolated tissue cell," *J. Natl. Cancer Inst*, vol. 9, p. 8, 1948.
- [28] B. B. Westfall, V. J. Evans, J. E. Shannon, and W. R. Earle, "The glycogen content of cell suspensions prepared from massive tissue culture comparison of cells derived from mouse connective tissue and mouse liver," *Journal of the National Cancer Institute*, vol. 14, pp. 655-664, 1953.
- [29] W. R. Earle, "Production of malignancy in vitro. IV. The mouse fibroblast cultures and changes seen in the living cells," *Journal of the National Cancer Institute*, vol. 4, pp. 165-212, Aug-Jun 1943.
- [30] K. K. Sanford and G. L. Hobbs, "The tumor-producing capacity of strain L mouse cells after 10 years in vitro," *Cancer Research*, vol. 16, p. 5, 1956.
- [31] W. R. Earle, K. K. Sanford, V. J. Evans, H. K. Waltz, J. E. Shannon, "The influence of inoculum size on proliferation in tissue cultures " *Journal of the National Cancer Institute*, vol. 12, pp. 133-153, 1951 1951.
- [32] P. Arnstein, D. O. N. Taylor, Nelsonre.Wa, R. J. Huebner, E. H. Lennette, "Propagation of human tumors in anithymocyte serum-treated mice," *Journal of the National Cancer Institute*, vol. 52, pp. 71-84, 1974.
- [33] R. S. Day and C. H. J. Ziolkowski, "Human-brain tumor-cell strains with deficient host-cell reactivation of n-methyl-n'-nitro-n-nitrosoguanidine-damaged adenovirus-5," *Nature*, vol. 279, pp. 797-799, 1979.
- [34] K. R. Jessen and R. Mirsky, "Glial-cells in the enteric nervous-system contain glial fibrillary acidic protein " *Nature*, vol. 286, pp. 736-737, 1980.
- [35] J. E. Castro, "Human tumors grown in mice," *Nature-New Biology*, vol. 239, pp. 83-&, 1972.
- [36] B. C. Giovanel, J. S. Stehlin, L. J. Williams, S. O. Yim, "Development of invasive tumors in nude mouse after injection of cultured human melanoma cells," *Journal of the National Cancer Institute*, vol. 48, pp. 1531-&, 1972.
- [37] D. Krex, B. Mohr, M. Hauses, G. Ehninger, H. K. Schackert, G. Schackert, "Identification of uncommon chromosomal aberrations in the neuroglioma cell line H4 by spectral karyotyping," *Journal of Neuro-Oncology*, vol. 52, pp. 119-128, Apr 2001.
- [38] G. Giordano and L. G. Costa, "Primary Neurons in Culture and Neuronal Cell Lines for In Vitro Neurotoxicological Studies," in *In Vitro Neurotoxicology: Methods and Protocols*. vol. 758, L. G. Costa, G. Giordano, and M. Guizzetti, Eds., ed: Humana Press Inc, 999 Riverview Dr, Ste 208, Totowa, Nj 07512-1165 USA, 2011, pp. 13-27.
- [39] G. Augusti-Tocco and G. Sato, "Establishment of functional clonal lines of neurons from mouse neuro blastoma " *Proceedings of the National Academy of Sciences of the United States of America*, vol. 64, pp. 311-315, 1969.

- [40] G. Meric, J. E. Dahl, I. E. Ruyter, "Cytotoxicity of silica-glass fiber reinforced composites," *Dental Materials*, vol. 24, pp. 1201-1206, Sep 2008.
- [41] M. Mueller, B. Krolitzki, B. Glasmacher, "Dynamic in vitro hemocompatibility testing - improving the signal to noise ratio," *Biomedical Engineering-Biomedizinische Technik*, vol. 57, Sep 2012.
- [42] C. L. Haycox and B. D. Ratner, "*in-vitro* platelet interaction in whole human blood exposed to biomaterial surface-insights on blood compatibility " *Journal of Biomedical Materials Research*, vol. 27, pp. 1181-1193, Sep 1993.
- [43] R. C. Jaeger, *Introduction to Microelectronic Fabrication* vol. V. New Jersey: Prentice Hall, 2002.
- [44] I. O. f. Standardization, "ISO 3696:1987," in *Water for analytical laboratory use -- Specification and test methods*, ed, 1987.
- [45] C. W. Locke, L. C. Frewin, S. E. Sadow, "3C-SiC epitaxial growth for advanced biomedical applications," in *Silicon Carbide Epitaxy*, F. La via, Ed., ed, 2012, pp. 225-258
- [46] D. Q. Zhang, A. Alkhateeb, H. M. Han, H. Mahmood, D. N. McIlroy, M. G. Norton, "Silicon carbide nanosprings," *Nano Letters*, vol. 3, pp. 983-987, Jul 2003.
- [47] Y. Q. Zhu, W. B. Hu, W. K. Hsu, M. Terrones, N. Grobert, J. P. Hare., "SiC-SiOx heterojunctions in nanowires," *Journal of Materials Chemistry*, vol. 9, pp. 3173-3178, 1999.
- [48] J. L. Goodwin, M. E. Kehrli Jr, E. Uemura, "Integrin Mac-1 and β -amyloid in microglial release of nitric oxide," *Brain Research*, vol. 768, pp. 279-286, 9/12/ 1997.
- [49] J. M. Pocock and A. C. Liddle, "Microglial signalling cascades in neurodegenerative disease," in *Progress in Brain Research*. vol. Volume 132, M. N.-S. B. Castellano Lopez, Ed., ed: Elsevier, 2001, pp. 555-565.
- [50] D. A. Wink, "The chemical mechanisms in regulatory, cytotoxic, and cytoprotective roles of nitric oxide.," *Abstracts of Papers of the American Chemical Society*, vol. 215, pp. U360-U360, Apr 2 1998.
- [51] D. A. Wink and J. B. Mitchell, "Chemical biology of nitric oxide: Insights into regulatory, cytotoxic, and cytoprotective mechanisms of nitric oxide," *Free Radical Biology and Medicine*, vol. 25, pp. 434-456, Sep 1998.
- [52] M. Nezafati, S. E. Sadow, C. L. Frewin, "Investigating the surface changes of silicon in vitro within physiological environments for neurological application," presented at the MRS, Boston MA, 2014.
- [53] H. Charkhkar, C. Frewin, M. Nezafati, G. L. Knaack, N. Peixoto, S. E. Sadow, J. J. Pancrasio., "Use of cortical neuronal networks for in vitro material biocompatibility testing," *Biosensors and Bioelectronics*, vol. 53, pp. 316-323, 2014.
- [54] G. Voskerician, M. S. Shive, R. S. Shawgo, H. von Recum, J. M. Anderson, M. J. Cima "Biocompatibility and biofouling of MEMS drug delivery devices," *Biomaterials*, vol. 24, pp. 1959-1967, May 2003.

- [55] M. Long and H. J. Rack, "Titanium alloys in total joint replacement - a materials science perspective," *Biomaterials*, vol. 19, pp. 1621-1639, Sep 1998.
- [56] B. Rubehn and T. Stieglitz, "In vitro evaluation of the long-term stability of polyimide as a material for neural implants," *Biomaterials*, vol. 31, pp. 3449-3458, 2010.
- [57] H. E. Koschwanetz and W. M. Reichert, "In vitro, in vivo and post explantation testing of glucose-detecting biosensors: Current methods and recommendations," *Biomaterials*, vol. 28, pp. 3687-3703, 9// 2007.
- [58] S. Zhang, X. Zhang, C. Zhao, J. Li, Y. Song, C. Xie, "Research on an Mg–Zn alloy as a degradable biomaterial," *Acta Biomaterialia*, vol. 6, pp. 626-640, 2010.
- [59] R. A. Green, J. S. Ordonez, M. Schuettler, L. A. Poole-Warren, N. H. Lovell, G. J. Suaning, "Cytotoxicity of implantable microelectrode arrays produced by laser micromachining," *Biomaterials*, vol. 31, pp. 886-893, Feb 2010.
- [60] G. Meriç, J. E. Dahl, I. E. Ruyter, "Cytotoxicity of silica–glass fiber reinforced composites," *Dental Materials*, vol. 24, pp. 1201-1206, 2008.
- [61] L. Scheideler, C. Füger, C. Schille, F. Rupp, H. P. Wendel, N. Hort, "Comparison of different in vitro tests for biocompatibility screening of Mg alloys," *Acta Biomaterialia*, vol. 9, pp. 8740-8745, 11// 2013.
- [62] CreightonUniversity. (2014). *Cell Counts using a Hemacytometer*. Available: http://medschool.creighton.edu/fileadmin/user/medicine/images/TeachResearchPatient/Research/Flow_Cytometry_Core_Files/Protocols/Using_a_Hemacytometer.pdf
- [63] M. Yang, F. Qu, Y. Lu, Y. He, G. Shen, R. Yu, "Platinum nanowire nanoelectrode array for the fabrication of biosensors," *Biomaterials*, vol. 27, pp. 5944-5950, 2006.
- [64] R. A. Sperling, P. Rivera gil, F. Zhang, M. Zanella, W. J. Parak, "Biological applications of gold nanoparticles," *Chemical Society Reviews*, vol. 37, pp. 1896-1908, Sep 2008.
- [65] R. P. Haugland, I. C. MacCoubrey, P. L. Moore, "Dual-fluorescence cell viability assay using ethidium homodimer and calcein AM," ed: Google Patents, 1994.
- [66] T. C. Sandy Hoopera, "Neurotoxicity screening test for deep brain stimulation leads," *Journal of Biomaterials Science, Polymer Edition*, vol. 18, p. 13, 2007.
- [67] M. Scudellari. (2013). *Penetrating the Brain*. Available: <http://www.the-scientist.com/?articles.view/articleNo/37957/title/Penetrating-the-Brain/>
- [68] K. Kottkemarchant, J. M. Anderson, Y. Umemura, R. E. Marchant, "Effect of albumin coating on the *in-vitro* blood compatibility of dacron arterial prostheses " *Biomaterials*, vol. 10, pp. 147-155, Apr 1989.
- [69] K. Kottkemarchant, J. M. Anderson, A. Rabinovitch, "The platelet reactivity of vascular graft prostheses - an *in-vitro* model to test the effect of preclotting " *Biomaterials*, vol. 7, pp. 441-448, Nov 1986.
- [70] B. D. Ratner, "Blood compatibility - a perspective," *Journal of Biomaterials Science-Polymer Edition*, vol. 11, pp. 1107-1119, 2000 2000.

- [71] A. Bolz and M. Schaldach, "Hemocompatibility optimization of implants by hybrid structuring " *Medical & Biological Engineering & Computing*, vol. 31, pp. S123-S130, Jul 1993.
- [72] K. Ishihara, H. Oshida, Y. Endo, T. Ueda, A. Watanabe, N. Nakabayashi, "Hemocompatibility of human whole-blood on polymers with a phospholipid polar group and its mechanism " *Journal of Biomedical Materials Research*, vol. 26, pp. 1543-1552, Dec 1992.
- [73] A. Chandler, "In vitro thrombotic coagulation of the blood; a method for producing a thrombus," *Laboratory investigation; a journal of technical methods and pathology*, vol. 7, p. 110, 1958.
- [74] N. Schettini, in *Silicon Carbide Biotechnology: A Biocompatible Semiconductor for Advanced Biomedical Devices and Applications*, S. E. Sadow, Ed., ed: Elsevier LTD, 2011.
- [75] J. P. Alper, M. S. Kim, M. Vincent, B. Hsia, V. Radmilovic, C. Carraro., R. Maboudian, "Silicon carbide nanowires as highly robust electrodes for micro-supercapacitors," *Journal of Power Sources*, vol. 230, pp. 298-302, May 2013.
- [76] K. Zekentes and K. Rogdakis, "SiC nanowires: material and devices," *Journal of Physics D-Applied Physics*, vol. 44, Apr 2011.
- [77] J. P. Alper, A. Gutes, C. Carraro, R. Maboudian, "Semiconductor nanowires directly grown on graphene - towards wafer scale transferable nanowire arrays with improved electrical contact," *Nanoscale*, vol. 5, pp. 4114-4118, 2013.
- [78] J. P. Alper, M. Vincent, C. Carraro, R. Maboudian, "Silicon carbide coated silicon nanowires as robust electrode material for aqueous micro-supercapacitor," *Applied Physics Letters*, vol. 100, Apr 2012.
- [79] F. Fabbri, F. Rossi, M. Negri, R. Tatti, L. Aversa, S. C. Dhanabalan., "Carbon-doped SiO_x nanowires with a large yield of white emission," *Nanotechnology*, vol. 25, May 9 2014.
- [80] F. Filippo, R. Francesca, A. Giovanni, S. Giancarlo, I. Salvatore, A. Lucrezia., "Enhancement of the core near-band-edge emission induced by an amorphous shell in coaxial one-dimensional nanostructure: the case of SiC/SiO₂ core/shell self-organized nanowires," *Nanotechnology*, vol. 21, p. 345702, 2010.
- [81] G. D. Wei, W. P. Qin, G. F. Wang, J. B. Sun, J. J. Lin, R. J. Kim, "The synthesis and ultraviolet photoluminescence of 6H-SiC nanowires by microwave method," *Journal of Physics D-Applied Physics*, vol. 41, Dec 2008.
- [82] R. B. Wu, B. S. Li, M. X. Gao, J. J. Chen, Q. M. Zhu, Y. Pan, "Tuning the morphologies of SiC nanowires via the control of growth temperature, and their photoluminescence properties," *Nanotechnology*, vol. 19, Aug 2008.
- [83] S. Perisanu, V. Gouttenoire, P. Vincent, A. Ayari, M. Choueib, M. Bechelany, "Mechanical properties of SiC nanowires determined by scanning electron and field emission microscopies," *Physical Review B*, vol. 77, Apr 2008.


- [84] D. Zhou and S. Seraphin, "Production silicon-carbide whiskers from carbon nanoclusters," *Chemical Physics Letters*, vol. 222, pp. 233-238, May 1994.
- [85] H. J. Dai, E. W. Wong, Y. Z. Lu, S. S. Fan, C. M. Lieber, "Synthesis and characterization of carbide nanorods," *Nature*, vol. 375, pp. 769-772, Jun 1995.
- [86] K. Zekentes, N. Becourt, M. Androulidaki, K. Tsagaraki, J. Stoemenos, J. M. Bluet, "Gas source molecular beam epitaxy of beta-SiC on Si substrates," *Applied Surface Science*, vol. 102, pp. 22-27, Aug 1996.
- [87] Y. F. Zhang, Y. H. Tang, Y. Zhang, C. S. Lee, I. Bello, S. T. Lee, "Deposition of carbon nanotubes on Si nanowires by chemical vapor deposition," *Chemical Physics Letters*, vol. 330, pp. 48-52, Nov 2000.
- [88] X. T. Zhou, N. Wang, H. L. Lai, H. Y. Peng, I. Bello, N. B. Wong, "beta-SiC nanorods synthesized by hot filament chemical vapor deposition," *Applied Physics Letters*, vol. 74, pp. 3942-3944, Jun 1999.

APPENDICES

Appendix A: Copyright Permissions

In this section the copyright permission from the websites and the journal publishers which, own the copyright of the corresponding figures will be presented. In figure 2.15 the AFM and figure 2.16 SEM micrographs were already published in MRS Fall 2013 the permission to reuse the micrographs was obtained in July 29, 2014 from Cambridge University Press the copyright owner and it is presented in figure A.1 of the appendix A. The figure 4.1 was presented from the website “to-BBB.com”, the permission obtained from © to-BBB institute administrator via email on July 30, 2014, the written permission is presented in figure A.2. The figure 5.1 SEM micrograph and XRD spectrum was already used in the Journal of Power Sources in Elsevier, the permission license is presented in figure A.3. The figure 5.2 and figure 5.3 used from Institute of Physics (IOP) publishing, journals, the name of journals and permission to use the figures from them is presented in figure A.4 of appendix A. The permission for these figures obtained from permissions@iop.org on July 30, 2014 and it was confirmed by Lucy Evans the publishing assistant of IOP.

7/31/2014 RightsLink - Your Account



RightsLink[®]

Welcome maysam@mail.usf.edu [Log out](#) | [Help](#)

[My Orders](#) [My Library](#) [My Profile](#)

[My Orders](#) > [Orders](#) > [All Orders](#)

License Details

This is a License Agreement between Maysam Nezzafati ("You") and Cambridge University Press ("Cambridge University Press"). The license consists of your order details, the terms and conditions provided by Cambridge University Press, and the [payment terms and conditions](#).

[Get the printable license](#)

License Number	3438411086035
License date	Jul 20, 2014
Order Content Publisher	Cambridge University Press
Order Content Publication	MRS Online Proceedings Library
Order Content Title	Investigating the surface changes of silicon in vitro within physiological environments for neurological application
Order Content Author	Maysam Nezzafati, Stephen E. Saddow and Christopher L. Frewin
Order Content Date	Mar 25, 2014
Volume number	1621
Issue number	-1
Start page	237
End page	242
Type of Use	Dissertation/Thesis
Requestor type	Author
Portion	Text extract
Number of pages requested	1
Author of this Cambridge University Press article	Yes
Author / editor of the new work	Yes
Order reference number	None
Territory for reuse	North America Only
Title of your thesis / dissertation	Biomaterial Testing Methodology for Long-Term in vivo Applications: Silicon Carbide Corrosion Resistance, Biocompatibility and Hemocompatibility
Expected completion date	Aug 2014
Estimated size(pages)	122
Billing Type	Invoice
Billing address	4501 Montego Bay Ct unit 5 TAMPA, FL 33613 United States
Tax(0.00%)	0.00 USD
Total	0.00 USD

← Back

Copyright © 2014 Copyright Clearance Center, Inc. All Rights Reserved. [Privacy statement](#) . Comments? We would like to hear from you. E-mail us at customerscare@copyright.com

<https://s100.copyright.com/MyAccount/ViewLicenseDetails?ref=3c6ec71e-5be0-4d1b-b402-6bc91a462392>
1/1

Figure A.1: Copyright permission to reuse the figures from Cambridge University Press, for figure 2.15 and 2.16.



Maysam Nezafati <maysam@mail.usf.edu>

Re: Maysam Nezafati

1 message

Marco de Boer | to-BBB <MarcoDeBoer@tobbb.com>
To: "maysam@mail.usf.edu" <maysam@mail.usf.edu>

Wed, Jul 30, 2014 at 5:17 AM

Dear Maysam,

Hereby, I would like to confirm that you can use the image as long as you include "© to-BBB" as reference of origin/copyright.

Good luck,

Marco

From: "to-BBB.website@gould.eatserver.nl" <to-BBB.website@gould.eatserver.nl>

Date: Tuesday, July 29, 2014 9:35 PM

To: Research | to-BBB <research@tobbb.com>

Subject: Maysam Nezafati

U heeft een bericht van de website

Naam: Maysam Nezafati
E-mail: maysam@mail.usf.edu
Department: Research
Telefoonnummer: 4043173313

Toelichting:

To Whom it may concern, This is maysam nezafati PhD from university of South Florida. I want to use the picture in your website that shows the brain vascular network. I was wondering how can I obtain the permission from the owner of the picture. According to my research the picture was published by your website. the url of the image that I want to use is as written here: http://www.tobbb.com/img/Sciencevasculature_s.png I will appreciate it if I have the permission to use the image in my phd dissertation. Regards
Maysam

Figure A.2: Copyright permission to reuse the figures from © to-BBB, for figure 4.1.



MyOrders > Orders > All Orders

License Details

Thank you very much for your order.

This is a License Agreement between Maysam Nezafei ("You") and Elsevier ("Elsevier"). The license consists of your order details, the terms and conditions provided by Elsevier, and the [payment terms and conditions](#).

[Get the printable license.](#)

License Number	3438380155258
License date	Jul 29, 2014
Order Content Publisher	Elsevier
Order Content Publication	Journal of Power Sources
Order Content Title	Silicon carbide nanowires as highly robust electrodes for micro-supercapacitors
Order Content Author	John P. Alper,Min Sek Kim,Maxime Vincent,Ben Hsia,Valimir Radmilovic,Carlo Carraro,Roya Maboudian
Order Content Date	15 May 2013
Licensed content volume number	230
Licensed content issue number	n/a
Number of pages	5
Type of Use	reuse in a thesis/dissertation
Portion	figures/tables/illustrations
Number of figures/tables/illustrations	1
Format	electronic
Are you the author of this Elsevier article?	No
Will you be translating?	No
Title of your thesis/dissertation	Biomaterial Testing Methodology for Long-Term in vivo Applications: Silicon Carbide Corrosion Resistance, Biocompatibility and Hemocompatibility
Expected completion date	Aug 2014
Estimated size (number of pages)	122
Elsevier VAT number	GB 494 8272 12
Price	0.00 USD
VAT/Local Sales Tax	0.00 USD / 0.00 GBP
Total	0.00 USD

[Back](#)

Copyright © 2014 Copyright Clearance Center, Inc. All Rights Reserved. [Privacy statement](#) . [Comments?](#) We would like to hear from you. E-mail us at customerscare@copyright.com

Figure A. 3: Copyright permission to reuse the figures from Elsevier, for figure 5.1.

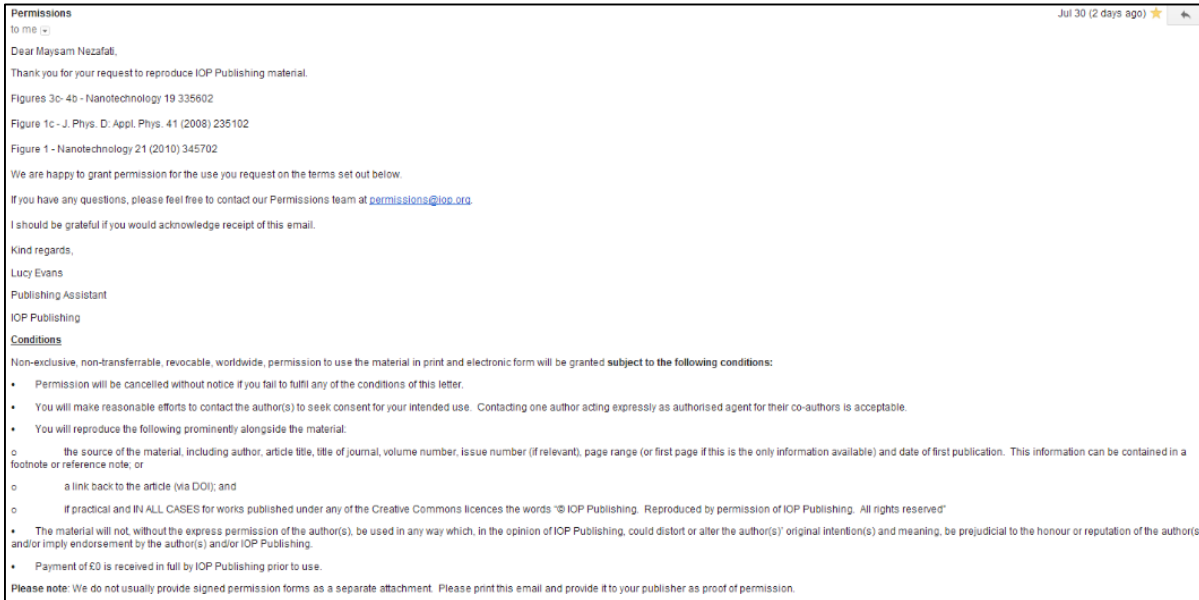


Figure A. 4: Copyright permission to reuse the figures from institute of physics publishing, for figure 5.2 and figure 5.3.

Appendix B: Chemical Composition of Electrolytes

The quantities that are mentioned in the following list, is to obtain 1 liter of the electrolytes.

- Phosphate Buffer Saline (1X-PBS):

1.37 M NaCl (58.44 g/M)80.0 g

27 mM KCl (74.55 g/M)2.01 g

100 mM Na₂HPO₄ (141.958 g/M)14.2 g

17.6 nM KH₂PO₄ (136.086 g/M)2.395 g

HCl (to adjust the pH)

NaOH (to adjust the pH)

- Artificial Plasma:

NaCl 6.800 g

CaCl₂..... 0.200 g

KCl 0.400 g

MgSO₄ 0.100 g

NaHCO₃..... 2.200 g

Na₂HPO₄ 0.126 g

NaH₂PO₄ 0.026 g

- Artificial Cerebrospinal Fluid (ACSF):

NaCl7.5975 g

KCl0.2236 g

NaH₂PO₄0.1500 g

Glucose1.8016 g

NaHCO₃1.6802 g

MgSO₄0.3204 g

CaCl₂-2H₂O0.3675 g